New Dynamic Modeling and Practical Control Design for MacPherson Suspension System

by

MOHAMMAD SABER FALLAH

A thesis
in
the Department
Mechanical and Industrial Engineering

Presented in partial fulfillment of the requirements
for the degree of Doctor of Philosophy at
Concordia University
Montreal, Quebec, Canada

April 2010   ©

NOTICE:

AVIS:

Canada

ABSTRACT

New Dynamic Modeling and Practical Control Design for MacPherson Suspension System

Mohammad Saber Fallah
Concordia University, 2010

The ride quality, handling, and stability are three main issues in vehicle suspension design. Different suspension systems have been designed in the past to fulfil these conflicting requirements. One of the popular suspension systems integrated in small and midsize passenger cars is MacPherson suspension system. A suspension system is either passive if a conventional damper is incorporated or is semi-active with a variable damper. A new control oriented dynamic model of the MacPherson suspension system is developed in this thesis to consider the effects of the suspension structure on the dynamic response and a new kinematic model is proposed to investigate those suspension kinematic parameters affecting both handling performance and stability of the vehicle.

The performance of MacPherson suspension system under alternative hybrid semi-active controls is evaluated. It is shown that the contribution of different control strategies on the ride quality enhancement of the vehicle could be similar whereas their effectiveness on the performance of suspension kinematc parameters is completely different.

Using the H_∞ robust control theory, a full state feedback controller is designed to improve MacPherson suspension specifications. The gain of the controller is optimized so that the trade-off between the requirements is achieved. To be more practical and to reduce the design cost, H_∞ output feedback control theory is employed to design a controller with the minimal cost design. To optimize the controller gain, the LMI and Genetic Algorithm

optimization tools are used. It is shown that the output controller can improve the suspension performance close to that of a full state feedback controller.

A magnetorheological damper with continuously variable damping is considered as the actuator to the system. In order to tune the current signal of the damper so as to track the desired force calculated from the controller unit, a mathematical dynamic model of the damper is required. For modelling the damper, the MR damper is characterized by a piece-wise polynomial model which is identified by using the data acquired from various tests in the laboratory. The dynamic behaviour of the MR damper on control performance is investigated. The Hardware-in-the-Loop Simulation is made and the effectiveness of the controllers is evaluated through experiments.

ACKNOLEDGEMENT

I, author of this thesis, am sincerely grateful to my supervisors Prof. Rama Bhat and Dr. Wen-Fang Xie for their excellent guidance, advice, and encouragement throughout the thesis work. I would like to acknowledge the support from Prof. Subash Rakheja for allowing the use of his laboratory and equipment for the experimental studies in this thesis work.

Special thanks are due to Prof. Ebrahim Esmailzadeh, the external examiner, for his thoughtful review and many helpful suggestions. In addition, I would like to thank the reading committee members, Prof. Stiharu, Dr. Hong, and Dr. Hashtrudi-zad for their valuable comments and suggestions.

Thanks are also due to all of my colleagues at the Concordia University who have helped me through the work.

I thank all the members of my family for the warmth and kindness they always offer, with special gratitude to my wife, Somi. Without her continuous support, encouragement, and love, my study would never have been done properly. Finally, my great appreciations and thanks are dedicated to my parents from whom I have taken the lesson of life. I am very proud of them.

Finally, I would like to dedicate this thesis to my dear son, Danial, my beloved wife, Somi, and my parents with love and gratitude.

TABLE OF CONTENTS

LIST OF FIGURES

LIST OF TABLES

NOMENCLATURE

A, B_1, B_2, B_3	State space matrices
A_i, B_i	Discrete state space matrices of jth vertex
C_p	Passive damping coefficient
C_{sky}	Sky-hook damping coefficient
e	Controlled output vector
f_a	Actuator force
f_d	Disturbance force
f_{sa}	Semi-active damper force
G	Constant controller gain
I_{ca}	Inertia moment of the wheel about the axis which is parallel to X axis and passing through its centre of the gravity
I_u	Inertia moment of the control arm about the axis which is parallel to X axis and passing through its centre of the gravity
K_s, K_t	Stiffness coefficients of the sprung and unsprung masses, respectively
K	Gain matrix
L_A	Length of the control arm
m_s, m_u, m_{ca}	Mass of the chassis, wheel, and control arm, respectively
n_1, n_2	Road roughness constants
$\bar{r}_c$	Position vector of point C
r_1, r_2	Weighting parameters
$S_g(\Omega_0)$	Road roughness coefficient
$x(t)$	Vector of states.

(x_A, y_A, z_A)	Position of point A
(x_B, y_B, z_B)	Position of point B
(x_C, y_C, z_C)	Position of point C
(x_D, y_D, z_D)	Position of point D
(x_J, y_J, z_J)	Position of point J
(x_P, y_P, z_P)	Position of point P
(x_M, y_M, z_M)	Position of point M
(u_x, u_y, u_z)	Cosine directions of line CD
(u_{x0}, u_{y0}, u_{z0})	Cosine directions of line GH
v	Control input vector
w	Plant input vector
y	Measurement vector
z_r	Road disturbance
$z(t)$	Vector of H_∞ performance controlled outputs
z_s	Vertical displacement of sprung mass (chassis)
z_u	Vertical displacement of unsprung mass (wheel)
α	Slope of the strut
β	The relative ratio between the skyhook and groundhook controllers
θ	Angular displacement of control arm
θ_I	Initial angle of the control arm resulting from the static deflection and structure design
φ	Rotation angle of the wheel with respect to a vertical line to the road
σ_{SKY}	skyhook component of the damping force
σ_{GND}	groundhook component of the damping force

γ	Upper bound of the H_∞ transfer matrix norm
(ϕ, ϑ, ψ)	Roll, Pitch and Yaw angles
Ω	Special frequency
Ω_0	References special frequency

ABBREVIATION

DOF	Degree of Freedom
LMI	Linear Matrix Inequality
LQG	Linear Quadratic Gaussian
LPV	Linear Parameter Variable
LVDT	Linear Variable Differential Transformers
OFC	Output Feedback Controller
MR	Magneto Rehological
RPY	Roll-Pitch-Yaw
RS	Revolute-spherical
PSD	Power Spectral Density
PTP	Peak to Peak
RMS	Root Mean Square
GA	Genetic algorithm
SC	Spherical-cylindrical
SS	Spherical-spherical

CHAPTER 1

INTRODUCTION, LITERATURE SURVEY, AND OBJECTIVES

1.1 Introduction

Vehicles are subjected to excitations due to road roughness. In order to alleviate the discomfort to the passengers and excessive fatigue damage to the various vehicle system components, the vehicle is equipped with a suspension system that cushions the vehicle. The main function of a suspension system is to provide sufficient ride quality (passenger comfort), superior handling performance, and adequate road-holding of the tire. A suspension system is a multilink dynamic system which absorbs the energy exerted from road to the vehicle by a spring and dissipates it through a damper.

Ride quality deals with the sense of comfort and feel of the passengers within the vibration environment of a moving vehicle. The vibrations mainly arise from road surface irregularities and on-board vibration sources. The on-board vibration sources can be classified as imbalances in the tire and wheel assemblies, engine vibration, aerodynamic forces and vibrations from transmission system. The engine and driveline vibrations are transmitted to the vehicle body via the engine and transmission mounts while the excitations from wheel and tire imbalances are applied to the vehicle body through the suspension system. However, the main vibration source is the road irregularities, transmitted to the vehicle body through the wheel and suspension system [1, 2]. The road vibrations are classified as shocks and vibration. Shocks from suddenly applied inputs

1

such as those by potholes and bumps are discrete events with short duration and high power, whereas vibrations include consistent excitations.

Another function of suspension system is to maintain sufficient contact force between the tires and the road (road holding ability) with minimal load variation. Based on the wheel position and its motions, different types of forces such as tractive, cornering and braking forces are generated by the tire on motion. It is known that all of these forces are a function of the vertical force acting between the tire and the road. The magnitude of the vertical force varies when the suspension system is undergoing vibrations. The vibration of the tire influences the road holding ability of the suspension and consequently affects the handling performance and stability condition of the vehicle. In order to avoid losing contact with the ground, the magnitude of the dynamic vertical force should not exceed the static load. This factor becomes important during cornering due to rapid variation of the vertical load [1].

Handling performance refers to the response of the vehicle subject to steering commands and environmental inputs. The kinematics and linkage of a suspension system with significant influence on the handling performance are important in controlling the direction of the vehicle motion and in its stability in the presence of external disturbances, such as wind gust and road disturbances. In the context of suspension design, kinematics describes the wheel motions during bottoming out and steering and kinematic suspension parameters refer to variations in the positions of the wheels subject to the changes in the forces and moments between the tires and road.

It is known that the above requirements of a suspension system are conflicting. For example, in order to achieve better isolation of the vehicle body from road roughness it is preferable to have low damping allowing a large suspension deflections while a large damping yields better road contact at the expense of high frequency isolation. Thus, it is hard to have simultaneously a high ride comfort, handling and body attitude control under all driving conditions.

1.2 Categories of Suspensions

Based on the principle of operation, the suspension systems are classified into three main categories: passive, active and semi-active systems. A passive suspension system dissipates the energy via the passive damper. In this case, the kinematic and dynamic parameters of the structure would be so chosen as to reach a compromise between road holding and ride comfort. While in active suspension system a hydraulic actuator is incorporated in place of the strut in order to exert a desired force to improve suspension performance, in semi-active suspension system the damping coefficient of the damper is controlled so that there is maximum energy absorption without compromising the ride comfort.

Traditionally used in automotive applications, the passive suspension systems provide a compromise between the specifications in a limited range of the road excitation frequencies, while the active suspensions offer good road roughness isolation, stability, and handling performance compared to those of passive type over a wide range of disturbance frequencies. However, complicated circuit components, expensive structure and heavy weight are the main obstacles in the implementation of this type of suspensions. In spite of the advantages of the active suspension systems, semi- active

3

suspensions are more attractive because of low energy requirement, simple structure and a performance in between those of passive and fully active systems.

Suspension systems are divided into two main groups, solid axles and independent suspensions based on the type of structure. A solid axle connects two wheels together by a rigid beam and therefore the motion of one-side wheel affects the motion and position of the opposite-side wheel directly. Such suspension systems are usually found as rear and front suspensions where a high load capacity is required such as in heavy trucks. The independent suspension systems, on the other hand, allow the motions of the two-side wheels to be free from each other. This type of suspensions is popular in nearly all passenger cars and light trucks since it provides a better space for the engine, superior steering and better suspension kinematic performance [1]. Some of the popular types of independent suspension systems integrated in small and middle size vehicles include MacPherson, double wishbone, and multi-link suspension systems [3].
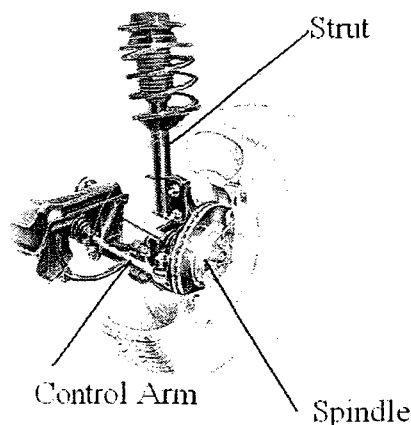
Figure 1.1 MacPherson strut wheel suspension[1]

---

[1] The figure is borrowed from: http://autospeed.com/cms/article.html?&A=1653

The MacPherson suspension (Figure 1.1) was proposed by Earl S. MacPherson in 1949. Ford Motor Company incorporated this type of suspension in its products. The MacPherson suspension is widely used in many modern vehicles due to its simple structure. It is usually implemented in the vehicle body as a front suspension; however, it has been used as both front and rear suspensions. This suspension is categorized as an independent suspension and it is an advanced development of a double wishbone suspension where the upper transverse link is replaced by the strut link including damper and spring. The main advantages of a MacPherson suspension are its simple structure, compact size, low weight and low maintenance cost, whereas it has some disadvantages such as less favourable kinematic performance, higher need for steering, higher tire wear and less isolation of the vehicle body from road roughness compared to other types of independent suspensions [3].

1.3 Literature Survey

The objective of the present thesis research is to attenuate the vehicle body vibration resulting from road irregularities using a suitable semi-active control strategy along with evaluation of the kinematic suspension performance and validation of the results with experimental data. The literature review is in three parts, modeling of the suspension system, suspension control strategies and experimental studies.

1.3.1 Modeling of the suspension system

In terms of the suspension control of a vehicle, three models are widely considered by researchers. The first model represents the vertical dynamic response of the quarter vehicle. It can be divided into two sub-models including the single degree-of-freedom (DOF) model and two degree-of-freedom model. While single DOF model shows the

vibration of the sprung mass (vehicle body), the two DOF model includes the wheel modes as well. The second model considers the half car of a vehicle and represents either the vertical and pitch motions corresponding to the bicycle model or the vertical and roll motions corresponding to the axle model. The third one represents a full vehicle and contains seven DOF including roll, pitch, vertical motions of wheels and vertical motion of the vehicle body [4]. However, in all those models, the unsprung mass, including suspension linkage and wheel mass, is connected to the sprung mass via a linear spring and damper. Among the above models the quarter car model with two DOF is much more popular for ride control applications compared to the other models.
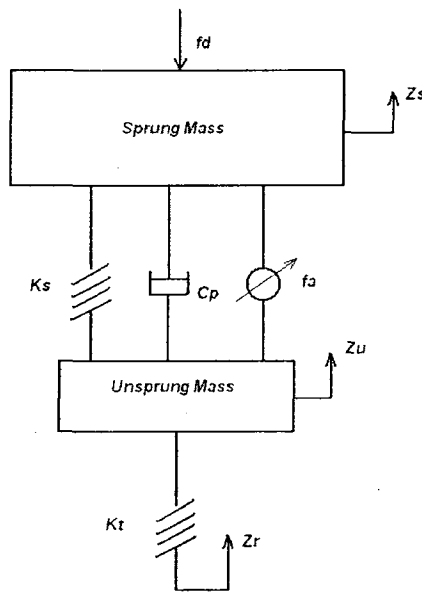
Figure 1.2 Conventional quarter-car model

A quarter-car model, shown in Figure 1.2, represents two dominant modes of two lumped masses connected via a spring and a damper. The dynamics of the tire is modelled as the spring stiffness. This model considers the vertical motions of the sprung and unsprung masses. It should be noted that without considering the effect of the suspension

6

kinematics and related linkage, this simple model may not be significantly effective. Studies related to the control-oriented modeling of a specific suspension system, such as MacPherson suspension, are rare. It is obvious that the need for an accurate model of the MacPherson suspension system to study the impact of suspension kinematics on the dynamic behaviour of the system becomes increasingly important for ride control design.

1.3.2 Ride control design strategies

The objective of ride control is to isolate the vibrations transmitted to the sprung mass from road disturbances while satisfying the handling and stability constraints. There are many semi-active control algorithms available in the literature; however, the main control architectures used can be classified into three categories including hybrid (skyhook-groundhook controller), optimal and robust control strategies. It is worth mentioning that in an active suspension system the controlled force is generated by a hydraulic actuator, while in the semi-active one, the idea is to reproduce a desired damping force obtained from ride control design by a semi-active damper located between the wheel and chassis. However, the procedure for the force control design is the same for both active and semi-active suspension systems.

Previous studies employed the root mean square acceleration of the sprung mass, suspension deflection, i.e. the relative displacement between the car body and wheel assembly, and tire deflection as measurement of the ride quality, rattle space constraint and road holding ability, respectively. It was concluded in [4] that there exists an excellent correlation between root mean square acceleration and the individual ride feeling. In addition, the smaller tire deflection results in better road holding and consequently a superior handling and stability performance. A large suspension

deflection may cause deterioration of ride comfort as well as structural damage. Accordingly, for optimal control of a suspension system, a performance index such as Equation (1.1) is defined which should be minimized subject to the system dynamics, represented by Equation (1.2) [4].

$$minimize\left\{ PI = \int_{0}^{\infty}(\ddot{z}_{s}^{2} + r_{1}(z_{s} - z_{u})^{2} + r_{2}(z_{u} - z_{r})^{2})dt \right\}$$ (1.1)

$$\dot{x} = Ax(t) + B_{1}f_{a}(t) + B_{2}z_{r}(t) + B_{3}f_{d}(t)$$ (1.2)

where $x(t) = \left[z_{s} - z_{u}, \dot{z}_{s}, z_{u} - z_{r}, \dot{z}_{u} \right]$ represents the states of the system. f_{a} and f_{d} stand for actuator and disturbance forces, respectively, and z_{r} is road profile input. In addition, r_{1} and r_{2} are weighting parameters indicating the contribution of the rattle space limitation and handling performance in improving the ride quality.

A comprehensive literature survey was carried out by Hrovat [4] pertaining to optimal control of active suspensions based on different suspension models. It was concluded that the performance of optimal control of active suspension is not superior compared to that of the passive one unless an adaptive control approach or gain scheduling is combined.

For semi-active control suspension applications, Tseng and Hedrick [5] showed that variable gain is needed for optimal control which makes it impractical. In order to cope with the variable gain problem of optimal control for semi-active suspension systems, they investigated two main sub-optimal approaches, including clipped optimal and steepest gradient that involved constant gain solutions. In the former approach, the performance index is in relation with the optimal active one while in the latter approach it

is pertaining to the optimal passive one. In addition, Giua et al [6] designed an optimal gain switching force controller for this application. In their work, an optimal controller was obtained based on the active control law; however, the gain would be changed under different conditions based on a gain scheduling approach. In their next work [7], they applied the proposed control strategy on the semi-active suspension by utilizing two types of actuators including MR and ER dampers and incorporating an observer.

In semi-active suspension systems, the force of a semi-active actuator is limited between $[f_{min}, f_{max}]$. In addition, the passivity requirement of dynamics of a semi-active suspension system leads to another constraint. The passivity constraint arises from the fact that the force generated by semi-active damper should play an energy dissipating role. Thus the following mathematical constraint should be satisfied during optimization procedure [44].

$$f_{sa}(\dot{z}_s - \dot{z}_u) \geq 0 \qquad (1.3)$$

Considering the abovementioned constraints and their effects on the future dynamic performance of the system, a Model Predictive Control (MPC) algorithm was employed by Canale et al [8] to handle the limitations. It was shown that the MPC significantly improves the ride comfort and handling performance. Since the computation load of this type of algorithm is high, they proposed a faster algorithm for optimization purposes. Sohn et al [9] tried to estimate the profile of the road using extended least square estimation approach and consequently designed a Linear Quadratic Gaussian (LQG) controller based on the road estimation. However, it is known that the LQG controller has poor stability margins with respect to model uncertainties thereby reducing the overall performance of the control system [10].

Although, in the literature, the abovementioned control strategies cover the major part of controllers applied to a vehicle suspension system, there are various other advanced control strategies such as adaptive, predictive, pole placement etc. control for this application.

Adaptive control strategy refers to a controller that is able to adapt its parameters in the presence of some system changes. In suspension systems, the main source of variations is dynamic parameter changes such as stiffness and mass. Song et al [11] employed a nonlinear adaptive control for magnetorheological suspension systems where its mass and stiffnesses were assumed to be unknown. In their study, the unknown parameters were first estimated by recursive least squares method and subsequently the cost function of the system including sprung mass acceleration and suspension deflection was minimized. Chen and Huang [12] considered the load of the vehicle as a time-varying parameter with known bound. In addition, they assumed that some uncertainties with unknown bounds exist in the plant. Accordingly, they designed an adaptive sliding controller to accommodate the uncertainties. Fialho and Balas [13], employed adaptive theory by gain scheduling tool for active suspension control. Two main specifications taken into account in this work were the suspension deflection and the sprung mass acceleration. Depending on the road profile conditions and suspension deflection, the weighting parameters were switched on specified values to overcome the limitations. In addition, the dynamics of hydraulic actuator was considered and a backstepping approach control was designed for voltage generation.

Leite and Peres [14] considered the damper coefficient, the spring coefficient, and the sprung mass as the uncertain parameters belonging to a polytope of uncertainty and then

proposed a parameter-dependent gain using pole location control approach for active suspension systems. Sie et al [15] employed the grey prediction fuzzy controller for active suspension control. A preview active suspension was studied in [16, 17] as well. In a preview controller, the future information of the system is available and utilized by the control law.

In conclusion, many studies on the advanced suspension control design have been carried out, however, the control objective mostly is either ride quality or road holding improvement while the concerns regarding the handling and steering are not sufficiently addressed.

1.4 Objectives and Research Scope

The survey of literature reveals that there are many studies carried out on vehicle suspension control, however, there are still challenges that are not adequately addressed in this area, which are highlighted as follows.

First of all, despite numerous advanced control strategies designed for active suspension system applications, there are not many advanced control algorithms available for semi-active suspension systems.

Secondly, almost all the control strategies were developed based on a simple quarter car model in which the effect of the kinematics of the system on the dynamic behaviour is not considered.

Thirdly, the performances of the main kinematic suspension parameters, that play an important role in the overall handling, steering and stability of a vehicle, have not received sufficient attention in the design procedure.

Finally, despite massive analytical studies, experimental investigations and validations of control strategies are rare.

Motivations for the present study are based on the above factors. The different investigations in the current thesis are summarized as:

1) Model modification for specific suspension system, namely MacPherson suspension system.

2) Control design together with the improvement of kinematic suspension performance.

3) Experimental validation of analytical results (hardware-in-the-loop).

The current research will present a novel approach for the semi-active control of MacPherson suspension system. The originality of the research lies in building both dynamic and kinematic models of the MacPherson suspension system, considering the structural effects on the dynamic behaviour of the system, and also evaluating the performance of the kinematic parameters influencing handling performance and stability of vehicle subject to robust semi-active control policy.

The main purpose of the research is to design an advanced controller with minimum cost design and consideration of practical limitations in order to satisfy the conflicting suspension system specifications simultaneously. Generally speaking, this work

comprises three main phases; i.e. modeling and dynamical analysis of the system, design of a novel advanced control, and experimental validation of the analytical results.

In this research, an MR damper will be considered as actuator for the system because of its desired performance in vehicle applications. In addition, a proper model describing nonlinear performance of MR damper will be employed. Using that model, the required current for producing desired force will be generated. A real MR damper will be incorporated in the feedback loop and the performance of the MacPherson suspension subjected to a MR damper force will be investigated in a hardware-in-the-loop experiment.

1.5 Thesis Outline

Considering the structure of MacPherson suspension system, a new control-oriented dynamic model of system is developed in Chapter 2. The frequency and time performances of the new model are compared with those of the conventional model. A three-dimensional kinematic model of the suspension system is developed to evaluate the kinematic performance of the system subjected to the damping force variation and road disturbances. The model is validated by a three-dimensional model developed by ADAMS software. It is shown that the kinematic model represents the performance of the suspension kinematic parameters with a reasonable accuracy.

In Chapter 3, three well-known semi-active control strategies are described and their contributions on ride quality enhancement are compared. It is shown that the controllers improve the ride quality close to each other while affecting the kinematic performance adversely.

Full states feedback and output feedback controllers are designed according to the H_∞ robust control theory in Chapter 4. Although the full state feedback controller has a better performance compared to output feedback controller, its implementation is difficult because of the need for a lot of sensors. In order to make the controller design more practical than the full state feedback controller, the output feedback control theory is employed and a controller with simpler structure is designed. It is shown that the controller has a performance close to the full states feedback controller. For the optimizations of controller gains, the Genetic Algorithm (GA) and Linear Matrix Inequality (LMI) toolboxes are used. The effectiveness of the controller is evaluated through simulation results.

To generate current signal of the MR damper, the dynamic performance of a candidate MR damper is characterized through experiments. In Chapter 5, using the data acquired in laboratory, a piece-wise polynomial model is developed for the MR damper. A practical approach for current signal estimation is described and the performance of the controller is validated through hardware-in-the-loop simulations.

The results of the research and possible future works are presented in Chapter 6.

CHAPTER 2

DYNAMIC AND KINEMATIC MODEL OF A MACPHERSON STRUT SUSPENSION SYSTEM

The previous chapter provides a survey of the literature treating the different aspects of MacPherson suspension systems including the control aspects, and presents the objectives and the scope of the present dissertation. This chapter will propose a new dynamic model of the MacPherson strut suspension system for ride control applications. The model includes the vertical acceleration of the sprung mass and incorporates the suspension linkage kinematics. This two degree-of-freedom (DOF) model provides a more accurate representation of the MacPherson suspension system for ride control applications since it considers the linkages of the system in the dynamic modeling and incorporates the rotational motion of the wheel. The performance of the nonlinear and linearized models is investigated and compared with that of the simple two DOF model.

Furthermore, this chapter describes the concepts of kinematic suspension parameters and the related effects of their variations on the handling, steering, and stability of a vehicle during either forward motion or cornering. The main kinematic parameters, introduced in this chapter, consist of camber, caster, king-pin, and toe angles as well as track width and roll centre. In addition, a new three dimensional kinematic model of the MacPherson suspension system for the evaluation of those parameters is established. The model is

validated with a virtual prototype of MacPherson suspension system developed by ADAMS software.

2.1 Introduction

There are numerous studies carried out on both active and semi-active control of suspension systems. However, as pointed out in the literature survey, the studies on the effect of the suspension kinematics on the dynamic response of the system are rare. In addition, the evaluation of the suspension kinematic parameters subjected to the controlled damping force has not received enough attention in previous studies. It should be noted that the evaluation of the suspension kinematic parameters opens another view to study aspects of the ride quality, stability, and handling performance of the vehicle. For instance, the roll variation affects the ride quality while camber angle and track width are important in handling performance.

Stensson et al [18] investigated the nonlinear dynamic performance of the MacPherson structure using three nonlinear models. A finite element analysis was carried out to assess the deformation of the components of this mechanism by Jonsson [19]. Fallah [20], Suh [21] and Mantaras et al [22] analyzed the kinematic and dynamic performances of the MacPherson suspension by formulating its spatial model. Chen and Beale [23] employed a three-dimensional model (3D) of a MacPherson suspension system to estimate its dynamic parameters. Habibi et al [24] developed a three dimensional kinematic model of this system and optimized its design characteristics such as linkage lengths and positions using Genetic Algorithm to optimize the suspension kinematic performance. However, the aforementioned models are not suitable for ride control design because they can not be written in the state space form. Ro and Kim [25] incorporated model reduction

technique to identify the parameters of the simplified quarter-car model based on a three-dimensional model of the MacPherson suspension system developed in ADAMS software. Hong et al and Sohn et al [26, 27] offered a two-dimensional model of the MacPherson suspension for ride control applications. However, the spindle structure was ignored in this model.

In the following, a new dynamic control-oriented suspension model is introduced so as to consider the structural effects on the dynamic behaviour of the system. In addition, the performance of those kinematic suspension parameters describing wheel motions is investigated using a new three-dimensional kinematic model of the MacPherson suspension system.

2.2 Displacement Matrix Method and Constraint Equations

The displacement matrix method is employed in order to analyze the mechanism of the MacPherson suspension system. The general three-dimensional displacement matrix is given in terms of a translation from a point $p_1(x_1, y_1, z_1)$ to another point $p_2(x_2, y_2, z_2)$ and a rotation about a fixed coordinate [28].

$$[D]_{12} = \begin{bmatrix} a_{11} & a_{12} & a_{13} & x_2 - (a_{11}x_1 + a_{12}y_1 + a_{13}z_1) \\ a_{21} & a_{22} & a_{23} & y_2 - (a_{21}x_1 + a_{22}y_1 + a_{23}z_1) \\ a_{31} & a_{32} & a_{33} & z_2 - (a_{31}x_1 + a_{32}y_1 + a_{33}z_1) \\ 0 & 0 & 0 & 1 \end{bmatrix} \qquad (2.1)$$

where a_{ij} are components of the rotation matrix.

A rotation matrix can be described as a product of successive rotations about the principal coordinate axes x_0, y_0 and z_0 taken in a specific order. These rotations define the roll,

pitch, and yaw angles, which are denoted as (ϕ, ϑ, ψ). The resulting rotation matrix is given by

$$\begin{bmatrix} a_{11} & a_{12} & a_{13} \\ a_{21} & a_{22} & a_{23} \\ a_{31} & a_{32} & a_{33} \end{bmatrix} = \begin{bmatrix} \cos\phi\cos\vartheta & -\sin\phi\cos\psi + \cos\phi\sin\vartheta\sin\psi & \sin\phi\sin\psi + \cos\phi\sin\vartheta\cos\psi \\ \sin\phi\cos\vartheta & \cos\phi\cos\psi + \sin\phi\sin\vartheta\sin\psi & -\cos\phi\sin\psi + \sin\phi\sin\vartheta\cos\psi \\ -\sin\vartheta & \cos\vartheta\sin\psi & \cos\vartheta\cos\psi \end{bmatrix} \quad (2.2)$$

The second part of the displacement matrix method is the holonomic constraint equation formulations which apply mathematical restrictions to the mobility of the model in order to take away degrees of freedom of the multi-body system, and are specifically related to the joints between adjacent bodies. The constraint equations for the spherical-spherical (SS) link, the revolute-spherical (RS) link and spherical-cylindrical (SC) link are explained in the following.

2.2.1 Spherical-Spherical (SS) Link Constraint Equations:

The Spherical-Spherical (SS) link is defined by a spherical joint at a point $P_0(x_0, y_0, z_0)$ on a fixed body and a spherical joint at a point $P_1(x_1, y_1, z_1)$ on the moving body and the constraint equation which specifies the property of constant length between the two spherical joints. The displacement constraint is:

$$(x_{P_2} - x_{P_0})^2 + (y_{P_2} - y_{P_0})^2 + (z_{P_2} - z_{P_0})^2 = (x_{P_1} - x_{P_0})^2 + (y_{P_1} - y_{P_0})^2 + (z_{P_1} - z_{P_0})^2 \quad (2.3)$$

where $P_2(x_2, y_2, z_2)$ is transformed position of the point $P_1(x_1, y_1, z_1)$.

2.2.2 Revolute-Spherical (RS) Link Constraint Equations:

A Revolute-Spherical (RS) link is defined as a revolute joint at a point $P_0(x_0, y_0, z_0)$ with rotation axis $U_0(u_{x0}, u_{y0}, u_{z0})$ on a fixed body and a spherical joint at a point $P_1(x_1, y_1, z_1)$

18

on a moving body and the constraint equations which specify the properties of constant length between the revolute and spherical joints and the perpendicularity between the revolute axis and the axis defined by the link.

$$(x_{P_2} - x_{P_0})^2 + (y_{P_2} - y_{P_0})^2 + (z_{P_2} - z_{P_0})^2 = (x_{P_1} - x_{P_0})^2 + (y_{P_1} - y_{P_0})^2 + (z_{P_1} - z_{P_0})^2 \qquad (2.4)$$

$$u_{x_0}(x_{P_2} - x_{P_0}) + u_{y_0}(y_{P_2} - y_{P_0}) + u_{z_0}(z_{P_2} - z_{A_0}) = 0 \qquad (2.5)$$

where $P_2(x_2, y_2, z_2)$ is the transformed position of the point $P_1(x_1, y_1, z_1)$.

2.2.3 Spherical-Cylindrical (SC) Link Constraint Equations:

The Spherical-Cylindrical (SC) link is defined as a spherical joint at a point $P_0(x_0, y_0, z_0)$ on a fixed body and a cylindrical joint at a point $P_1(x_1, y_1, z_1)$ on a moving body with an axis of translation /rotation $U_1(u_x, u_y, u_z)$ along the link axis, and the constraint equations specify that the straight line defined by the link, or cylindrical joint axis remains a straight line during any displacement.

$$u_z(x_{P_2} - x_{P_0}) - u_x(z_{P_2} - z_{P_0}) = 0 \qquad (2.6)$$

$$u_z(y_{P_2} - y_{P_0}) - u_y(z_{P_2} - z_{P_0}) = 0 \qquad (2.7)$$

$$u_x^2 + u_y^2 + u_z^2 = 1 \qquad (2.8)$$

2.3 New Model of MacPherson Suspension for Semi-active/active Ride Control Applications

Using the displacement matrix method and the abovementioned constraint equation, a two-dimensional control oriented model of MacPherson suspension system will be developed in this section.

19

A MacPherson suspension, shown in Figure 2.1, consists of the control arm, the strut including spring and damper, the spindle, and the piston rod. The control arm is a rigid body and connected to the chassis with a rotational joint. A spherical joint connects the control arm and the spindle. Wheels are installed on the strut's spindle. A cylindrical joint connects the strut to the piston rod. The piston rod is connected to the chassis with a spherical joint. A spring and damper are installed between the strut and the chassis along the piston rod to absorb the vibration and shock caused by a bumpy road.
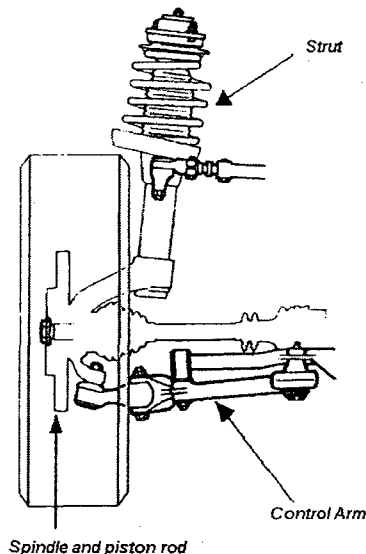
Figure 2.1 Schematic of the MacPherson strut suspension

2.3.1 Kinematics

A two-dimensional model of the MacPherson suspension system is illustrated in Figure 2.2. It is formed of a quarter-car body, a spindle and tire. a helical spring, a control arm and a load disturbance. If the joint between the strut and the car body at point D is assumed as a bushing, it is a three DOF system. However, if the mass of the strut is ignored and the bushing is assumed to be a pin joint. the number of DOF will reduce to

two, including the vertical displacement of the sprung mass and the rotational motion of the control arm [26]. In this model, the strut is shown by link CD while link AB depicts the control arm which is modelled as a rod. The revolute joint at point B in which the control arm and the chassis are connected together, is modelled as a rotational joint. This model is more general than the conventional model since it integrates the linkage kinematics and is more accurate than that was proposed in references [20-23] where the wheel camber motion was not considered.

The detailed assumptions made in this model are as follows:

1- The sprung mass has only vertical displacement while the motion of the vehicle body in other directions is assumed to be zero.

2- The unsprung mass (spindle and tire) is connected to the car body through both the strut and the control arm.

3- The values of z_s and θ are measured from the static equilibrium position and are considered as generalized coordinates.

4- The camber angle is assumed to be zero when the suspension system is at static equilibrium.

5- Compared to other links, the mass of the strut is negligible.

6- The coil spring, the tire, and the damper are assumed to be linear.
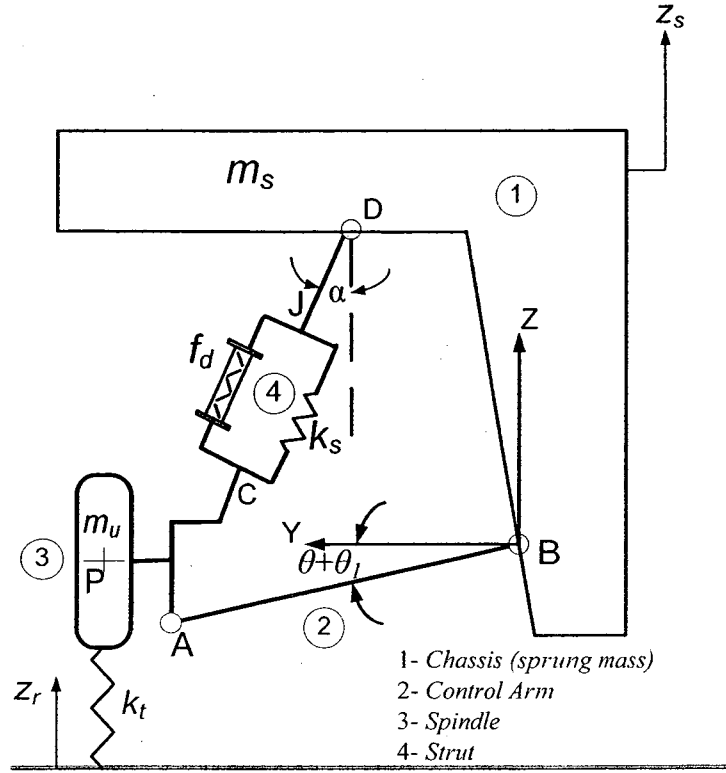
Figure 2.2 Model of the MacPherson strut suspension

It is assumed that, under static equilibrium conditions, points A, B, C, D, J, and P, respectively, are located at (y_{A1}, z_{A1}), (y_{B1}, z_{B1}), (y_{C1}, z_{C1}), (y_{D1}, z_{D1}), (y_{J1}, z_{J1}), and (y_{P1}, z_{P1}) with the origin of the coordinate system, O, at B. In addition, the vertical displacement of the sprung mass, z_s, to be upward and the rotation angle of the control arm, θ, to be in the counter clockwise direction.

By developing the displacement matrix [25], the main points on the spindle change as:

$$\begin{bmatrix} y_C & y_J & y_P \\ z_C & z_J & z_P \\ 1 & 1 & 1 \end{bmatrix} = \begin{bmatrix} a_{11} & a_{12} & y_A - (a_{11}y_{A_1} + a_{12}z_{A_1}) \\ a_{21} & a_{22} & z_A - (a_{21}y_{A_1} + a_{22}z_{A_1}) \\ 0 & 0 & 1 \end{bmatrix} \begin{bmatrix} y_{C_1} & y_{J_1} & y_{P_1} \\ z_{C_1} & z_{J_1} & z_{P_1} \\ 1 & 1 & 1 \end{bmatrix} \tag{2.9}$$

Further,

$$a_{11} = a_{22} = \cos\phi$$
$$a_{21} = -a_{12} = \sin\phi$$

(2.10)

where φ is the rotation angle of the wheel about x axis.

In Equation (2.9), the unknown parameters are (y_A, z_A), (y_J, z_J), (y_P, z_P), (y_C, z_C) and φ with 6 equations in terms of 9 unknowns. In order to solve this set of equations, it is necessary to employ the kinematic constraints of the mechanism. Since a link including cylindrical joint and spherical joint establishes the strut of the MacPherson suspension, the constraint of this link at the points C and J can be described as follows:

$$z_C = \alpha(y_C - y_D) + z_D$$
$$z_J = \alpha(y_J - y_D) + z_D$$

(2.11)

where α is the slope of the strut with respect to the vertical axis and is less than 15 degree in Macpherson strut suspension system

The control arm is a link between a revolute joint and a spherical joint. It rotates around a fixed axis and has a constant length. Thus the constraint equations of this link are:

$$y_A = L_A \cos(\theta + \theta_1) + y_B$$
$$z_A = L_A \sin(\theta + \theta_1) + z_B$$

(2.12)

where L_A is the length of the control arm and θ_1 is the initial angle of the control arm resulting from static deflection and structure design. Moreover, the positions of the key points on the chassis are changing under road disturbances as below:

$$y_B = 0, \quad z_B = z_s, \quad y_D = y_{D_1}, \quad z_D = z_{D_1} + z_s$$

(2.13)

23

With addition of Equations (2.11), (2.12), and (2.13) the number of unknowns, (y_A, z_A), (y_J, z_J), (y_P, z_P), (y_C, z_C), α and φ, increases to 10 which is equal to the number of equations. Thus, the following system of equations can be established:

$$
\begin{aligned}
y_C &= (y_{C_1} - y_{A_1})a_{11} + (z_{A_1} - z_{C_1})a_{21} + y_A \\
z_C &= (y_{C_1} - y_{A_1})a_{21} + (z_{C_1} - z_{A_1})a_{11} + z_A \\
y_J &= (y_{J_1} - y_{A_1})a_{11} + (z_{A_1} - z_{J_1})a_{21} + y_A \\
z_J &= (y_{J_1} - y_{A_1})a_{21} + (z_{J_1} - z_{A_1})a_{11} + z_A \\
y_P &= (y_{P_1} - y_{A_1})a_{11} + (z_{A_1} - z_{P_1})a_{21} + y_A \\
z_P &= (y_{P_1} - y_{A_1})a_{21} + (z_{P_1} - z_{A_1})a_{11} + z_A \\
z_C &= \alpha(y_C - y_{D_1}) + (z_{D_1} + z_s) \\
z_J &= \alpha(y_J - y_{D_1}) + (z_{D_1} + z_s) \\
y_A &= L_A \cos(\theta + \theta_1) \\
z_A &= L_A \sin(\theta + \theta_1) + z_s
\end{aligned}
\qquad (2.14)
$$

Upon solving the above system of equations, φ would be determined as a function of the generalized coordinates θ and z_s. The value of φ as a function of θ and z_s is:

$$
\varphi = -\frac{[s_1 + s_2 \cos(\theta + \theta_1) + s_3 \sin(\theta + \theta_1)]}{2} + \frac{\sqrt{[(s_1 + s_2 \cos(\theta + \theta_1) + s_3 \sin(\theta + \theta_1)]^2 - 4[s_4 + s_2 \sin(\theta + \theta_1) + s_4 \cos(\theta + \theta_1)]}}{2}
\qquad (2.15)
$$

where

$$
s_1 = \frac{(y_{C_1} - y_{J_1})y_{D_1} + (z_{J_1} - z_{C_1})z_{D_1}}{(y_{C_1} - y_{A_1})(z_{J_1} - z_{A_1}) + (z_{A_1} - z_{C_1})(y_{J_1} - y_{A_1})}
$$

$$
s_2 = \frac{(y_{J_1} - y_{C_1})L_A}{(y_{C_1} - y_{A_1})(z_{J_1} - z_{A_1}) + (z_{A_1} - z_{C_1})(y_{J_1} - y_{A_1})}
$$

$$
s_3 = \frac{(z_{C_1} - z_{J_1})L_A}{(y_{C_1} - y_{A_1})(z_{J_1} - z_{A_1}) + (z_{A_1} - z_{C_1})(y_{J_1} - y_{A_1})}
$$

$$s_4 = 1 + \frac{(z_{C_1} - z_{J_1})y_{D_1} + (y_{C_1} - y_{J_1})z_{D_1}}{(y_{C_1} - y_{A_1})(z_{J_1} - z_{A_1}) + (z_{A_1} - z_{C_1})(y_{J_1} - y_{A_1})}$$

and subsequently the other unknown parameters including (y_A, z_A), (y_J, z_J), (y_P, z_P), (y_C, z_C) and α can be specified. So far, the displacements of all key points have been determined as functions of the independent variables θ and z_s.

The next step is to find the velocities of the key points. The system of velocity components of the main points are obtained from the derivation of the system of Equations (2.14) as below:

$$
\begin{aligned}
\dot{y}_C &= \dot{\varphi}(z_A - z_C) + \dot{y}_A \\
\dot{z}_C &= \dot{\varphi}(y_C - y_A) + \dot{z}_A \\
\dot{y}_J &= \dot{\varphi}(z_A - z_J) + \dot{y}_A \\
\dot{z}_J &= \dot{\varphi}(y_J - y_A) + \dot{z}_A \\
\dot{y}_P &= \dot{\varphi}(z_A - z_P) + \dot{y}_A \\
\dot{z}_P &= \dot{\varphi}(y_P - y_A) + \dot{z}_A \\
\dot{z}_C &= \alpha \dot{y}_C + \dot{\alpha}(y_C - y_D) + \dot{z}_s \\
\dot{z}_J &= \alpha \dot{y}_J + \dot{\alpha}(y_J - y_D) + \dot{z}_s \\
\dot{y}_A &= -L_A \sin(\theta + \theta_1)\dot{\theta} \\
\dot{z}_A &= L_A \cos(\theta + \theta_1)\dot{\theta} + \dot{z}_s
\end{aligned}
\tag{2.16}
$$

In solving the above system of equations, the value of $\dot{\varphi}$ is determined as follows

$$\dot{\varphi} = \frac{(\dot{z}_A - \alpha \dot{y}_A - \dot{z}_s)(y_C - y_J)}{h} \tag{2.17}$$

where

$$h = (y_C - y_A + \alpha z_C - \alpha z_A)(y_J - y_D) - (y_J - y_A + \alpha z_J - \alpha z_A)(y_C - y_D) \tag{2.18}$$

2.3.2 Equations of motion

The equations of motion of the new model can be derived using Lagrange's method. The kinetic energy, T, is given by

$$T = \frac{1}{2}(m_s + m_{ca})(\dot{z}_s)^2 + \frac{1}{2}m_u(\dot{y}_P^2 + \dot{z}_P^2) + \frac{1}{2}I_u\dot{\varphi}^2 + \frac{1}{2}I_{ca}^B\dot{\theta}^2 \qquad (2.19)$$

where m_s, m_u, and m_{ca} are masses of the body, wheel and control arm, respectively. I_u and I_{ca}^B are the inertia moments of the wheel and control arm where the latter is taken about point B. The potential energy, V, is

$$V = \frac{1}{2}K_s(\Delta L)^2 + \frac{1}{2}K_t(\Delta z)^2 \qquad (2.20)$$

where K_s and K_t are the stiffness coefficients of the sprung and unsprung masses, respectively. Moreover, the deflection of the spring, ΔL, and the deflection of the tire, Δz, are:

$$\Delta L = [(y_C - y_D)^2 + (z_C - z_D)^2]^{(1/2)} - [(y_{C_1} - y_{D_1})^2 + (z_{C_1} - z_{D_1})^2]^{(1/2)} \qquad (2.21)$$

$$\Delta z = z_P - z_r = (y_{A_1} - y_{P_1})\varphi + (z_{P_1} - z_{A_1}) + L_A \sin(\theta + \theta_1) + z_s - z_r \qquad (2.22)$$

The damping function, D, is given by

$$D = \frac{1}{2}C_p(\Delta \dot{L})^2 \qquad (2.23)$$

where C_p is the damping coefficient and the relative velocity of damper $\Delta \dot{L}$ is:

$$\Delta \dot{L} = [\dot{y}_C(y_C - y_D) + (\dot{z}_C - \dot{z}_D)(z_C - z_D)][(y_C - y_D)^2 + (z_C - z_D)^2]^{-(1/2)} \qquad (2.24)$$

26

Using Lagrange's equations along the generalized coordinates z_s and θ and by substituting the values of $\dot{y}_p$ and $\dot{z}_p$, taken from (2.16) and $\dot{\varphi}$ from (2.17), respectively, into (2.19) one can obtain the equations of motion:

$$\overbrace{(m_s + m_u + m_{ca})}^{f_1}\ddot{z}_s + m_u L_A \overbrace{\left[\cos(\theta+\theta_1)+\left[\cos(\theta+\theta_1)+\alpha\sin(\theta+\theta_1)\right]\frac{(y_C - y_J)(y_P - y_A)}{h}\right]}^{f_2}\ddot{\theta} =$$

$$\overbrace{\frac{\partial \vec{r}_C}{\partial z_s}\cdot f_a + f_d + H_3 - H_1 - H_2}^{F_1}$$

(2.25)

and

$$\left[m_u L_A\left[\{(\cos(\theta+\theta_1)+\alpha\sin(\theta+\theta_1)\}\frac{(y_C - y_J)(z_A - z_P)}{h} - \sin(\theta+\theta_1)\right]\left[-L_A\sin(\theta+\theta_1)+(z_A - z_P)\frac{\partial\dot{\varphi}}{\partial\theta}\right]+\right.$$

$$m_u L_A\left[L_A\cos(\theta+\theta_1)+(y_P - z_A)\frac{\partial\dot{\varphi}}{\partial\theta}\right]\left[\{(\cos(\theta+\theta_1)+\alpha\sin(\theta+\theta_1)\}\frac{(y_C - y_J)(y_P - y_A)}{h}+\cos(\theta+\theta_1)\right]+$$

$$\left.I_u L_A(\cos(\theta+\theta_1)+\alpha\sin(\theta+\theta_1)\frac{\partial\dot{\varphi}}{\partial\theta}+I_{ca}\right]\ddot{\theta}+m_u\overbrace{\left[L_A\cos(\theta+\theta_1)+(y_P - z_A)\frac{\partial\dot{\varphi}}{\partial\theta}\right]}^{f_3}\ddot{z}_s$$

$$=\overbrace{-\frac{\partial\vec{r}_C}{\partial\theta}\cdot f_a + H_6 - H_4 - H_5}^{F_2}$$

(2.26)

where

$$H_1 = -\frac{\partial T}{\partial \dot{z}_s}, \qquad H_2 = \frac{\partial V}{\partial z_s}, \qquad H_3 = -\frac{\partial D}{\partial \dot{z}_s} \tag{2.27}$$

$$H_4 = -\frac{\partial T}{\partial \dot{\theta}}, \qquad H_5 = \frac{\partial V}{\partial \theta}, \qquad H_6 = -\frac{\partial D}{\partial \dot{\theta}} \tag{2.28}$$

27

Since the equations are highly nonlinear, the higher order nonlinearities are ignored in

Equations (2.25) and (2.26). Therefore, the equations of motion are obtained as:

$$f_1(z_s, \dot{z}_s, \theta, \dot{\theta})\ddot{z}_s + f_2(z_s, \dot{z}_s, \theta, \dot{\theta})\ddot{\theta} = F_1(z_s, \dot{z}_s, \theta, \dot{\theta})$$
$$f_3(z_s, \dot{z}_s, \theta, \dot{\theta})\ddot{z}_s + f_4(z_s, \dot{z}_s, \theta, \dot{\theta})\ddot{\theta} = F_2(z_s, \dot{z}_s, \theta, \dot{\theta})$$

(2.29)

Solving the above system of equations, the accelerations along the generalized

coordinates are obtained as follows:

$$\ddot{z}_s = \frac{f_4 F_1 - f_2 F_2}{f_4 f_1 - f_2 f_3} = g_1(z_s, \dot{z}_s, \theta, \dot{\theta})$$
$$\ddot{\theta} = \frac{f_1 F_2 - f_3 F_1}{f_4 f_1 - f_2 f_3} = g_2(z_s, \dot{z}_s, \theta, \dot{\theta})$$

(2.30)

At this point, introducing the state variables as $[x_1, x_2, x_3, x_4]^T = [z_s, \dot{z}_s, \theta, \dot{\theta}]^T$ yields the

state space representation of Equation (2.30).

$$\dot{x}_1 = x_2$$
$$\dot{x}_2 = g_1(z_s, \dot{z}_s, \theta, \dot{\theta}, f_a, f_d, z_r)$$
$$\dot{x}_3 = x_4$$
$$\dot{x}_4 = g_2(z_s, \dot{z}_s, \theta, \dot{\theta}, f_a, f_d, z_r)$$

(2.31)

2.3.3   Linearization of the Equations

The highly nonlinear equations of motion are linearized at the equilibrium state $(x_{1e}, x_{2e}, x_{3e}, x_{4e}) = (0, 0, 0, 0)$. The resulting linearized equations are:

$$\dot{x} = Ax(t) + B_1 f_a(t) + B_2 z_r(t) + B_3 f_d(t)$$
$$x(0) = x_e$$

(2.32)

where

28

$$A = \begin{bmatrix} 0 & 1 & 0 & 0 \\ \dfrac{\partial g_1}{\partial x_1} & 0 & \dfrac{\partial g_1}{\partial x_3} & \dfrac{\partial g_1}{\partial x_4} \\ 0 & 0 & 0 & 1 \\ \dfrac{\partial g_2}{\partial x_1} & 0 & \dfrac{\partial g_2}{\partial x_3} & \dfrac{\partial g_2}{\partial x_4} \end{bmatrix}_{x_e}$$

$$B_1 = \begin{bmatrix} 0 \\ \dfrac{\partial g_1}{\partial f_a} \\ 0 \\ \dfrac{\partial g_2}{\partial f_a} \end{bmatrix}^{T}_{f_a=0} \qquad B_2 = \begin{bmatrix} 0 \\ \dfrac{\partial g_1}{\partial z_r} \\ 0 \\ \dfrac{\partial g_2}{\partial z_r} \end{bmatrix}^{T}_{z_r=0} \qquad B_3 = \begin{bmatrix} 0 \\ \dfrac{\partial g_1}{\partial f_d} \\ 0 \\ \dfrac{\partial g_2}{\partial f_d} \end{bmatrix}^{T}_{f_d=0}$$

2.4 Modified Model for Semi-active Ride Control Applications

The implementation of active control components on MacPherson suspension is difficult due to the limited space available in this type of the suspension system. In the semi-active case, there is no actuator to supply an active force, and the passive damper is replaced by a damper with a controllable variable damping coefficient. Magnetorheological (MR) dampers are commonly recommended for the semi-active control applications due to their small size, low energy requirements and desired performance which is in between that of passive and fully active devices [29-31]. Thus, the idea of incorporating semi-active controller is more attractive. For the semi-active control applications, the process of modeling is the same as that for active control applications except that the damping function is equal to zero in Equation (2.23) and f_{sa}, representing the semi-active control force is used in place of f_a in Equations (2.25) and (2.26) [5, 26]. Therefore, the state space equations are modified as:

$$\dot{x} = Ax(t) + B_1 f_{sa}(t) + B_2 z_r(t) + B_3 f_d(t) \tag{2.33}$$

where

$$A = \begin{bmatrix} 0 & 1 & 0 & 0 \\ \dfrac{\partial g_1}{\partial x_1} & 0 & \dfrac{\partial g_1}{\partial x_3} & 0 \\ 0 & 0 & 0 & 1 \\ \dfrac{\partial g_2}{\partial x_1} & 0 & \dfrac{\partial g_2}{\partial x_3} & 0 \end{bmatrix}_{x_e}$$

$$B_1 = \begin{bmatrix} 0 \\ \dfrac{\partial g_1}{\partial f_{sa}} \\ 0 \\ \dfrac{\partial g_2}{\partial f_{sa}} \end{bmatrix}^T_{f_{sa}=0}, \quad B_2 = \begin{bmatrix} 0 \\ \dfrac{\partial g_1}{\partial z_r} \\ 0 \\ \dfrac{\partial g_2}{\partial z_r} \end{bmatrix}^T_{z_r=0}, \quad B_3 = \begin{bmatrix} 0 \\ \dfrac{\partial g_1}{\partial f_d} \\ 0 \\ \dfrac{\partial g_2}{\partial f_d} \end{bmatrix}^T_{f_d=0}$$

2.5 Comparison of Three Models (nonlinear, linear and conventional)

2.5.1 Comparison of the conventional and linear models

Representing the two dominant modes of a quarter-car model, the conventional model is composed of two lumped masses connected via a spring and a damper, with one of them connected to the ground through the tire stiffness. This model, shown in Figure 1.2, considers the vertical motions of the sprung (vehicle body) and the unsprung (wheel) masses. It should be noted that all the coefficients are assumed to be linear. The equations of motion are given as:

$$\sum f_{m_s} = -k_s(z_s - z_u) - c_p(\dot{z}_s - \dot{z}_u) + f_a - f_d = m_s \ddot{z}_s$$

$$\sum f_{m_u} = k_s(z_s - z_u) + c_p(\dot{z}_s - \dot{z}_u) + k_t(z_u - z_r) - f_a = m_u \ddot{z}_u \tag{2.34}$$

where f_a and f_d represent actuator and disturbance forces, respectively.

The state vector is defined in state space as $[76] x = [z_s, \dot{z}_s, z_u, \dot{z}_u]$. The state equations are expressed in matrix form as:

$$\dot{x} = Ax + B_1 f_a + B_2 z_r + B_3 f_d \qquad (2.35)$$

where

$$A = \begin{bmatrix} 0 & 1 & 0 & 0 \\ -\dfrac{k_s}{m_s} & -\dfrac{c_p}{m_s} & \dfrac{k_s}{m_s} & \dfrac{c_p}{m_s} \\ 0 & 0 & 0 & 1 \\ \dfrac{k_s}{m_u} & \dfrac{c_p}{m_u} & \dfrac{k_t - k_s}{m_u} & -\dfrac{c_p}{m_u} \end{bmatrix}$$

$$B_1 = \begin{bmatrix} 0 \\ \dfrac{1}{m_s} \\ 0 \\ -\dfrac{1}{m_u} \end{bmatrix}^T , \quad B_2 = \begin{bmatrix} 0 \\ 0 \\ 0 \\ -\dfrac{k_t}{m_u} \end{bmatrix}^T , \quad B_3 = \begin{bmatrix} 0 \\ -\dfrac{1}{m_s} \\ 0 \\ 0 \end{bmatrix}^T$$

With the displacement of the sprung mass, z_s, as the output and the road disturbance, z_r, as the input to the system, the following transfer function will be obtained from Equation (2.35).

$$H(s) = \frac{z_s(s)}{z_r(s)} = \frac{k_t(c_p s + k_s)}{\Delta(s)} \qquad (2.36)$$

where

$$\Delta(s) = m_s m_u s^4 + (m_s + m_u) c_p s^3 + \{(m_s + m_u) k_s + m_s k_t\} s^2 + k_t c_p s + k_s k_t$$

In the conventional model, the output variables are the displacement of the sprung mass, z_s, and unsprung mass, z_u, whereas in Equation (2.32) the outputs are the displacement of the sprung mass, z_s, and angular displacement of the control arm, θ. Therefore, the output variable compared between two models is in terms of the displacement of the sprung mass, z_s.

In order to show the advantage of the new model, the acceleration response of the new model is compared with that of the conventional and nonlinear models in Figure 2.3 with values taken from [26] and ADAMS software:

$$m_s = 453 \ Kg, \ m_u = 71 \ Kg, \ K_s = 17658 \ N/m, \ K_t = 183887 \ N/m$$
$$I_u = 0.021 \ Kg.m^2, \ C_p = 1950 \ N.sec/m$$

As can be seen, the linearized system shows a good response in the most parts of the range of frequencies while the conventional model presents some discrepancies in frequency domain response.

In addition, the displacement transmissibility of the new linearized and conventional models are shown in Figure 2.4 and Figure 2.5 for two different cases.

The positions of the key points on the MacPherson suspension are considered as below for three cases (the origin of the coordinate system at the equilibrium position assumed to be at point B_1, denoted as O, and all dimensions are in mm):

Case 1:

$A_1 = (206.5, 249, -60.8), \ C_1 = (222, 152.6, 236.2), \ J_1 = (229.2, 134.5, 374.8),$
$P_1 = (211.1, 292.1, 27.5), \ D_1 = (240, 107.4, 582.5)$

Case 2: The position of point D_1 is changed to (240, 94.3, 682.5). In this case, the length

of strut given by $L_S = \sqrt{(y_{C_1} - y_{D_1})^2 + (z_{C_1} - z_{D_1})^2}$ is larger than that in case 1.

Case 3: In this case all points are the same as those in case 1 except that C_1 corresponds

to point P_1.

As presented in Table 2-1, the first resonance frequency is lower than that of the

conventional model in Cases 1 and 2 and equal to it in Case 3. Hence, the new model

behaves in almost the same way as the conventional model when point C_1 is close to

point P_1. Since in the MacPherson suspension the strut is inclined with respect to the

vertical axis, there is a little discrepancy between pole locations of the conventional

model and those of Case 3. However, the second resonance frequency is higher in Case 1

and lower in Case 2.

Table 2-1 Comparison of new linear model and conventional model

	Conventional Model	Case 1 L_A= 256 (mm) L_S= 349 (mm)	Case 2 L_A= 256 (mm) L_S=450 (mm)	Case 3 point C=P
Poles	$-1.8475 \pm 5.7855i$ $-14.0372 \pm 50.3982i$	$-1.5430 \pm 5.2770i$ $-10.9611 \pm 50.0895i$	$-1.5805 \pm 5.3414i$ $-11.2035 \pm 49.9305i$	$-1.8213 \pm 5.7434i$ $-13.8058 \pm 50.4499i$
Resonances (Damping Ratio)	0.99 Hz (0.30) 7.70 Hz (0.27)	0.89 Hz (0.28) 7.81 Hz (0.21)	0.91 Hz (0.29) 7.68 Hz (0.22)	0.99 Hz (0.30) 7.70 Hz (0.27)
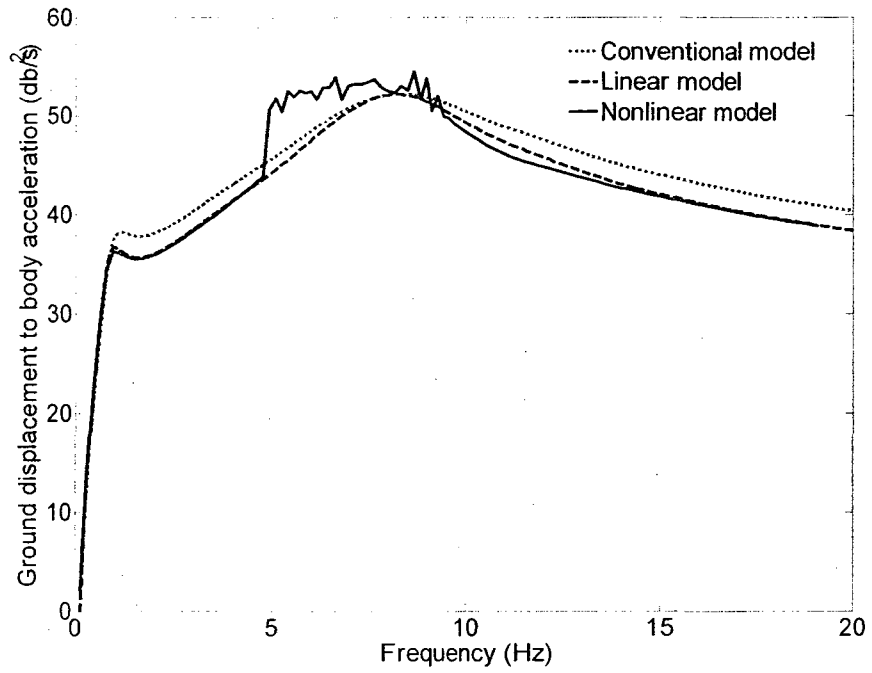
Figure 2.3 Frequency responses of the three models
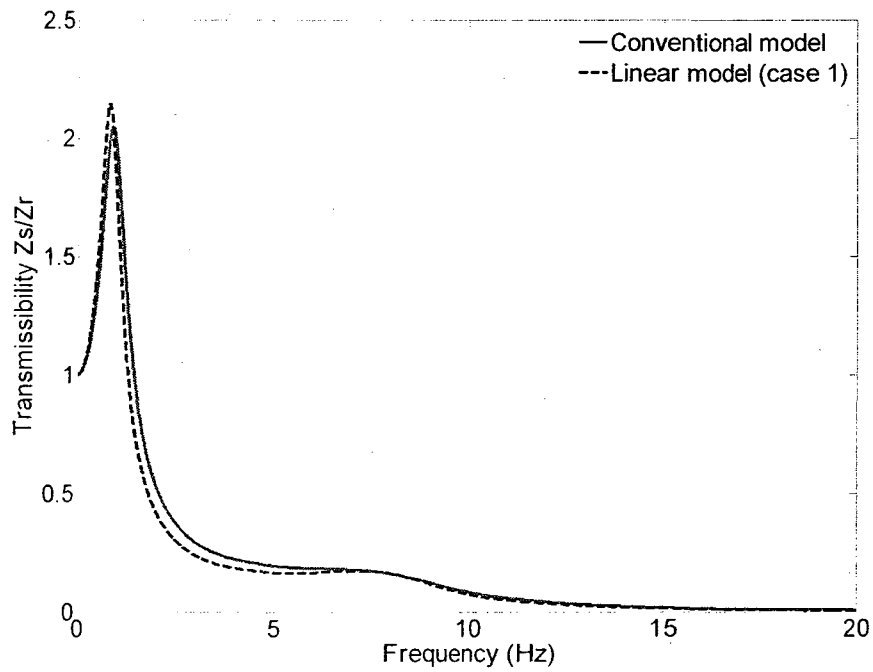
Figure 2.4 Frequency responses of the new model (Case 1) and the conventional model
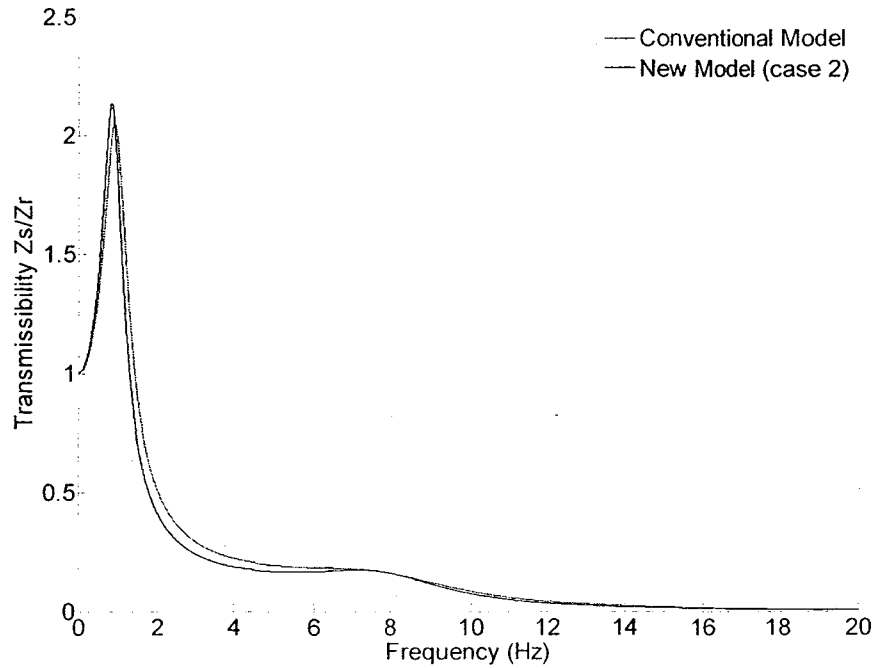
Figure 2.5 Frequency responses of the new model (Case 2) and the conventional model

The results show that the change of the strut length influences the first resonance frequency slightly. The results are summarized below:

1- The new model and the conventional model are identical when $C_1=P_1$ as well as the angle between the strut and the vertical axes is zero ($\alpha=0$).

2- The resonance frequencies are weakly dependent on the length of the strut in the new model.

3- For the first resonance frequency, the damping ratio and resonance frequency are smaller than those of the conventional model in Cases 1 and 2.

4- For the second resonance frequency, the damping ratio is smaller than that of the conventional model in both cases, while the resonance frequency is larger than that of conventional model in Case 1 and smaller in Case 2.

2.5.2 Comparison of the linear and the nonlinear models

The vertical acceleration of the sprung mass and the angular displacement of the control arm for the linear and nonlinear models for a step input are illustrated in Figure 2.6 and Figure 2.7, respectively. For simulation purposes, the step input, z_r, is chosen as 100 (*mm*) and the sampling time is 0.0001 (*s*). In Figure 2.6, the maximum acceleration response is 15 (m/s^2) which is approximately close to the step input magnitude times the transmissibility ratio at resonance in Figure 2.4 multiplied by the square of the natural frequency in radian per second. It is also shown that the difference in the responses between the two models is small and the linear model could be used to analyze the dynamic behaviour of the structure and to form a base line model for the controller design. In order to solve the nonlinear equations, the fourth order Runge-Kutta method is used. Finally, Figure 2.7, represents the angular displacement of the control arm of the linear model with reasonable estimation.
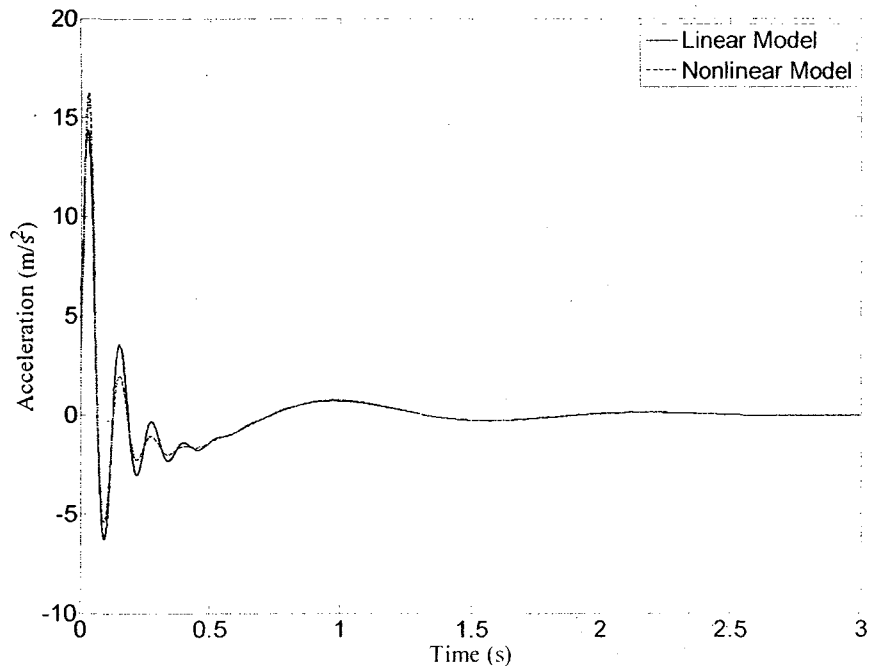
Figure 2.6 Vertical acceleration of the sprung mass for a step input (z_r=100 mm)
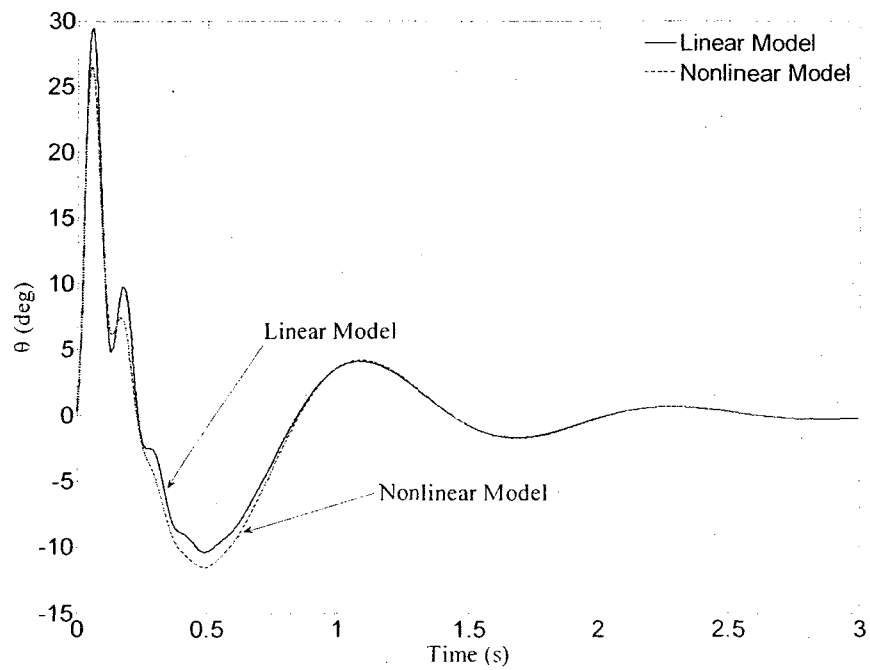
Figure 2.7 Angular displacement of the control arm for a step input (z_r=100 mm)

37

2.6 Suspension Kinematic Parameters

Kinematics and geometry of a suspension system are important from the point of view of the overall performance of a vehicle especially in the handling and stability analysis. The forces generated by the tire are greatly dependent on the position and motion of the tire and the motion of the suspension linkage. Based on this fact, different parameters which describe the position of the wheel as well as determine the location of the forces acting on the tire are defined. Some of these parameters are camber, caster, kingpin and toe angles as well as track width and roll centre. It is worth mentioning that the proper kinematic parameter performance ensures: greater driving safety, easier steering, longer tire life, greater fuel economy and, less strain in suspension components [3]. In the following, the definition of the kinematic parameters of the MacPherson suspension and corresponding mathematical representations are described.

2.6.1 Camber angle

In accordance with the standard DIN 70 000, the angle between the wheel centre plane and a vertical line to the road plane is defined as camber angle [32]. It is positive if the wheel inclination is outward of the vehicle body while it is negative if it is inward (see Figure 2.8). Camber angle alteration results in the reduction of tire life because it increases the abrasion between the tire and ground as well as increases the temperature of the tire in forward motion. During cornering, camber angle variation generates lateral forces acting on the tire which result in deterioration of stability. The camber angle alteration in MacPherson suspension behaves unfavourably when the switching occurs between compression and expansion of the wheel during cornering. Thus, it is necessary

38

to reduce the camber change during either forward motion or cornering to improve tire life, steering and handling.

POSITIVE CAMBER   NEGATIVE CAMBER
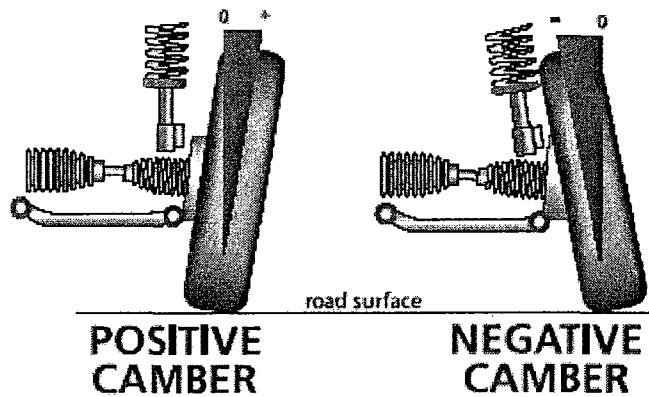
Figure 2.8 Camber angle representation

2.6.2 King-pin and Caster angles

In accordance with standard DIN 70 000, the king-pin angle is the angle between the projection of the steering axis on the yz plane and the vertical line to the road, while caster angle is the angle between the projection of the steering axis on the xz plane and the vertical line to the road, passing through the wheel centre (see Figure 2.9 and Figure 2.10). In MacPherson suspension, the steering axis is the line crossing between the MacPherson strut mount (point D in Figure 2.10) and the ball pivot of the guiding joint (Point A in Figure 2.10) in the 3D case [3, 32].

The variations of caster and kingpin angles are critical because they play an important role in the generation of the self-aligning torques which in turn deteriorates the steering and stability of the vehicle during cornering. In forward motion, variations of these

angles affect the steering and handling of the vehicle. Less changes in caster and kingpin

angles in forward motion causes better steering and stability as well.
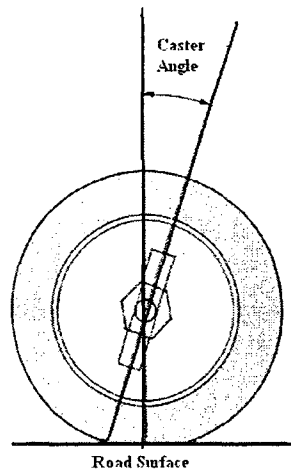
Figure 2.9 Caster angle representation
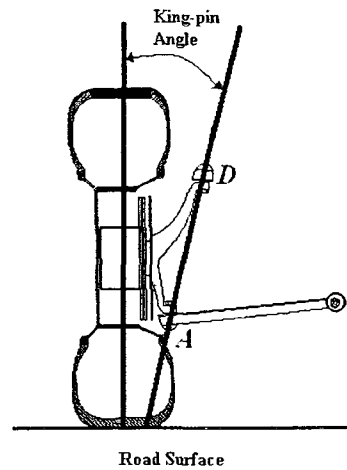
Figure 2.10 King-pin angle representation

2.6.3 Toe Angle

According to standard DIN 70 000, toe angle is the angle between wheel and vehicle

centre planes both in longitudinal direction (see Figure 2.11). It is positive when the

wheel is turned towards the vehicle longitudinal centre plane and negative if it is turned

away. Lower toe angle alterations result in reduction of tire wear and rolling resistance as

well as in having a better directional stability. Hence, to avoid increased tire wear and

rolling resistance or impending directional stability, no toe angle change should occur

when the wheels compress or rebound.
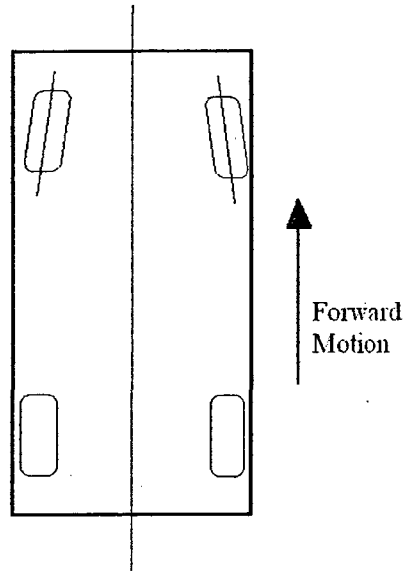
Figure 2.11 Toe angle representation

2.6.4 Track width

Track width is the lateral distance between the centres of the front wheels. In the MacPherson suspension, track width changes cause the deterioration in the directional stability of the vehicle and reduction of the rolling resistance. In addition, there exist a direct relation between the track variations and the height of the roll centre of a vehicle. Track changes of the MacPherson suspension cause the body roll centre to drop below the ground which is undesirable. In addition, the track change reduces the tire life by increasing lateral abrasion between tire and road.
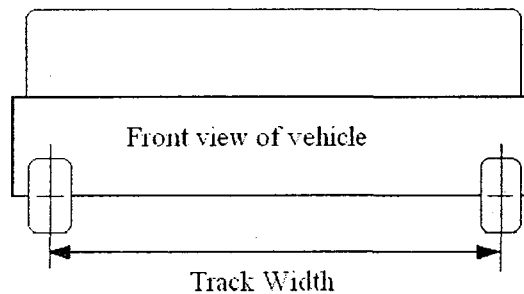
Figure 2.12 Track width representation

2.6.5 Roll Centre

In accordance with the standard DIN 70 000, the body roll centre is a virtual point in the centre of the vehicle (from the front view) located between the road surface and axle which is defined for the front and rear axles separately. In fact, the vehicle body starts to roll when a lateral force acts, the front and rear axles roll around the front and rear roll centres, respectively. The type of the suspension, length and location of the linkage determines the height of the roll centre from the ground. It is usually designed near to ground for the front axle and slightly high for the rear axle in the case of independent suspensions. Smaller variation of the body roll centre results in having a better handling performance and stability as well as a superior ride quality.
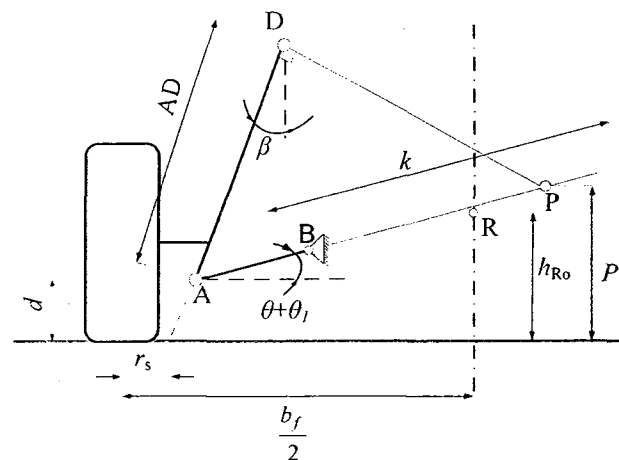
Figure 2.13 Roll center calculation for the MacPherson suspension system

A kinematic representation of the roll centre, R, and its height, h_{Ro}, is shown in Figure 2.13. Roughly speaking, the height of the roll centre is related to the generalized coordinates of the dynamic system for small vehicle roll angles as follows [3]:

$$h_{Ro} = \frac{b_f}{2} \frac{p}{k\cos(\theta + \theta_1) + d\tan(\beta) + r_s}$$ (2.37)

where,

42

$$p = k\sin(\theta + \theta_1) + (d + \Delta d), \quad \Delta d = \Delta z_A \tag{2.38}$$

$$k = \frac{AD}{\sin(\theta + \theta_1 + \beta)} \tag{2.39}$$

$$AD = \sqrt{(y_A - y_D)^2 + (z_A - z_D)^2}, \quad \tan(\beta) = \frac{|y_A - y_D|}{|z_A - z_D|} \tag{2.40}$$

Using Eq. (2.37), it is possible to evaluate the roll centre variation during forward vehicle motion. It should be noted that, in the above formulation, the variations of the track width (b_f) and scrub radius (r) are ignored compared to their initial values. The positions of the key points used in the above equations can be obtained by the kinematic relations explained in the next section.

2.7 Kinematic Model

It is feasible to investigate the camber angle and track width alterations using dynamic model explained in the section 2.3 [33], however, that model does not show their accurate variations. Further, an investigation of the toe angle alteration is not possible using that model. In order to evaluate the effect of the controlled damping force variation on wheel motions accurately, a three dimensional kinematic model of MacPherson suspension system is developed using displacement matrix method.

A three-dimensional kinematic model of MacPherson suspension system is shown in Figure 2.14. Generally, a MacPherson suspension connects the chassis to the wheel through three links, namely the control arm, the tie rod, and the strut. While the tie rod and the control arm are rigid links, the length of the strut including a damper and a spring varies because of the relative motions between two ends. The tie rod connects the

steering gear to the front wheel and the function of the control arm is to control the wheel motion. It should be noted that effects of the tie rod in the dynamic model were ignored.
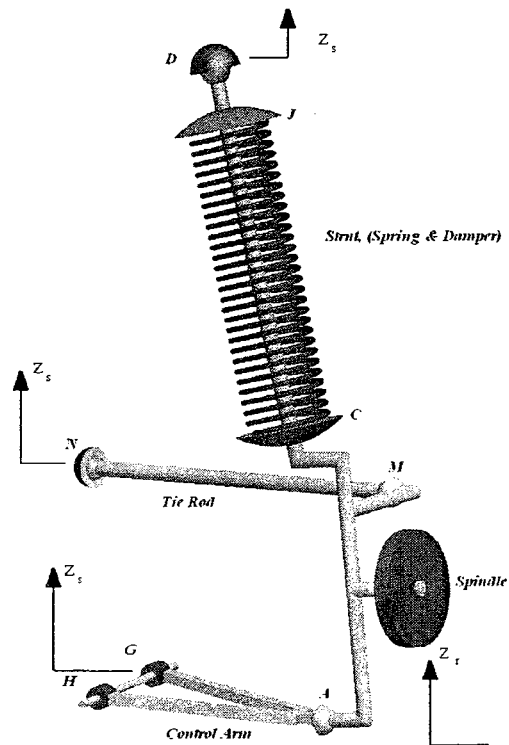
Figure 2.14 Kinematic model of MacPherson suspension system

The assumptions in developing the kinematic model are; 1) all bodies are rigid; 2) the control arm is modelled by a rod 3) the chassis has only the vertical displacement and the motion of the body in other directions is zero. A kinematic model of the system is illustrated in Figure 2.14. The model includes two DOF, including the vertical displacement of the sprung mass, z_s, and the rotational motion of the control arm, θ, where the road disturbance, z_r, is considered as the input of the system. In this model, control arm is connected to the chassis through a revolute joint and to the wheel through a spherical joint. The tie rod is connected to both the chassis and the wheel via spherical

44

joints. In addition, the strut is considered as a prismatic joint connected to the chassis through a spherical joint. It should be noted that the wheel (spindle) is considered as a rigid body which has three rotational motions around fixed RPY coordinates and three displacements along the coordinate axes. The displacement matrix is formed for the spindle as the following

$$[D]_{Spindle} = \begin{bmatrix} a_{11} & a_{12} & a_{13} & x_A - (a_{11}x_{A_1} + a_{12}y_{A_1} + a_{13}z_{A_1}) \\ a_{21} & a_{22} & a_{23} & y_A - (a_{21}x_{A_1} + a_{22}y_{A_1} + a_{23}z_{A_1}) \\ a_{31} & a_{32} & a_{33} & z_A - (a_{31}x_{A_1} + a_{32}y_{A_1} + a_{33}z_{A_1}) \\ 0 & 0 & 0 & 1 \end{bmatrix} \quad (2.41)$$

where a_{ij} is component of an RPY rotation matrix as explained in Eq. (2.2). The position of the key points on the spindle therefore can be found using displacement matrix as below

$$\begin{bmatrix} x_M & x_C & x_J \\ y_M & y_C & y_J \\ z_M & z_C & z_J \\ 1 & 1 & 1 \end{bmatrix} = [D]_{Spindle} \begin{bmatrix} x_{M_1} & x_{C_1} & x_{J_1} \\ y_{M_1} & y_{C_1} & y_{J_1} \\ z_{M_1} & z_{C_1} & z_{J_1} \\ 1 & 1 & 1 \end{bmatrix} \quad (2.42)$$

It should be noted that in abovementioned equations subscripts ($_1$) denotes initial position of each component.

In Equation (2.41), there are 15 unknown parameters which are (x_A, y_A, z_A), (x_J, y_J, z_J), (x_C, y_C, z_C), (x_M, y_M, z_M) and (ϕ, ϑ, ψ) while there are just 9 equations. To solve the kinematic equations, the holonomic constraint equations are required to be added to the system of Equation (2.42). Since a link including the cylindrical and spherical joints

45

establish the strut of the MacPherson suspension, the constraint of this link at points C and J can be described as follows:

For line CD:

$$u_z(x_C - x_D) - u_x(z_C - z_D) = 0 \qquad (2.43)$$

$$u_z(y_C - y_D) - u_y(z_C - z_D) = 0 \qquad (2.44)$$

$$u_x^2 + u_y^2 + u_z^2 = 1 \qquad (2.45)$$

For line JD:

$$u_z(x_J - x_D) - u_x(z_J - z_D) = 0 \qquad (2.46)$$

$$u_z(y_J - y_D) - u_y(z_J - z_D) = 0 \qquad (2.47)$$

In addition, the control arm is a link between a revolute joint and a spherical joint. It rotates around a fixed axis and has a constant length. In this model, the control arm is considered as a rod. The point B on line GH is chosen so that line AB is vertical to GH. Therefore, the constraint equations of this link are:

$$(x_B - x_A)^2 + (y_B - y_A)^2 + (z_B - z_A)^2 = (x_{B_1} - x_{A_1})^2 + (y_{B_1} - y_{A_1})^2 + (z_{B_1} - z_{A_1})^2 \qquad (2.48)$$

$$u_{x_0}(x_B - x_A) + u_{y_0}(y_B - y_A) + u_{z_0}(z_B - z_A) = 0 \qquad (2.49)$$

Moreover, the tie rod is a moving body and the constant length between the two spherical joints is expressed as

$$(x_M - x_N)^2 + (y_M - y_N)^2 + (z_M - z_N)^2 = (x_{M_1} - x_{N_1})^2 + (y_{M_1} - y_{N_1})^2 + (z_{M_1} - z_{N_1})^2 \qquad (2.50)$$

Furtherer, under road disturbances, the positions of the key points on the chassis are given by

$$
\begin{aligned}
&x_B = 0, && y_B = 0, && z_B = z_s \\
&x_D = x_{D_1}, && y_D = y_{D_1}, && z_D = z_{D_1} + z_s \\
&x_N = x_{N_1}, && y_N = y_{N_1}, && z_N = z_{N_1} + z_s
\end{aligned}
\qquad (2.51)
$$

Considering Equations (2.42)-(2.51), the number of unknowns increases to 18, (x_A, y_A, z_A), (x_J, y_J, z_J), (x_C, y_C, z_C), (x_M, y_M, z_M), (u_x, u_y, u_z) and (ϕ, ϑ, ψ).

It is worth mentioning that in order to connect the kinematic and dynamic models together, the values of the generalized coordinate z_s obtained from Equation (2.32), is considered as the input of the kinematic model in addition to road disturbances. Additionally, the vertical displacement of the point A which belongs to both the wheel and the control arm is considered as:

$$z_A \approx z_{A_1} + z_r \approx L_A \sin(\theta + \theta_1) + z_s \qquad (2.52)$$

By considering the above equations, the number of unknown parameters reduces to 17. Thus, the following system of equations can be established:

$$
\begin{cases}
1: x_M = a_{11}x_{M_1} + a_{12}y_{M_1} + a_{13}z_{M_1} + a_{14} \\
2: x_C = a_{11}x_{C_1} + a_{12}y_{C_1} + a_{13}z_{C_1} + a_{14} \\
3: x_J = a_{11}x_{J_1} + a_{12}y_{J_1} + a_{13}z_{J_1} + a_{14} \\
4: y_M = a_{21}x_{M_1} + a_{22}y_{M_1} + a_{23}z_{M_1} + a_{24} \\
5: y_C = a_{21}x_{C_1} + a_{22}y_{C_1} + a_{23}z_{C_1} + a_{24} \\
6: y_J = a_{21}x_{J_1} + a_{22}y_{J_1} + a_{23}z_{J_1} + a_{24} \\
7: z_M = a_{31}x_{M_1} + a_{32}y_{M_1} + a_{33}z_{M_1} + a_{34} \\
8: z_C = a_{31}x_{C_1} + a_{32}y_{C_1} + a_{33}z_{C_1} + a_{34} \\
9: z_J = a_{31}x_{J_1} + a_{32}y_{J_1} + a_{33}z_{J_1} + a_{34} \\
10: (x_M - x_N)^2 + (y_M - y_N)^2 + (z_M - z_N)^2 = (x_{M_1} - x_{N_1})^2 + (y_{M_1} - y_{N_1})^2 + (z_{M_1} - z_{N_1})^2 \\
11: u_z(x_C - x_D) - u_x(z_C - z_D) = 0 \\
12: u_z(y_C - y_D) - u_y(z_C - z_D) = 0 \\
13: u_z(x_J - x_D) - u_x(z_J - z_D) = 0 \\
14: u_z(y_J - y_D) - u_y(z_J - z_D) = 0 \\
15: u_x^2 + u_y^2 + u_z^2 = 1 \\
16: (x_A - x_B)^2 + (y_A - y_B)^2 + (z_A - z_B)^2 = (x_{A_1} - x_{B_1})^2 + (y_{A_1} - y_{B_1})^2 + (z_{A_1} - z_{B_1})^2 \\
17: u_{x_0}(x_A - x_B) + u_{y_0}(y_A - y_B) + u_{z_0}(z_A - z_B) = 0
\end{cases}
\tag{2.53}
$$

The above nonlinear equations set is solved numerically using Newton-Raphson method [34] and all unknown parameters are determined. Now, the displacement matrix of the spindle is known. Using this matrix, the motion of the wheel can be evaluated.

Since (ϕ, ϑ, ψ) angles rotate about principal axes [Reference axis (X,Y,Z)], according to definition of camber and toe angles, ψ demonstrates the trend of toe angle alteration and ϕ indicates the trend of camber angle alteration. Moreover, track alteration is equal to:

$$
Track\ alteration = y_A - y_{A_1}
\tag{2.54}
$$

The mathematical representations of the caster and king-pin angles are as following:

$$
King\text{-}pin\ angle = \tan^{-1}\left(\frac{y_D - y_A)}{z_D - z_A)}\right)
\tag{2.55}
$$

48

$$\text{Caster angle} = \tan^{-1}\left(\frac{x_D - x_A}{z_D - z_A}\right) \tag{2.56}$$

2.8 Model Verification

A virtual prototype of the MacPherson suspension system based on the key point positions and dynamic properties is developed in ADAMS/Chassis software package as shown in Figure 2.15. ADAMS is commercial multi-body dynamic analysis software that provides a virtual atmosphere, similar to that of the actual system. In Figure 2.15, the connections between the strut and car body and also between the control arm and car body are through bushings. The road input is given at the right side wheel.

In order to investigate variations of the wheel motions, it is assumed that the chassis (sprung mass) is fixed. The input is considered as $80 \sin(\pi t/5)$ (mm) for both the kinematic and ADAMS models. Figure 2.16, Figure 2.17, and Figure 2.18 represent the camber angle, toe angle and track width alterations, respectively, for the kinematic model as well as those of the model developed in ADAMS. As shown, all parameters for both models are in good agreement. There is a slight discrepancy between the models due to the initial assumptions. In fact, in ADAMS model the road displacement acts on the centre of the wheel (point P) while in the kinematic model developed in this work the road displacement is inserted at point A. In brief, the results from the kinematic model reasonably agree with those from the simulations in ADAMS. Thus, the kinematic model represents the wheel motions of the MacPherson suspension with reasonable accuracy. It should be noted that although modeling of a special type of suspension is studied in this research, the approach is applicable to other kinds of suspension systems such as double wishbone, trailing arm and so on.
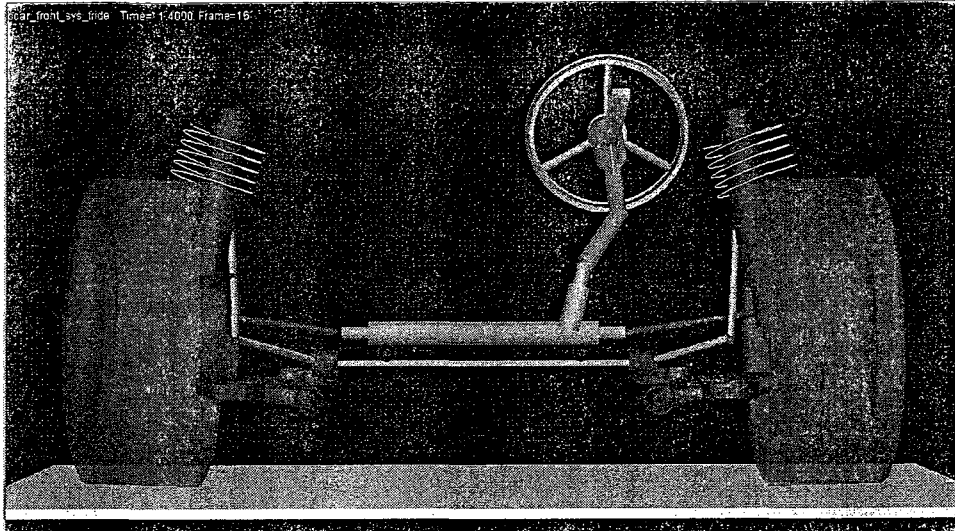
Figure 2.15 A virtual prototype of the MacPherson suspension system in ADAMS
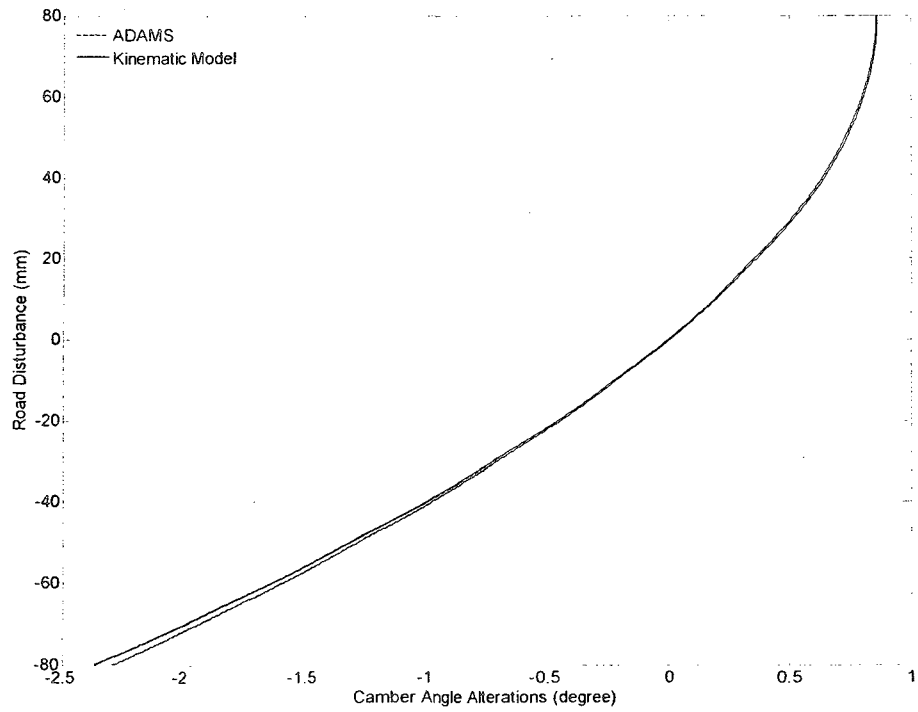
Figure 2.16 Camber angle alteration of kinematic model and that of ADAMS
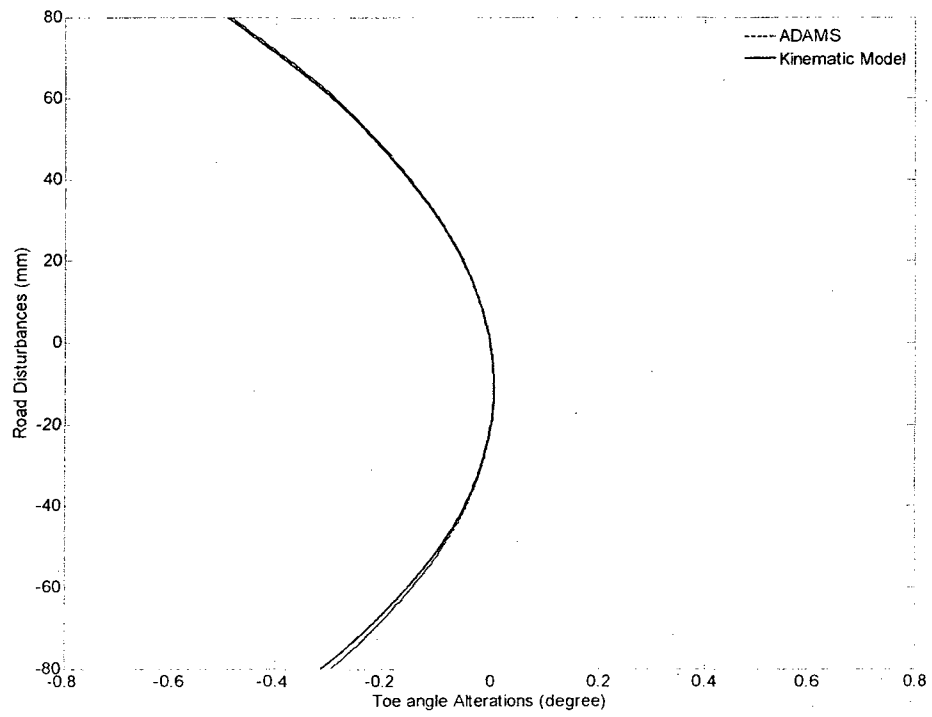
Figure 2.17 Toe angle alteration of kinematic model and that of ADAMS
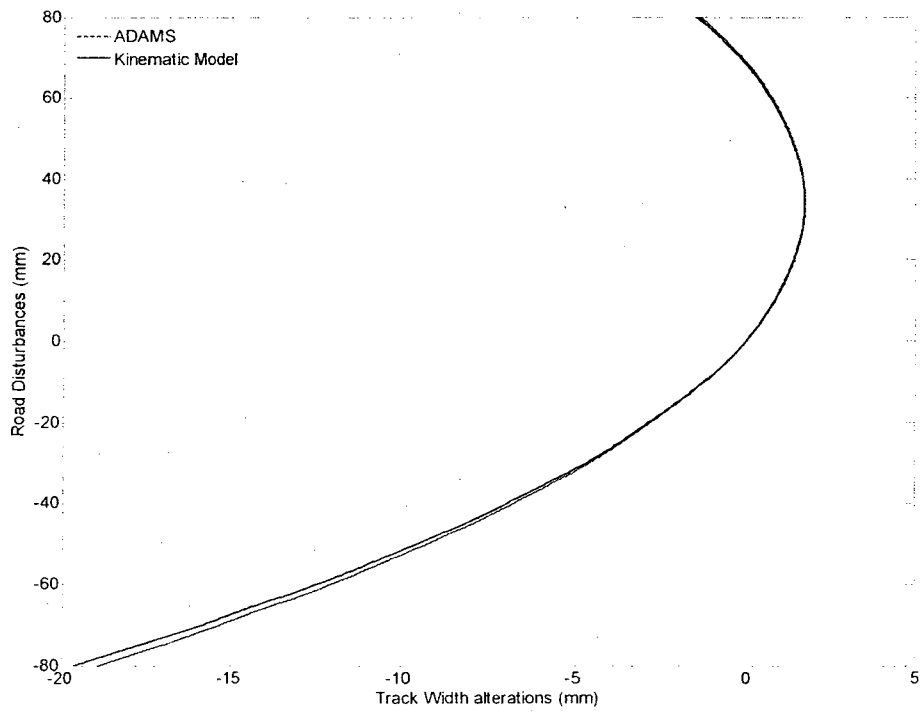
Figure 2.18 Track width alteration of kinematic model and that of ADAMS

51

2.9 Summary

A new nonlinear model of the MacPherson suspension is proposed and equations of motion are derived. This model provides one more degree of freedom than the conventional model where the bushing and mass of strut are taken into account. From the simulation results, it has been concluded that the frequency responses of conventional and linearized new model are similar for a specific case in which the angle between the strut and the vertical line to the road is zero and also the strut and tire are connected together at the centre of the wheel. The new model is more accurate than conventional model where the structure of suspension and wheel rotation resulting from kinematics of the system is considered.

In addition, a three-dimensional kinematic model of the suspension is developed to evaluate the performance of the MacPherson suspension kinematic parameters in conjunction with the dynamic response of the system. It is shown that the kinematic model represents the kinematic performance of the system with a reasonable accuracy by comparing its results with the results obtained from a virtual prototype of the MacPherson suspension system developed in ADAMS software..

The next chapter will deal with the semi-active control systems for application in MacPherson suspension systems.

CHAPTER 3

EVALUATION OF SEMI-ACTIVE CONTROLS IN MACPHERSON SUSPENSION SYSTEMS

The previous chapter dealt with the dynamic and kinematic modeling of the MacPherson suspension systems. In this chapter, the importance of three different hybrid semi-active control strategies on the ride quality, road holding ability, and performance of kinematic parameters of the MacPherson suspension are investigated analytically. The three control methods compared in this chapter are of hybrid skyhook-groundhook, modified skyhook, and passive-skyhook types. The comparison includes an evaluation of different aspects of suspension dynamics, vehicle body response and suspension kinematic performance. The results indicate that the passive-skyhook policy improves the MacPherson suspension performance significantly compared to the two other controllers. In addition, the results show that, unlike the previous findings, neither the ideal skyhook nor pure ground-hook controllers are perfectly appropriate for MacPherson suspension system due to structural kinematics. Finally, the frequency response of a modified hybrid control policy developed by the new generalized coordinates of the system is studied and discussed.

3.1 Introduction

The skyhook control methodology, proposed by Karnopp [35] in the early 1970's, is widely used to improve the ride quality due to its simplicity and high efficiency. The name "skyhook" comes from the assumption that the damper is hooked between the mass body and an imaginary inertia reference point in the sky (Figure 3.1). In fact, the mathematical description of this controller comes from the optimal solution to the cost

function of the quarter-car model with one degree of freedom when the cost function contains the sprung mass acceleration and weighted control force [4].

Skyhook control policy significantly decreases the resonant peak of the sprung mass, resulting in improvement of the ride quality, at the expense of increasing peak resonance of the unsprung mass which causes a deterioration of the handling performance. In order to improve the efficiency of the skyhook controller, different modifications of that control policy have been suggested by the researchers for semi-active suspension applications. For instance, to suppress the vibration of the unsprung mass, a fictitious damper is inserted between the sprung mass and the ground, called groundhook controller (Figure 3.2), by Novak et al [36].
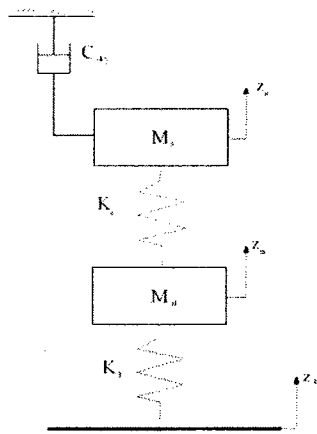
Figure 3.1 Skyhook damper configuration   Figure 3.2 Groundhook damper configuration
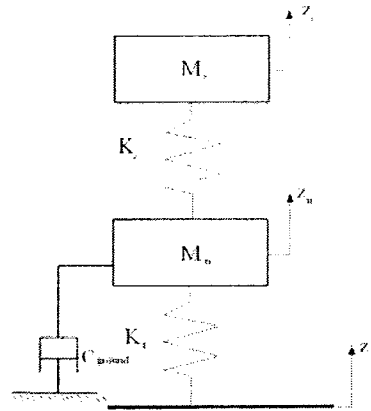
Ahmadian et al proposed a hybrid semi-active control strategy combining skyhook and groundhook controllers and analyzed the frequency domain and time domain responses for different values of controller's gain, experimentally and analytically [37, 38] and [39]. Also, they proposed a solution to the discontinuity of the damping force occurring in the

54

skyhook controller [40]. Batterbee and Sims [41] considered the advantages of the passive damping force and skyhook controller, and based on that developed a modified skyhook controller as a set-point force for a feedback linearization force tracking control of a MR damper. Yi and Song [42] proposed a modification of the skyhook controller in which the passive, skyhook, and groundhook damper forces were included for the computation of the desired force, and designed an adaptive controller for different road frequency disturbances. Sohn et al [43] implemented a modified skyhook controller on the MacPherson suspension by mixing the passive and skyhook damper forces. The performances of four different balance (hybrid) semi-active damping control strategies on a single degree-of-freedom body for vibration isolation have been compared and discussed by Liu et al [44]. Shen et al [45] have investigated the effects of the three different semi-active control methods on the acceleration and relative displacement transmissibility of the suspension system analytically and experimentally. For the comfort enhancement, Savaresi and Spelta combined the benefits of the skyhook and a new control approach called acceleration driven damping which was based on the optimal control solution [46]. The theoretical concepts of semi-active vibration-control design, control techniques and their implementation on related applications were reviewed by Jalili [47]. Furthermore, the performance of the skyhook controller is considered as a reference for the evaluation of the advantages of other advanced control strategies which were designed for ride and handling enhancement in references [48, 49].

From the above survey of the literature, although various combinations of the skyhook and groundhook controllers are used to handle the conflicting requirements of road holding and ride quality, the concerns regarding the contribution of those controllers to

the suspension kinematic performances and subsequently steering and stability are ignored. Meanwhile the kinematic effects on the dynamic response are not taken into account.

3.2 Description of the Hybrid Control Strategies

The purpose of the semi-active control suspension system is to regenerate an ideal damping force by a semi-active damper, located between the wheel and chassis.

The function of the skyhook damper, hooked between the stationary sky and the sprung mass, is to develop an ideal damping force in order to suppress the vibration of the sprung mass. This damping force can be written as

$$f_{sa} = c_{sky}\dot{z}_s \qquad (3.1)$$

where $\dot{z}_s$ is the velocity of the sprung mass and c_{sky} is the damping coefficient of the skyhook damper. Note that since the function of a damper is to dissipate the energy of the system, the product of the semi-active force and relative velocity of the sprung and unsprung masses, $\dot{z}_s - \dot{z}_p$, must satisfy the passivity constraint [44]

$$f_{sa}(\dot{z}_s - \dot{z}_p) \geq 0 \qquad (3.2)$$

Thus, a skyhook damper force acts as an ideal force when $\dot{z}_s$ and $\dot{z}_s - \dot{z}_p$ have the same sign. Otherwise, the force generated by the damper is opposite to that of the desired force, in which case, the damper needs to produce no force. Hence the skyhook controller was modified as

$$f_{sa} = \begin{cases} c_{sky} \dot{z}_s & \dot{z}_s(\dot{z}_s - \dot{z}_p) \geq 0 \\ 0 & \dot{z}_s(\dot{z}_s - \dot{z}_p) < 0 \end{cases} \tag{3.3}$$

It is known that this controller can greatly improve the frequency response of the sprung mass, while deteriorating that of the unsprung mass. Based on the skyhook controller methodology, an alternative control policy named groundhook control was developed to improve the handling performance. In the groundhook controller, a fictional damper was inserted between the unsprung mass and the ground in order to control the unsprung mass vibration. The groundhook control strategy is defined [38] as

$$f_{sa} = \begin{cases} c_{ground} \dot{z}_p & -\dot{z}_p(\dot{z}_s - \dot{z}_p) \geq 0 \\ 0 & -\dot{z}_p(\dot{z}_s - \dot{z}_p) < 0 \end{cases} \tag{3.4}$$

where c_{ground} is the damping coefficient of the groundhook damper. The logic of the groundhook controller is the same as that of the skyhook controller except that the control effort is on the unsprung mass. The direction of the semi-active damper force on the unsprung mass body is in the opposite direction of that acting on the sprung mass, and therefore the negative sign appears in the inequality in Equation (3.4). In contrast to the skyhook controller, this controller improves the wheel oscillation whilst reducing the comfort. In order to maximize the advantages of the skyhook and groundhook controllers, different hybrid control policies combining the two controllers have been proposed. However, these two controllers and their modifications were developed based on the simple quarter-car model. Moreover, their effects on kinematic suspension performance have not been taken into account. The focus of this study is to scrutinize the performance of three different recent hybrid control policies and their effects on the ride quality, road

holding ability and especially on the performance of the MacPherson suspension kinematic parameters.

It should be noted that in this work the velocity of the unsprung mass corresponds to the velocity of point P where it is the centre of the wheel as shown in Figure 2.2. In addition, since most of the contribution of the velocity of point P comes from it's the vertical velocity component, it is assumed that the velocity of the unsprung mass is equal to $\dot{z}_p$.

3.2.1 Hybrid skyhook-groundhook controller

The first hybrid control algorithm, so-called SA1, is the controller proposed by [37-40]. In this controller, a linear combination of the skyhook and groundhook controllers is employed. Mathematical expression for that controller is

$$\begin{cases} \dot{z}_s(\dot{z}_s - \dot{z}_p) > 0 & \sigma_{SKY} = \dot{z}_s \\ \dot{z}_s(\dot{z}_s - \dot{z}_p) < 0 & \sigma_{SKY} = 0 \end{cases}$$

$$\begin{cases} -\dot{z}_p(\dot{z}_s - \dot{z}_p) > 0 & \sigma_{GND} = \dot{z}_p \\ -\dot{z}_p(\dot{z}_s - \dot{z}_p) < 0 & \sigma_{GND} = 0 \end{cases}$$

$$f_{sa} = G\left[(1-\beta)\sigma_{SKY} - \beta\sigma_{GND}\right] \qquad (3.5)$$

where the variables σ_{SKY} and σ_{GND} are the skyhook and groundhook components of the damping force. The relative ratio between the skyhook and groundhook controllers is β, which varies between 0-1, and G is a constant gain. Reducing β near to zero causes the controller to become a pure skyhook controller. In contrast, increasing β yields a groundhook controller.

3.2.2 Modified skyhook controller

The second controller, SA2, which is used by Sammier et al [49] considers a skyhook controller for isolation of the chassis from road disturbances and tunes the groundhook controller to improve the handling performance. The mathematical description of this controller is as shown

$$f_{sa} = c_{sky}\dot{z}_s - \beta c_{sky}\dot{z}_p = G\left[\dot{z}_s - \beta \dot{z}_p\right] \tag{3.6}$$

However, this control law needs to satisfy the passivity constraint. Thus, this controller is modified as

$$
\begin{cases}
\dot{z}_s(\dot{z}_s - \dot{z}_p) > 0 & \sigma_{SKY} = \dot{z}_s \\
\dot{z}_s(\dot{z}_s - \dot{z}_p) < 0 & \sigma_{SKY} = 0
\end{cases}
$$
$$
\begin{cases}
-\dot{z}_p(\dot{z}_s - \dot{z}_p) > 0 & \sigma_{GND} = \dot{z}_p \\
-\dot{z}_p(\dot{z}_s - \dot{z}_p) < 0 & \sigma_{GND} = 0
\end{cases}
\qquad f_{sa} = G[\sigma_{SKY} - \beta \sigma_{GND}] \tag{3.7}
$$

The advantage of this control law, in comparison to that of SA1, is that the tuning of the control gain, β, only requires acting on one parameter, σ_{GND}.

3.2.3 Passive-skyhook controller

The third hybrid controller suggested by Yi and Song [42] is called SA3 which includes the advantages of the skyhook, groundhook and passive dampers. But, this control policy increases the degree of freedom of the control law to three. For simplicity, the advantages of the skyhook controller and conventional damper force together are considered in the following. The mathematical control description is

$$\begin{cases} \dot{z}_s(\dot{z}_s - \dot{z}_p) > 0 & \sigma_{SKY} = \dot{z}_s \\ \dot{z}_s(\dot{z}_s - \dot{z}_p) < 0 & \sigma_{SKY} = 0 \end{cases} \quad f_{sa} = c_{sky}\sigma_{SKY} + \beta c_{sky}\Delta\dot{L} = G\left[\sigma_{SKY} + \beta\Delta\dot{L}\right] \quad (3.8)$$

where β is the ratio of the conventional and skyhook damping coefficients and $\Delta\dot{L}$ is the relative velocity between the sprung and unsprung masses. Since the conventional damping force always satisfies the passivity constraint, the switching only occurs to the sprung mass velocity.

3.2.4 Numerical problems

Two main numerical problems related to the semi-active control strategies for simulation of response of a semi-active system are chatter and jerk. Chatters start whenever a rapid switching occurs between the on and off states of the system. Referring to [44], it is noted that the changes of the sign of the sprung mass, $\dot{z}_s$, are important for inducing the chatter in the on-off skyhook control systems due to the large damping forces. Two other reasons for chattering [44] are related to the sign and amplitude, respectively, of the damping force. Either having a different sign between the damper and spring forces or having larger amplitude of the damper force than that of the instantaneous spring force makes the system prone to chatter. In order to eliminate the chatter a different logic has been proposed. More detailed information on this problem can be found in [44] and references therein. Jerk refers to the sharp jump in sprung mass acceleration due to the discontinuity of the damping force which causes the reduction of isolation advantages of the skyhook controller. In [40], two different continuous functions for damping coefficient are proposed to avoid any jerk.

Moreover, it is worth mentioning that although the aforementioned hybrid controllers employ a linear combination of two linear control policies, they are inherently nonlinear due to switching between on and off states. The transient dynamic response of the MacPherson suspension system subject to those control strategies are compared in the following section.

3.3 Comparison of the Control Strategies

From the point of view of the ride and handling of a vehicle, the main vibration source is the road irregularities, transmitted to the vehicle body through the wheel and suspension system. In the following, the performance of the MacPherson suspension system is evaluated under both shock and vibration environments.

In order to compare the control strategies with that of the passive case, the following values have been taken from [26] and from ADAMS software default:

$m_s = 453$ (Kg)
$m_u = 71$ (Kg)
$K_s = 17658$ (N/m)
$K_t = 183887$ (N/m)
$I_u = 0.021$ (Kg.m^2)
$C_p = 1950$ (N.sec/m)

The positions for the key points on the MacPherson suspension are considered as below (the origin of the coordinate system at equilibrium position is assumed to be at point B and all dimensions are in *mm*):

$A_1 = (206.5, 249, -60.8)$ $P_1 = (211.1, 292.1, 27.5)$
$C_1 = (222, 152.6, 236.2)$ $D_1 = (240, 107.4, 582.5)$
$J_1 = (229.2, 134.5, 374.8)$

A measure of the road-holding ability of a vehicle, frequently used in the literature, is the contact force variation between the tire and ground which depends on the tire deflection (z_p-z_r). Accordingly, a vehicle has good stability if a strong contact force exists between the road and tire. However, in the case of MacPherson suspension system, the control of wheel motion is the function of the control arm, and thus, a low rotation of control arm results in a low wheel motion and consequently a better road holding. Therefore, in this study, the variation of the control arm, θ, is chosen to quantify the road holding instead of the tire deflection.

In the following, Root Mean Square (RMS) and Peak to Peak (PTP) values of the acceleration response and control arm rotation are investigated to quantify the ride quality and road holding ability, respectively. Those of the camber angle and track width alterations are evaluated as well using the dynamic model described in Section 2.3. For brevity, the results related to variations of the caster and kingpin angles are ignored.

3.3.1 Bump response

In the case of bump response study, the control gain, G, is taken as 4000 N.s/m and the variable, β, is chosen as 0.5 for all of the controllers. These two values are usually recommended by researchers so that the best trade-off between ride quality and handling performance is achieved [37, 49]. The corresponding ground displacement is given by

$$z_r = \begin{cases} \dfrac{A}{2}(1-\cos(\dfrac{2\pi V}{L}t)) & 0 \le t \le \dfrac{L}{V} \\ 0 & \dfrac{L}{V} < t \end{cases} \qquad (3.9)$$

where A and L are the height and the length of the bump. A= 0.08 m, L= 5 m and the vehicle forward velocity of V= 45 Km/h are considered in the following analysis.

The related system acceleration response and control arm rotation subject to each controller along with those of the passive system are shown in Figure 3.3 and Figure 3.4. As can be seen, all controllers show large overshoot of the acceleration response and reduce the oscillation of the control arm. The effects of these control laws on the camber angle and track width alterations are shown in Figure 3.5 and Figure 3.6. Referring to these figures, one can see that all the controllers significantly improve camber angle and track width alterations where SA3 has the most effect compared to the others by diminishing camber angle and acceleration vibration as well as by reducing overshot of the responses.
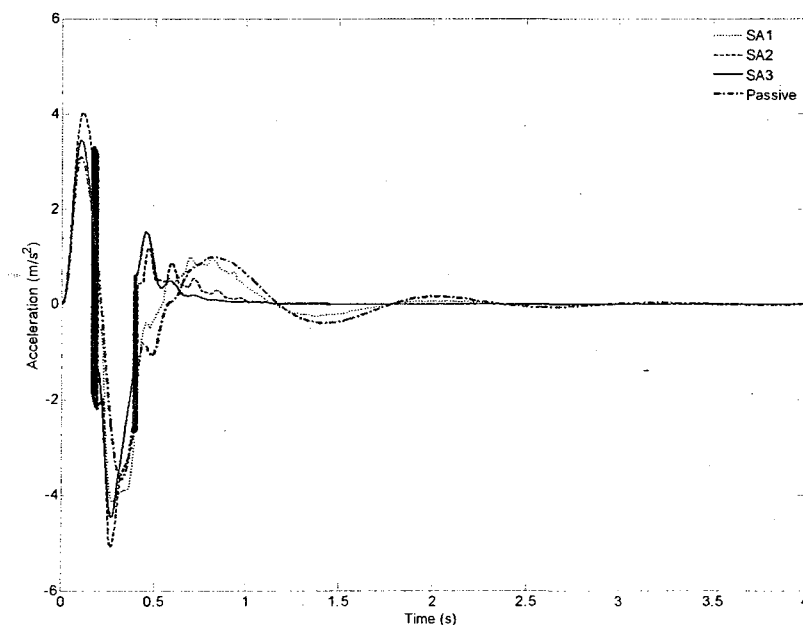
Figure 3.3 Vertical acceleration of the sprung mass for bump disturbance
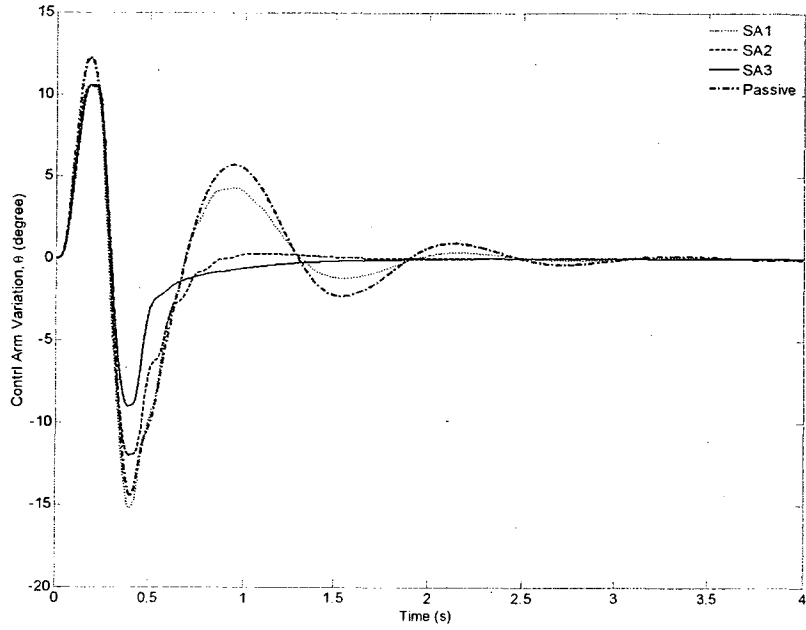
Figure 3.4 Control arm variation for bump disturbance
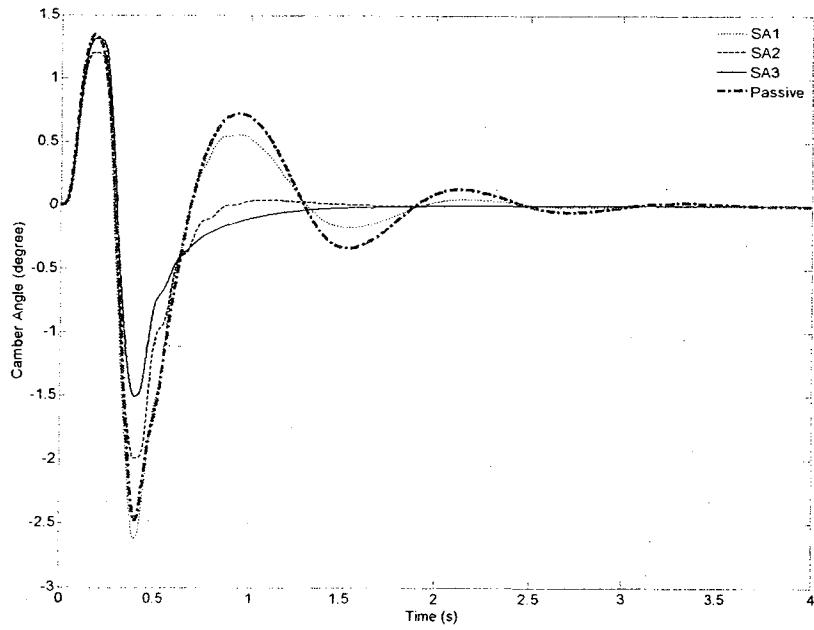
Figure 3.5 Camber angle alterations for bump disturbance
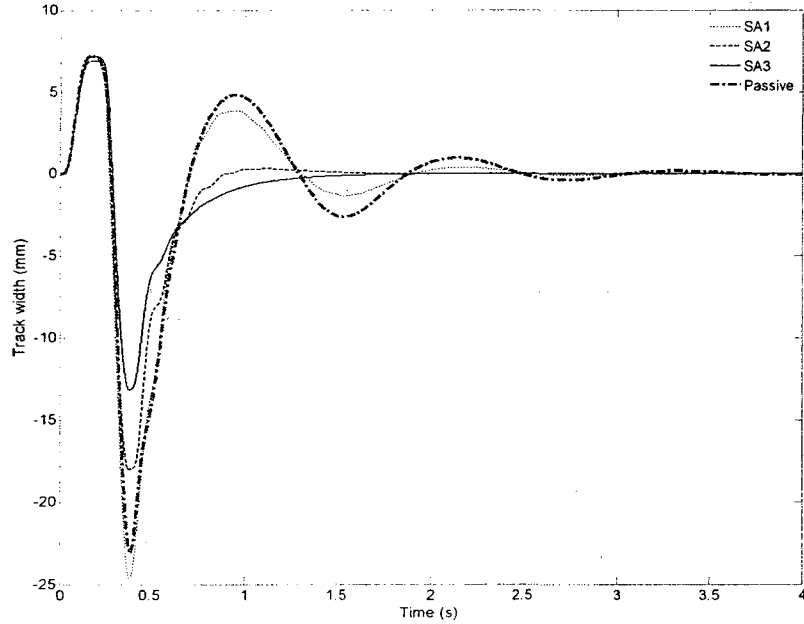
Figure 3.6 Track alteration for bump disturbance

In addition, peak to peak values and RMS of the acceleration response, control arm rotation, camber angle and track width variations are compared for different values of G and β. Peak to Peak (PTP) value shows the maximum variation of the response and is given by [39]:

$$PTP = max(x(t)) - min(x(t)) \tag{3.10}$$

where $x(t)$ is either any kinematic suspension parameter or the acceleration of the sprung mass.

Figure 3.7 to Figure 3.10 illustrate PTP values of the acceleration response, the control arm rotation, camber angle and track width alterations for different values of β and constant value of G equal to 4000 N.s/m. According to Figure 3.7, increasing β results in deterioration of PTP value of acceleration response, however, Figure 3.8 indicates that

increasing β reduces PTP value of the control arm rotation response for SA2 and SA3 and increases for that of SA1. In terms of the acceleration response, the performances of SA1 and SA3 are close to each other compared to that of SA2 while the performance of SA2 and SA3 are similar in terms of road holding ability. The interesting results come from Figure 3.9 and Figure 3.10 where the PTP values of the camber angle and track width alterations are shown. From these figures, one can realize that increasing β reduces the PTP values of camber angle in SA2 and SA3 from 3.37 to 3.18 and 3.34 to 2.59 degree, respectively, while it increases in SA1 significantly from 3.38 to 5.68 degree. However, increasing β results in reduction of PTP track width variation in SA3 from 24.1 to 19.1 mm whereas in SA1 and SA2 they are increased from 24.5 to 47.5 and 24.4 to 26.6 mm, respectively.
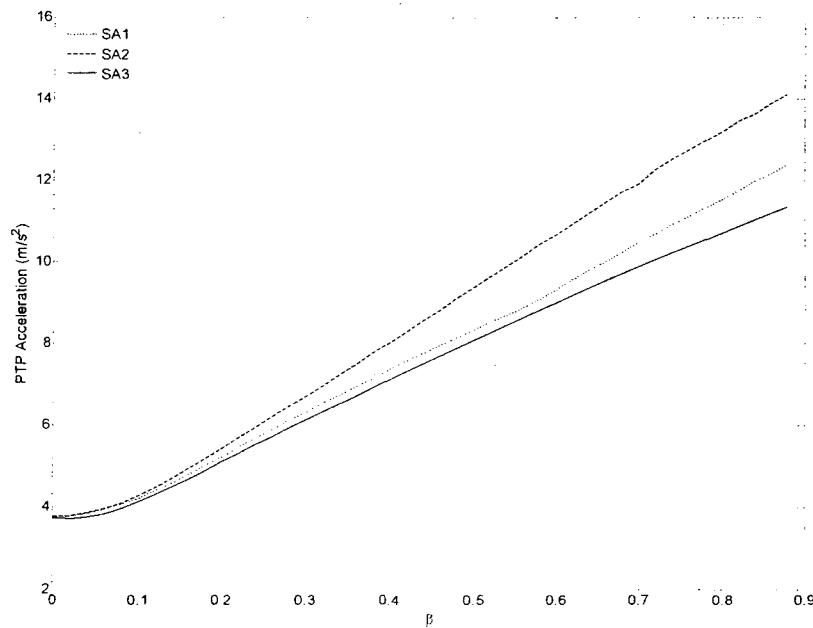
Figure 3.7 PTP acceleration response for different values of β
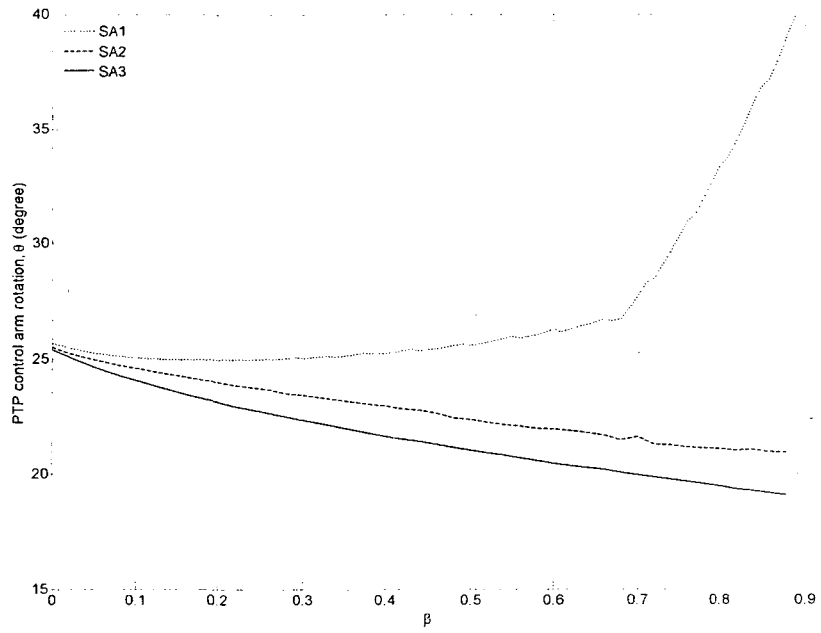
Figure 3.8 PTP control arm variation for different values of β
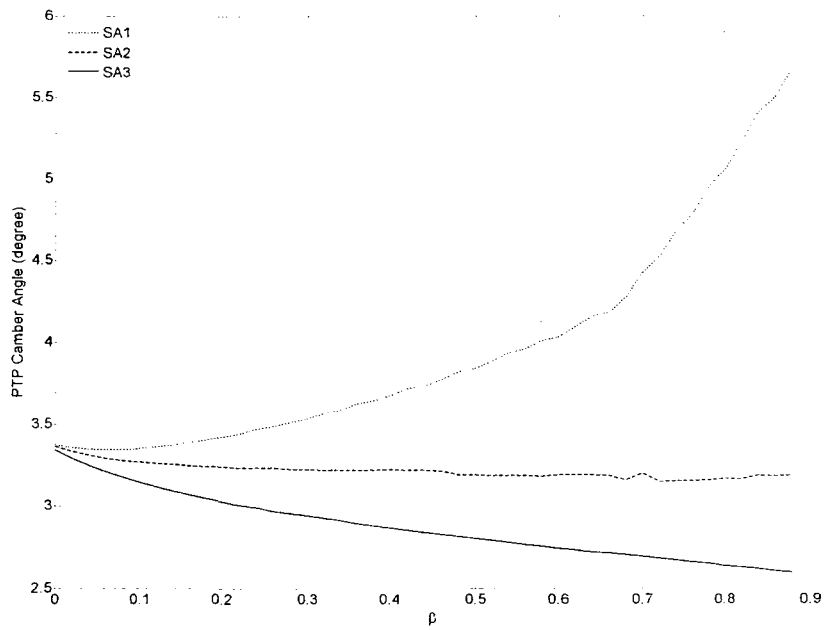
Figure 3.9 PTP camber angle alteration for different values of β
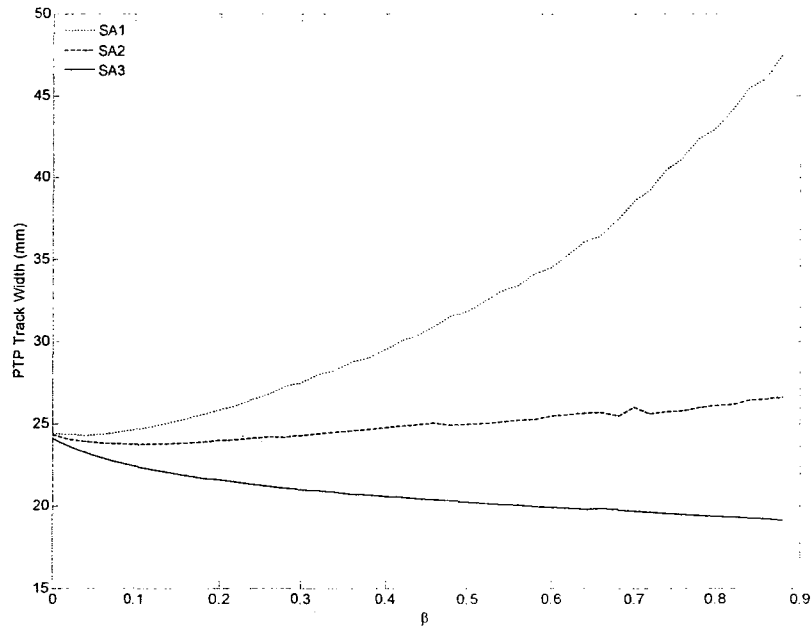
Figure 3.10 PTP Track width alteration for different values of β
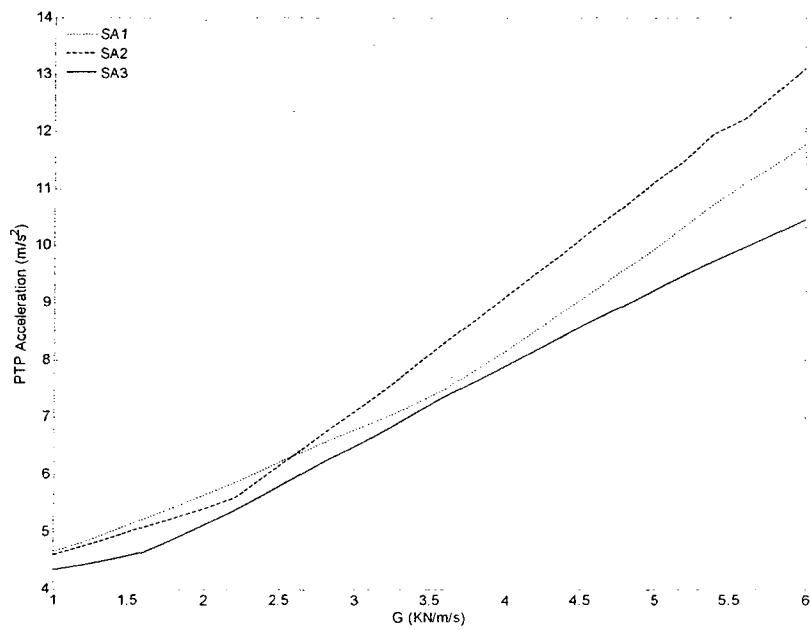
Figure 3.11 PTP acceleration response for different values of G

68
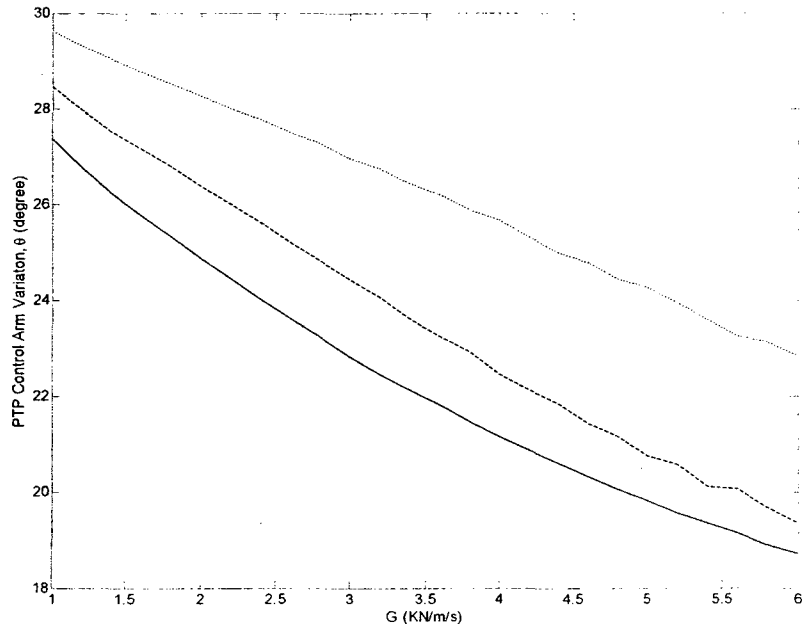
Figure 3.12 PTP control arm variation for different values of *G*
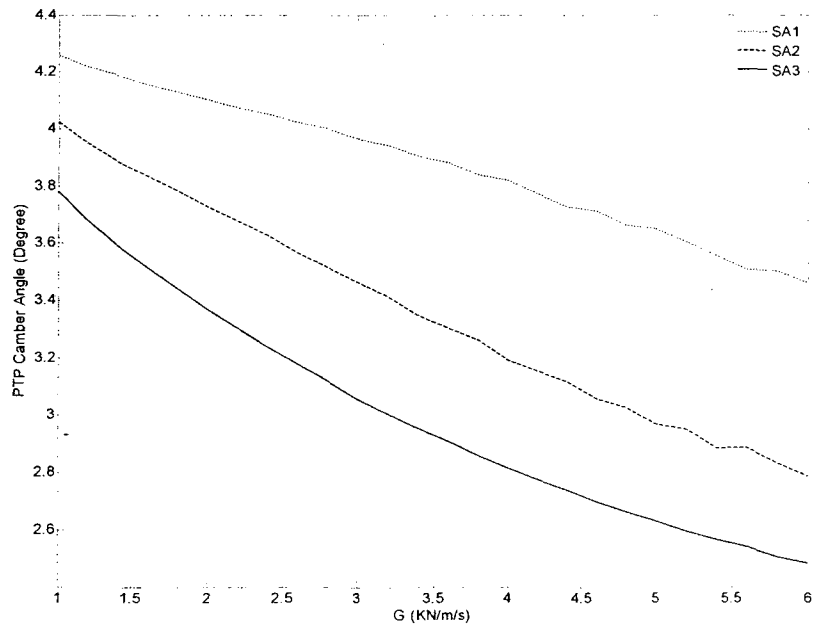
Figure 3.13 PTP camber angle alteration for different values of *G*
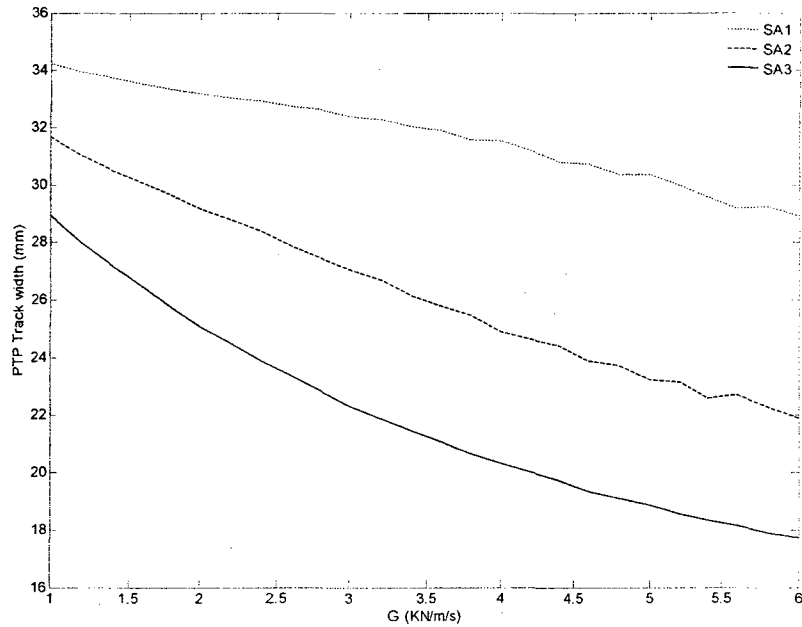
Figure 3.14 PTP Track width alteration for different values of _G_

In addition, the PTP values of the parameters are plotted in Figure 3.11 to Figure 3.14 for different controller gains and constant $\beta= 0.5$. In all the strategies, increasing G causes deterioration of the PTP value of the acceleration response, resulting in worse ride quality, and reduction of that of the control arm oscillation, indicating better road holding of the wheel. In addition, it results in reduction of PTP values of camber angle and track width variations for all controllers, resulting in better handling performance. It is seen from Figure 3.7 to Figure 3.14 that SA3 has the best performance for different values of β and G in terms of PTP values of ride quality, road holding ability, and handling performance. The RMS values of the performance parameters are calculated and summarized in Table 3-1 to Table 3-4 for different values of β. Referring to those Tables, one can see that by increasing β, RMS of acceleration response, control arm rotation, camber angle variation, and track width alteration will be increased in case of SA1, while

acceleration and track width will be increased and control arm rotation and camber angle variation will be almost constant in SA2. However, in SA3, increasing β improves road holding and handling performances whereas ride quality is deteriorated. In other words, these tables show that for each specific values of β the SA3 has less RMS values compared to the other control strategies.

The abovementioned results indicate that increasing β in SA1, meaning that the controller goes towards a pure groundhook strategy deteriorates the performance parameters of the system. As an important result of this study, the pure groundhook strategy is not applicable on the MacPherson suspension system. In fact, the chassis and wheel are connected to each other through the strut, including spring and damper, as well as through the control arm. It should be noted that the control arm is a rigid link and its function is to control the wheel motions. Thus, the motion of the chassis affects the wheel motion via the control arm other than the spring and damper. This fact is ignored in the simple quarter-car model and since developing the groundhook strategy was based on the simple model, its performance is not applicable in the MacPherson suspension system.

Table 3-1   RMS acceleration response (m/s²) for different values of β

Acceleration	$\beta=0.2$	$\beta=0.4$	$\beta=0.6$	$\beta=0.8$
SA1	0.3912	0.5479	0.7302	0.9530
SA2	0.3878	0.5591	0.7667	0.9856
SA3	0.3532	0.4830	0.6319	0.7812

Table 3-2 RMS control arm variation (degree) for different values of β

Theta	β=0.2	β=0.4	β= 0.6	β= 0.8
SA1	2.2491	2.2703	2.6291	3.8840
SA2	2.1873	2.0707	1.9544	1.8972
SA3	2.1249	1.9240	1.7481	1.6081

Table 3-3 RMS camber angle alteration (degree) for different values of β

Camber Angle	β=0.2	β=0.4	β= 0.6	β= 0.8
SA1	0.3157	0.3389	0.4063	0.5792
SA2	0.3015	0.2991	0.2931	0.2945
SA3	0.2837	0.2591	0.2369	0.2197

Table 3-4 RMS track width alteration (mm) for different values of β

Track Width	β=0.2	β=0.4	β= 0.6	β= 0.8
SA1	2.5062	2.8415	3.5174	4.9454
SA2	2.3464	2.4231	2.4512	2.5340
SA3	2.1313	1.9491	1.7853	1.6636

3.3.2 Random road disturbance

A road disturbance of $z_r(t)=25.4\sin(2\pi t)+d(t)$ mm, where $d(t)=5\sin(10.5\pi t)+\sin(21.5\pi t)$ mm represents the high frequency disturbances, is applied to the system [12]. The root mean square values of the performance parameters subjected to this disturbance, with β=

0.5 and G= 4000 Nm/s is summarized in Table 3-5. It is seen from the table that all hybrid control strategies reduce the control arm rotation, camber angle variation and track width alteration in comparison to those of the passive one. However, the RMS acceleration decreases in SA3 and consequently; the ride quality of the vehicle is improved by this controller while the other two control strategies slightly increase it compared to the passive case. It should be noted that although the RMS values of the acceleration response are close to that of the passive case, the RMS values of the other performance parameters are reduced. Among the above mentioned control policies, which are applied to the MacPherson suspension, the SA3 shows a significant improvement of the suspension performance especially on the reduction of the camber angle and track width variations compared to the other two hybrid control policies.

Table 3-5   RMS of the responses for different hybrid control strategies

	SA1	SA2	SA3	Passive
Acceleration(m/s^2)	1.5786	1.5130	1.2130	1.3689
Control arm rotation (degree)	6.0020	4.3373	3.6322	7.0073
Camber angle (degree)	0.8472	0.6093	0.5124	0.9908
Track width (mm)	6.5899	4.6469	3.9071	7.8102

3.4   Frequency Response Analysis of the Passive-skyhook Controller

It is important to note that the previous studies employed the vertical displacement of the sprung mass, z_s, and the vertical displacement of the unsprung mass, z_P, as the

generalized coordinates of the system while in the present study the generalized coordinates are the vertical displacement of the sprung mass, z_s, and the rotational motion of the control arm, θ. Using the new generalized coordinates, a modified hybrid control strategy is developed according to SA3 in the following.

The simulations show that the discrepancy between the vertical velocity components of point P and A is small. Thus, as an approximation, it is assumed that $\dot{z}_p \approx \dot{z}_A$. Hence, using Equation (2.12), one obtains

$$\dot{z}_p \approx L_A \dot{\theta} \cos(\theta + \theta_1) + \dot{z}_s \tag{3.11}$$

For small variation of θ, the above equation is reduced to

$$\dot{z}_p \approx L_A \cos(\theta_1)\dot{\theta} + \dot{z}_s \tag{3.12}$$

Based on the above equation, one has

$$\dot{z}_s - \dot{z}_p \approx -L_A \cos(\theta_1)\dot{\theta} \tag{3.13}$$

Therefore, for the purpose of the frequency analysis of the system, the hybrid control policy SA3 is modified as below based on the generalized coordinates

$$\left. \begin{cases} -\dot{z}_s \cos(\theta_1)\dot{\theta} > 0 & \sigma_{SKY} = \dot{z}_s \\ -\dot{z}_s \cos(\theta_1)\dot{\theta} < 0 & \sigma_{SKY} = 0 \end{cases} \right\} \quad f_{sa} = G\left[\sigma_{SKY} - \beta L_A \cos(\theta_1)\dot{\theta}\right] \tag{3.14}$$

Figure 3.15 and Figure 3.16 show the transmissibility of the vertical motion of the sprung mass and the rotational motion of the control arm subject to road disturbance for different values of β and a constant value of control gain of 4000 Ns/m.

As concluded in the earlier studies [38, 41, 44], the skyhook controller improves the motion of the sprung mass in the whole frequency range, however, as shown in Figure 3.15, for MacPherson suspension system, the vibration of the sprung mass is not attenuated at the second resonant frequency subject to pure skyhook controller (β =0). This stems from the fact that the structural effects on the frequency performance of a typical suspension such as MacPherson suspension have been ignored in the conventional model. In the MacPherson suspension, the sprung and unsprung masses are connected to each other by the control arm. In other words, there is an extra connection between the two lumped masses other than through the damper and spring that changes the frequency performance of the system. In addition, a pure skyhook controller improves the peak resonant response of the rotational motion of the control arm at the expense of greatly increasing the transmissibility at the second resonant frequency (see Figure 3.16). From Figure 3.15 and Figure 3.16, one can realize that the values of β around 0.5 would be a good candidate for improving both the transmissibility of the sprung mass and the rotational motion of the control arm throughout the frequency range. Increasing β above 0.5 results in the control arm rotation transmissibility improvement at the expense of the isolation reduction of the sprung mass in the moderate frequency range. In contrast, decreasing the value of β below 0.5 improves sprung mass transmissibility with a corresponding increase in the amplitude at the second resonant peak of the rotational motion.

As mentioned before, due to the switching between the on and off states, all semi-active control strategies and consequently, the acceleration response are strongly nonlinear. Thus, the conventional frequency response analysis is not applicable to the acceleration

frequency response analysis of this type of system. In this study, an approximation of the frequency response for nonlinear semi-active control systems named *variance gain* [46] is adopted. Based on this method, a finite set of pure harmonic excitations as $z_{ri}=Asin(\omega_i t)$ is exerted to the system and the squared root of the related response would be recorded. Using the variance gain method, the acceleration frequency response of the semi-active MacPherson suspension system due to road disturbance for different values of β and specific value of G equal to 4000 Ns/m is plotted in Figure 3.17. It should be noted that 20log of the acceleration response is plotted in the vertical axis in order to have a more comprehensible plot. As shown, by increasing β, the vibration isolation is reduced. The best vibration isolation occurs at β=0.25 at the cost of increasing the peak at the second resonant frequency. However, all values of β improve the ride quality compared to the passive case in the low frequency range between 0-2 Hz. As can be seen, at $\beta = 0.5$ there is a good acceleration transmissibility in the low frequency range and a vibration isolation similar to that of passive case for the rest of the frequency range.
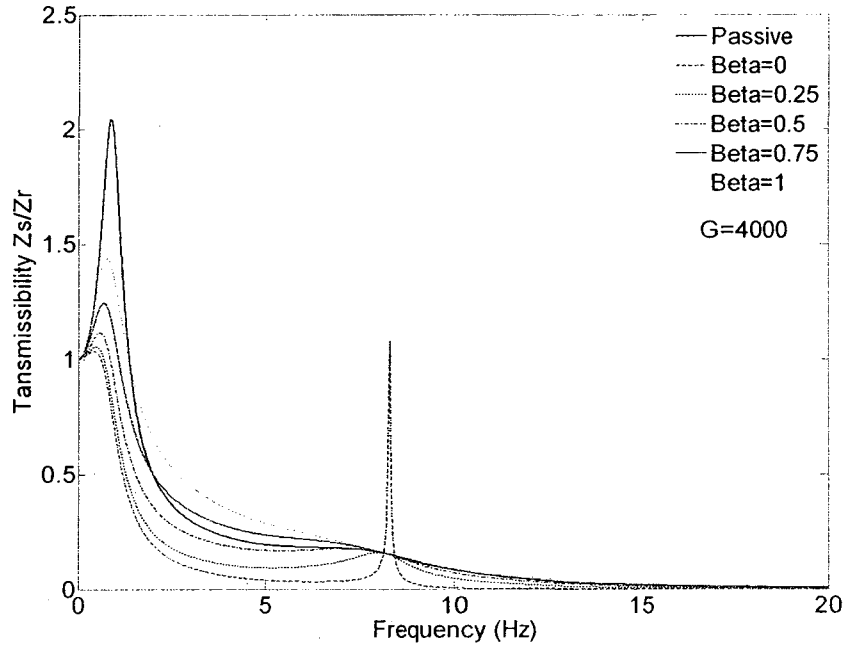
Figure 3.15 Transmissibility of the sprung mass for different values of β
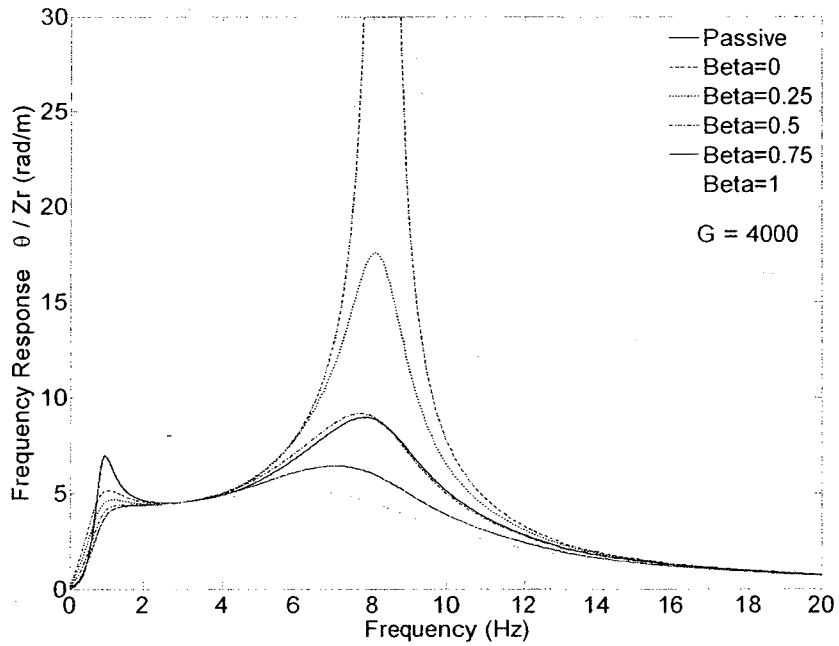
Figure 3.16 Frequency response of the control arm rotation for different values of β
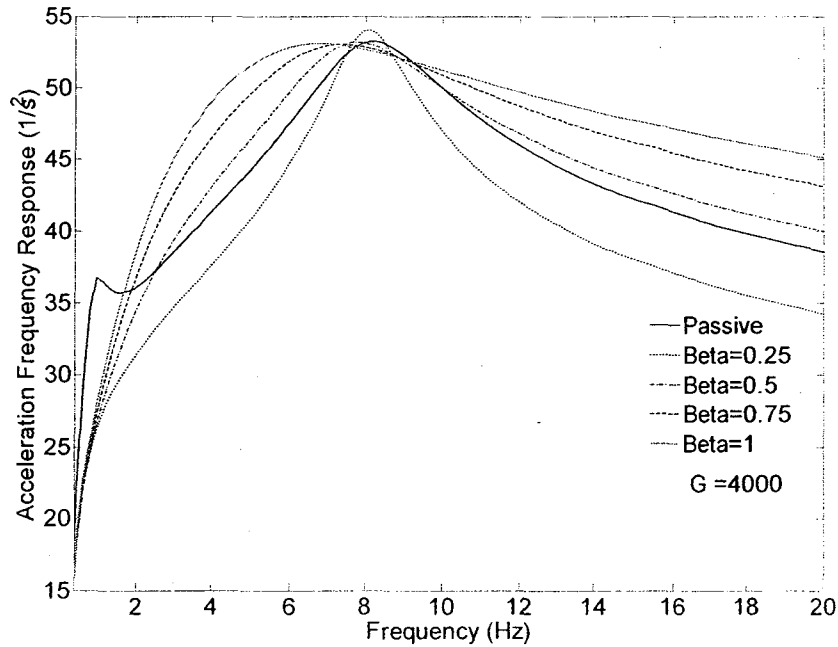
Figure 3.17 Frequency response of the sprung mass for different values of β

3.5 Summary

The influences of three different hybrid control strategies on the different aspects of performances of MacPherson suspension system such as ride quality, road holding, and suspension kinematic parameters are investigated. It is shown that the form of combination of the basic semi-active control strategies is really important in improving the overall performance of the vehicle. It is concluded that the combination of the skyhook controller and the passive damping force can significantly improve the kinematic parameter performance of the MacPherson suspension in addition to ride quality and road holding ability. The results indicate that a pure groundhook controller is not an applicable controller for MacPherson suspension since it makes the system unstable. Moreover, the frequency analysis of the system shows that, unlike previous

findings, the skyhook controller amplifies the resonant response at the second natural frequency of the system.

CHAPTER 4

SUSPENSION CONTROLLER FORMULATION

In this chapter, the H_∞ robust control theory is employed to generate a desired semi-active control force to boost the ride quality, road holding ability, and handling performance of MacPherson suspension system. After briefly introducing the concept of H_∞ robust control theory and Linear Matrix Inequality (LMI) optimization, a full state feedback control is formulated to fulfill the specifications. Full state feedback control needs the measurements of all the states of the system which results in increasing design cost and even causing implementation difficulties. Thus, the Static Output Feedback (SOF) H_∞ robust control theory is employed to generate the desired force command. Since the SOF leads the optimization procedure to the Bilinear Matrix Inequalities (BMI), Genetic Algorithm (GA) is used to solve the nonlinear optimization of the SOF. It is shown that the SOF has a performance close to that of full state feedback with lower cost design and more reliable implementation design.

4.1 Introduction

The robust control has gained much attention recently for vehicle suspension control, due to its ability of dealing with frequency specifications and model uncertainties. The main attempt in robust control is on minimization of the energy exerted from the road to the vehicle. The major approaches have been defined based on either L_2 (H_2) or L_∞ (H_∞) norms optimization of the transfer function between road disturbances to suspension responses. While in the former method the transfer function is minimized in the whole frequency range, in the latter it is optimized in the worst case of disturbance. A common

way used in formulating H_2 and H_∞ robust control is Linear Fractional Transformation (LFT) as shown in Figure 4.1.
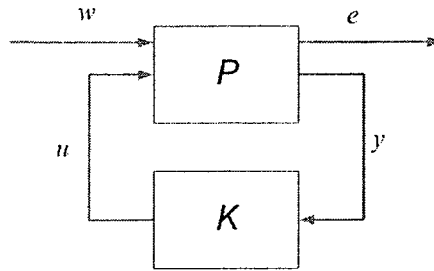
Figure 4.1 Linear fractional transformation configuration

where $P(s)$ is a generalized plant given by

$$\begin{pmatrix} e \\ y \end{pmatrix} = \begin{bmatrix} p_{11}(s) & p_{12}(s) \\ p_{21}(s) & p_{22}(s) \end{bmatrix} \begin{pmatrix} w \\ v \end{pmatrix} \tag{4.1}$$

In Equation (4.1), w and v stand for plant and control input vectors. e is the controlled output vector and y shows the measurement vector. The purpose is to design a controller K so that the system is kept stable and either H_2 or H_∞ norm of the transfer function $T_{ew}(s)$ between the input w to the controlled output e is minimized. Accordingly,

for H_2 control
$$min\|T_{ew}(s)\|_2 \tag{4.2}$$

for H_∞ control
$$\|T_{ew}\|_\infty = max\,\bar{\sigma}(T_{ew}) \le \gamma \tag{4.3}$$

where γ is a finite scalar and $\sigma(T_{ew})$ is the maximal singular value of T_{ew}. Typically, some weight functions are assumed on the controlled output, reference input and actuator force to show the performance specifications and normalize the signals with different units in an optimal setting. Generally speaking, these optimization problems are solved by using

Riccati equations, however; the Linear Matrix Inequality (LMI) is another formulation considered by researchers for solving robust control problem.

Sammier et al [49], specified proper weighting functions in terms of industrial specifications and designed a H_∞ control for semi-active suspension systems to improve ride quality and investigated the controller performance by applying it on a nonlinear model of a suspension system. Du et al [50] developed an inverse model of MR damper using experimental data and designed a H_∞ controller using two feedback signals including suspension deflection and sprung mass velocity. Hayakawa et al [51, 52] designed an active H_∞ control based on the full car model and utilized the output feedback instead of the state feedback in order to reduce the number of measurement devices. That controller was then applied to a real passenger car to show its superior performance. The novelty of their architecture arose from the decoupling of the roll and pitch motions of the full car model resulting in reducing the complexity of the control design while the model uncertainties were considered in the input channel. Zribi and Karkoub [53] proposed two robust schemes including robust inverse dynamics control and robust sliding mode control schemes. While the former scheme needs the exact knowledge of the system parameters, the latter does not. In order to overcome the shortcoming of the former controller, additional variables are considered in the parameter matrix. It was concluded that the modified inverse dynamics and sliding mode controllers were robust in the presence of the parameter uncertainties. In addition, it was shown that the latter had a better performance compared to the former one at the expense of some small chattering in the response of the system.

The μ analysis is a powerful tool to investigate the stability of the system in the presence of model uncertainties and μ synthesis is a robust control design counterpart of μ theory. Using a full car model, Gaspar et al [54] considered both structural and dynamical uncertainties and developed a robust controller by means of mixed μ synthesis for active suspension systems. In a similar way, Dai et al considered the active quarter-car model and developed a robust controller using H_∞ and μ synthesis [55]. Kashani and Kiriczi [56] analyzed the robust stability of LQG controlled active suspension systems in the presence of parameter variations by converting it in H_2 framework and using maximum singular value and structured singular value synthesis. It was shown that the structured value was a more reliable criterion than the maximum one for stability robustness test of LQG controlled active suspension systems. In addition, they investigated the effects of uncertainties, resulting from unmodeled high frequency dynamics of the plant, on the stability of the closed loop system and concluded that the effect of the structured uncertainties was more important than that of unstructured ones.

Extending further, some researchers defined different constraints arising from the performance limitation of the system and actuator, such as suspension stroke limitation, road holding ability and actuator saturation, and then tried to design an appropriate robust control to improve ride quality in accordance with fulfilment of those constraints. For instance, Chen and Guo [57, 58] designed a H_∞ active suspension controller using LMI approach in the case where the constraints were captured utilizing the concept of reachable sets and a state-space ellipsoid defined by a quadratic storage function. In order to modify the performance of the proposed active controller in the case of large unforeseen disturbances, they solved H_∞ problem based on moving horizon strategy,

making possible the on-line optimization procedure [59]. Even though Fialho and Balas [60] considered a linear time invariant model of an active vehicle and designed a typical H_∞ controller for performance enhancement, they assumed that the weighting functions considered for the constraints were varying based on the suspension deflection. With this assumption, they employed the linear parameter varying technique and designed a controller to fulfil the specifications in the wide range of frequencies. Son et al [62] considered H_∞ approach in LMI framework for ride control of semi-active suspension system, however, the handling performance and stability requirements were neglected in their design. Lucente and Rossi [63] proposed two multi-objective controllers including H_∞ optimization and backstepping approach for semi-active suspension systems. In that design, the friction and dynamics of damper were taken into account along with constraint limitations. It was shown that the H_∞ algorithm has a superior performance compared to backstepping nonlinear approach and passive system in the justification of vehicle performance. A H_∞/GH_2 static output feedback approach was presented by Du and Zhang in [64]. In that approach, the H_∞ norm of ride performance transfer function was minimized while the generalized H_2 norm of performance constraints were restricted to be less than their hard limits to keep them in allowable region. Since the solution to that optimization was bilinear and difficult to obtain, they employed genetic algorithm to search for the possible control gain matrices.

Loop shaping is a design technique that offers a trade-off between system robustness and good performance. Choi et al [65] used Loop Shaping method to design a H_∞ control for a full vehicle model system.

4.2 Robust Control Theory

Robust control deals with the control of those dynamic systems with uncertain parameters and subjected to unknown disturbance inputs. The purpose is to find a fixed controller to achieve an acceptable system performance in the presence of uncertainties and disturbances. This controller has gained great attention among the researchers because of its ability in dealing with disturbance attenuation and frequency domain specifications.

Different methodologies and syntheses such as loop shaping and LQG are available, however, in terms of the disturbance rejection, H_∞ robust control is a better candidate. The main problem in H_∞ robust is the design of a stabilizing controller that minimizes or at least imposes an upper bound on the H_∞ norm of the closed loop transfer function from objective vector to disturbance inputs [66].

Optimal H_∞ Control: *find all acceptable controllers K(s) so that* $\left\| T_{zw} \right\|_\infty$ *is minimized.*

where $\left\| T_{zw} \right\|_\infty$ shows H_∞ norm of the transfer function between the objective vector and the disturbance inputs. By definition, H_∞ indicates the space of all complex valued functions that are analytic and bounded in the open right half of the complex plane and are bounded on the imaginary axis jR .

It should be noted that finding the minimized value of the H_∞ norm of a function is complicated both numerically and theoretically. However, in practice, it is not necessary to obtain an accurate optimal controller and thus it is usually much more realistic to find controllers that are very close to the optimal, which will be called suboptimal controllers.

Suboptimal H$_\infty$ Control: *Given $\gamma > 0$, find all acceptable controllers $K(s)$, if there are any, such that $\|T_{zw}\|_\infty < \gamma$*

The H$_\infty$ norm can be defined as the maximum gain of the closed-loop system frequency response to the sinusoidal inputs in the frequency domain [67]

$$\|T_{zw}(j\omega)\|_\infty = \sup_{\omega \in R} \bar{\sigma} |T_{zw}(j\omega)| < \gamma \qquad (4.4)$$

In time domain, it is equivalent to the upper bound on the energy (L_2) gain from disturbances (w) to the objective vector (z), for $w \in L_2$

$$\|T_{zw}\|_\infty = \sup_{w \neq 0} \frac{\|z(t)\|_2}{\|w(t)\|_2} < \gamma$$

Alternatively, the H$_\infty$ norm can be represented as

$$\int_0^T \|z(t)\|^2 dt < \gamma^2 \int_0^T \|w(t)\|^2 dt, \quad x(0) = 0, \quad \forall w \in L_2[o,T), \quad \forall T \geq 0$$

Usually the abovementioned suboptimal problem can be solved by the Riccati equations, however, Linear Matrix Inequality (LMI) is an alternative method which is widely used by researchers.

4.3   Linear Matrix Inequality

A linear matrix inequality is of the type

$$F(x) > 0$$

where F is a polynomial function mapping a finite dimensional vector space χ to the set $\kappa := \left\{ M \middle| \exists n > 0 \text{ such that } M = M^T \in R^{n \times n} \right\}$, of real symmetric matrices. The LMI is a convex constraint on x that means the set $\{x | F(x) > 0\}$ is convex.

Definition: Set C is convex if

$$x_1, x_2 \in C \Rightarrow x := \alpha x_1 + (1 - \alpha)x_2 \in C \text{ for all } \alpha \in [0,1]$$

Definition: The convex hull co(Ω) of a set Ω is the intersection of all convex sets containing Ω.

Unlike the special form of LMI, the wide variety of convex constraints on x can be represented by LMI. For example, linear inequalities, quadratic inequalities, matrix norm inequalities and constraints which are important in control theory such as Lyapunov and convex quadratic matrix inequalities can all be rearranged in the form of an LMI [69].

A powerful tool to cast most of mathematical problems in the form of LMI is Schur complement lemma.

Lemma(Schur complement): A given LMI

$$\begin{bmatrix} Q(x) & S(x) \\ S(x)^T & R(x) \end{bmatrix} > 0$$

where $Q(x)$ and $R(x)$ are symmetric matrices, and $S(x)$ depends polynomially on x, is equivalent to

$$R(x) > 0 \qquad Q(x) - S(x)R(x)^{-1}S(x)^T > 0$$

provided $R(x)^{-1}$ exists.

4.4 Linear Parameter Variable (LPV) Systems

In terms of the parameter variation of a system, the dynamic systems are divided in two groups. First group includes Linear Time Invariant (LTI) systems in which parameters are known and constant while in the second one, namely Linear Parameter Variable (LPV) systems, some parameters vary with time. It is obvious that there is difference between stability analysis of the LTI and LPV systems. According to the Routh-Hurwitz theorem, a LTI system is stable if all of its eigenvalues are located on the left hand side of the complex plane. However, the theory is not applicable for a LPV system. The Lyapunov functions are an alternative criterion for examining the stability of the LTV systems which is widely used by researchers. According to the Lyapunov stability theorem, the LPV system described as

$$\dot{x}(t) = A(t)x(t)$$

is stable if 1) there exists a quadratic Lyapunov function $V(x) = x^T P x > 0$, where x^T is the transpose of x, and P is a symmetric positive definite matrix (all eigenvalues of P are positive) with constant arrays. 2) The derivative of $V(x) < 0$ *i.e.*

$$\dot{V}(x) = x^T [A^T(t)P + PA(t)]x < 0$$

Accordingly, the LPV system is asymptotically stable if and only if there is a constant positive definite matrix such as P such that:

$$A^T(t)P + PA(t) < 0 \qquad \forall t \in R$$

As mentioned earlier, one of the main advantages of the robust control is its ability in dealing with system uncertainties. A system with uncertainties can be represented by a polytopic or norm-bounded characterization during control design procedure. Polytopic representation is a popular way to describe system parameter uncertainties without any conservatism. It is known that this presentation of uncertainties results in less conservative controller compared with norm-bounded representation. In this representation, the uncertain system belongs to a polytope which is the convex hull of finite set of model parameters (vertices).

Definition: A vertex is a point that is independent and can not be generated as the convex combination of two distinct points.

Every point p in a polytope P can be represented as the convex combination of the vertices of P as follows

$$p = \sum_{i=1}^{n} \xi_i p_i \qquad \sum_{i=1}^{n} \xi_i = 1, \qquad \xi_i \geq 0$$

The constraint set of ξ_i is called the unit simplex.

A LPV system in state-space form can be described as follows

$$\dot{x}(t) = A(t)x(t) + B(t)u(t)$$

where $A(t)$ and $B(t)$ include r time-varying parameters $m_i(t)$ ($i=1,\ldots,r$) which are bounded in their extreme values:

$$m_i^{min} \leq m_i(t) \leq m_i^{max}$$

Thus, the polytope representation of the system is as following

$$(A(t), B(t)) = \sum_{i=1}^{n} \xi_i (A_i, B_i), \qquad \xi_i \geq 0, \qquad \sum \xi_i = 1$$

where A_i and B_i are the vertices of the polytope. The aforementioned polytope is stable if and only if there exists a Lyapunov matrix $P>0$ such that

$$A_i^T P + P A_i < 0$$

Considering the control input $u(t)=Kx$, the LPV system is stable if and only if there is a Lyapunov matrix $P>0$ and

$$(A_i + B_i K)^T P + P(A_i + B_i K) < 0$$

4.5 H∞ State Feedback Formulation

A common approach used in robust vehicle suspension control formulation is that all requirements, including ride quality, rattle space constraint, and road holding ability are weighted and formulated in a single objective function. The purpose is to design a controller K so that the system is kept stable and the transfer characteristics from road disturbance input to the controlled output are minimized [49, 50, 60, 61]. On the contrary, in another formulation, the attempt is on minimization of H_∞ norm of the vehicle body acceleration from road disturbance while keeping the other requirements within the given bounds [57-59].

In vehicle suspension design, ride comfort, road holding ability, and suspension deflection are the main performance criteria. As mentioned already, it is well known that the RMS value of the acceleration response is a suitable measurement of ride quality.

Consequently, it is essential to keep the transfer characteristics from road irregularities to the chassis acceleration small. A measure of the road-holding ability of a vehicle, frequently used in the literature, is the contact force variation between the tire and ground which depends on the tire deflection (z_p-z_r). Accordingly, a vehicle has good stability if a strong contact force between the road and tire is held. However, in the case of the MacPherson suspension, the wheel motion is function of the control arm rotation as explained in Section 3.3 , and thus, a low rotation of the control arm results in a low vertical motion of the wheel and consequently a better road holding can be achieved. Therefore, in this study, the transfer function from road irregularities to the control arm rotation, θ, is chosen to quantify the road holding instead of that of the tire deflection. In addition, the relation derived for suspension deflection in Equation (2.21) shows that the suspension deflection is strongly a function of the control arm rotation. Thus, keeping the transfer function characteristics from road disturbance to the control arm rotation small results in having both superior tire contact and better suspension deflection. From a design view point, measuring the tire deflection is difficult or even impractical while measuring the control arm rotation is much easier.

In the suspension control techniques proposed in the literature, the lateral motion of the wheel and its rotational motions are ignored. It is explained in the next section that the vertical chassis displacement directly affects the performance of the wheel. Therefore, in formulating the controlled output vector, the state z_s should be incorporated to improve the wheel motion. In other words, it is important to keep the magnitude of the transfer function from road disturbance to the vehicle body small over the whole frequency range, the fact that was ignored in previous studies.

In relation to the abovementioned conditions, an H_∞ control problem is formulated in the following to deal with different objectives of the suspension control system. The dynamics of the system is described by the following system of equations

$$\dot{x}(t) = Ax(t) + B_1 f_{sa} + B_2 z_r,$$
$$z(t) = C_1 x(t) + D_1 f_{sa} \tag{4.5}$$

subject to input constraint

$$\left| f_{sa}(t) \right| \leq f_{sa,\max}$$

where $x(t)$, z_r, A, B_1 and B_2 are defined as (2.33) and

$$z(t) = \begin{bmatrix} \ddot{z}_s \\ z_s \\ \theta \end{bmatrix}, \quad C_1 = \begin{bmatrix} A(2,1) & A(2,2) & A(2,3) & A(2,4) \\ \lambda_1 & 0 & 0 & 0 \\ 0 & 0 & \lambda_2 & 0 \end{bmatrix}, \quad D_1 = \begin{bmatrix} B_1(1,1) \\ 0 \\ 0 \end{bmatrix} \tag{4.6}$$

In order to compromise the control objectives and normalize the controlled output vector, λ_1 and $\lambda_2 > 0$ which are scalar weights for suspension displacement and control arm rotation, respectively, are considered in the above formulation.

The value of m_s will change under different conditions such as mass transformation between the rear and front axles during acceleration or deceleration or due to passenger and load mass variations. Thus, it is important to take this uncertainty into account through control design procedure. To do that the procedure proposed in Ref. [68] is employed in the following. The system in Equation (4.5) is a function of the variable m_s given by

$$A(m_s) = \begin{bmatrix} 0 & 1 & 0 & 0 \\ \dfrac{\rho_1}{m_s} & 0 & \dfrac{\rho_2}{m_s} & 0 \\ 0 & 0 & 0 & 1 \\ \rho_3 & 0 & \rho_4 & 0 \end{bmatrix}, \quad B_1 = \begin{bmatrix} 0 \\ \dfrac{\rho_5}{m_s} \\ 0 \\ \rho_6 \end{bmatrix}, \quad B_2 = \begin{bmatrix} 0 \\ \dfrac{\rho_7}{m_s} \\ 0 \\ \rho_8 \end{bmatrix} \qquad (4.7)$$

where ρ_i ($i=1,\ldots,8$) are constant values obtained from system linearization.

Assuming that $m_{s_{min}} \le m_s \le m_{s_{max}}$, the above system can be described as [69]

$$(A(m_s), B_1(m_s), B_2(m_s), C_1(m_s), D_1(m_s)) = \sum_{i=1}^{2} \xi_i (A_i, B_{1i}, B_{2i}, C_{1i}, D_{1i}) \qquad (4.8)$$

$$\xi_i \ge 0, \qquad \sum \xi_i = 1$$

where $i = 1, 2$ stands for $m_{s_{min}}$ and $m_{s_{max}}$, respectively, and the values of ξ_1 and ξ_2 are equal

to $\left(\dfrac{1}{m_{s_{max}}} - \dfrac{1}{m_s}\right) \Big/ \left(\dfrac{1}{m_{s_{max}}} - \dfrac{1}{m_{s_{min}}}\right)$ and $\left(\dfrac{1}{m_s} - \dfrac{1}{m_{s_{min}}}\right) \Big/ \left(\dfrac{1}{m_{s_{max}}} - \dfrac{1}{m_{s_{min}}}\right)$, respectively.

Theorem 4.1 Consider the system (4.5) subject to changing m_s. The control signal $f_{sa} = Kx$, the gain matrix, K, shall be designed so that the resulting closed-loop system is asymptotically stable and the H_∞-norm from the road disturbance to the performance output, $z(t)$, is minimized. For the existence of such a control gain and for a given $\gamma > 0$, the necessary and sufficient conditions are equivalent to the existence of matrices $Q^T = Q$ and Y satisfying the following Linear Matrix Inequality (LMI):

$$\begin{bmatrix} A_i Q + Q A_i^T + B_{1i} Y + Y^T B_{1i}^T & B_{2i} & Q^T C_{1i}^T + Y^T D_{1i}^T \\ B_{2i}^T & -\gamma I & 0 \\ C_{1i} Q + D_{1i} Y & 0 & -\gamma I \end{bmatrix} \le 0, \quad i = 1, 2 \qquad (4.9)$$

in which the feedback gain is equal to $K=YQ^{-1}$.

Proof:

Suppose there is a quadratic function $V(x)=x^{\mathrm{T}}Px$, $P>0$ and $\gamma>0$ such that for all t

$$\frac{d}{dt}V(x)+z^{T}z-\gamma^{2}w^{T}w\leq 0 \quad \text{for all } x \text{ and } w \text{ satisfying (4.5)} \qquad (4.10)$$

where z is defined in Equation (4.6) and w represents disturbance vector which in this case is road disturbance z_r. Then the Equation (4.9) is satisfied. To show this, we integrate (4.10) from 0 to T, assuming that $x(0)=0$, to obtain

$$V(x(T))+\int_{0}^{T}(z^{T}z-\gamma^{2}w^{T}w)dt\leq 0 \qquad (4.11)$$

Since $V(x(T))\geq 0$, one has

$$\frac{\|z\|_{2}}{\|w\|_{2}}\leq \gamma \qquad (4.12)$$

Condition (4.12) is equivalent to LMI (4.9). To show this, again consider quadratic function $V(x)=x^{\mathrm{T}}Px$, with symmetric matrix $P>0$. Thus,

$$\frac{d}{dt}V(x)=\frac{d}{dt}x^{T}Px=\dot{x}^{T}Px+x^{T}P\dot{x} \qquad (4.13)$$

Substituting the value of $\dot{x}(t)$ from Equation (4.5) with assumption $w=z_r$ and $f_{sa}=Kx(t)$, Equation (4.13) is equal to

$$\frac{d}{dt}V(x)=x^{T}(A+B_{1}K)^{T}Px+x^{T}P(A+B_{1}K)x+w^{T}B_{2}^{T}Px+x^{T}PB_{2}w \qquad (4.14)$$

In addition,

$$z^T z = x^T (C_1 + D_1 K)^T (C_1 + D_1 K) x \qquad (4.15)$$

Thus, the Equation (4.13) is equivalent to

$$x^T (A + B_1 K)^T P x + x^T P (A + B_1 K) x + w^T B_2^T P x + x^T P B_2 w + x^T (C_1 + D_1 K)^T (C_1 + D_1 K) x - \gamma^2 w^T w \leq 0$$

$$(4.16)$$

Defining $\zeta(t) = [x^T(t) \quad w^T(t)]^T$, the matrix form of the above equation is shown as follows

$$\zeta^T(t) \begin{bmatrix} (A + B_1 K)^T P + P(A + B_1 K) + (C_1 + D_1 K)^T (C_1 + D_1 K) & P B_2 \\ B_2^T P & -\gamma^2 I \end{bmatrix} \zeta(t) \leq 0 \qquad (4.17)$$

Therefore, the following inequality should be satisfied

$$\begin{bmatrix} (A + B_1 K)^T P + P(A + B_1 K) + (C_1 + D_1 K)^T (C_1 + D_1 K) & P B_2 \\ B_2^T P & -\gamma^2 I \end{bmatrix} \leq 0 \qquad (4.18)$$

By defining the new variables $Q^{-1} = P$ and $Y = KP$ and transformation matrix

$$T = \begin{bmatrix} Q & 0 \\ 0 & I \end{bmatrix} \qquad (4.19)$$

the inequality (4.18) will be

$$T \begin{bmatrix} (A + B_1 K)^T P + P(A + B_1 K) + (C_1 + D_1 K)^T (C_1 + D_1 K) & P B_2 \\ B_2^T P & -\gamma^2 I \end{bmatrix} T^T \leq 0 \qquad (4.20)$$

which is equal to

$$\begin{bmatrix} Q(A+B_1K)^T + (A+B_1K)Q + Q(C_1+D_1K)^T(C_1+D_1K)Q & B_2 \\ B_2^T & -\gamma^2 I \end{bmatrix} \leq 0 \qquad (4.21)$$

By using Schur complement and redefining $Q=(1/\gamma)Q$, the above inequality is equivalent to

$$\begin{bmatrix} QA^T + Y^T B_1^T + AQ + B_1Y & B_2 & QC_1^T + Y^T D_1^T \\ B_2^T & -\gamma I & 0 \\ C_1Q + D_1Y & 0 & -\gamma I \end{bmatrix} \leq 0 \qquad (4.22)$$

It should be pointed out that the force range which is generated by a semi-active actuator (damper) is limited and the force saturation constraint should be integrated in the control design. Thus, the matrices Q and Y in Equation (4.9) should satisfy the LMI which explains the saturation constraint as following [69],

$$\begin{bmatrix} f_{sa,max}^2 & Y \\ Y^T & Q \end{bmatrix} \geq 0 \qquad (4.23)$$

The matrices Q and Y can be obtained from the solution to the following minimization problem

$$\min_{\gamma, Q=Q^T, Y} \gamma \quad \text{subject to LMIs (4.9) and (4.23)} \qquad (4.24)$$

Subsequently, a state feedback control law with $K=YQ^{-1}$ can be obtained by solving the above convex optimization problem. In order to solve the above-mentioned LMI, SeDuMi LMI solver which is a MATLAB tool box that has been developed by the Advanced Optimization Lab of McMaster University is used. Based on the afore-

mentioned data and by setting λ_1 and λ_2 equal to 2500 and 250, respectively, the control gain matrix obtained from Equation (4.24) is equivalent to

$$K = 10^4 \times [-3.7027 \quad -0.6685 \quad 0.4781 \quad 0.0241] \quad \text{and} \quad \gamma^* = 71.9$$

4.6 H∞ Output Feedback Formulation

A main drawback of the state feedback controller designed in previous section needs either full state measurements or the estimation of partial states of the system. While the former increases the design cost, the latter has difficulties in both the controller design and its implementation. In order to address this problem, the use of the output feedback control theory appears to be a reasonable solution.

The main focus of this section is on the design of a modified sky-hook control for a semi-active MacPherson suspension system by means of H_∞ Output Feedback Control (OFC) theory. The combination of a Linear Matrix Inequality (LMI) solver and Genetic Algorithm (GA) is adopted to regulate the static output feedback control gain so that the stability conditions are fulfilled and control objectives are achieved.

Consider the dynamic system and the objective vector, $z(t)$ shown in Equation (4.5) in which the damping force changes based on the output measurements as

$$f_{sa} = Ky(t) = KCx(t) \tag{4.25}$$

where K is the gain control vector and C is defined as follows

$$C(t) = \begin{bmatrix} 0 & 1 & 0 & 0 \\ 0 & 0 & 0 & 1 \end{bmatrix}$$

97

Considering the mass uncertainty, the objective of this controller design is to find a suitable gain controller, K, such that the closed-loop polytopic system is robustly stable and the H_∞-norm of the transfer function from road disturbances to the objective vector is minimized.

Theorem 4.2 The above closed-loop polytopic system is robustly stable, with minimum H_∞-norm, if the following constraint holds:

Minimize γ subject to $P > 0$ and

$$\begin{bmatrix} P(A_i + B_iKC)^T + (A_i + B_iKC)P & PB_{1_i} & (C_{1_i} + D_{1_i}KC)^T \\ B_{1_i}^T P & -\gamma^2 I & 0 \\ (C_{1_i} + D_{1_i}KC) & 0 & -I \end{bmatrix} < 0 \qquad (4.26)$$

The proof of the abovementioned LMI is analogous to proof of the LMI (4.9). However, since the above optimization problem is bi-linear due to multiplication of the optimization parameters P and K in LMI (4.26), there is no analytical solution to that optimization problem. Hence, the Genetic Algorithm (GA) is adopted to find the optimization solution according to GA stochastic search capability.

4.6.1 GA/LMI Algorithm

GA is a stochastic search method and is based on the principles of natural selection and genetic modification. It has shown great potential in global optimization in different controller synthesis problems. This approach of optimization runs on a population of points (individuals). Each of the individuals belonging to the population is considered as a possible solution of the optimization problem. By evaluating the individuals based on

their fitness, indicating how well an individual solves the optimization problem, the rough individuals will be eliminated in the next population generation.

GA launches the optimization process with random selection of the population. The genetic operators such as *selection, crossover,* and *mutation* deal with the transition of one population to the next generation. In the selection phase, the fittest individuals will be picked to go to the next population. Using crossover, the genetic material of two individuals will be exchanged in order to create two new individuals. Mutation operates some changes on the genetic properties of an individual arbitrary. The genetic algorithm and its operators continue until a satisfactory solution of optimization problem is achieved. The process is terminated when a predefined stop condition, i.e., a certain number of generations, is reached [70].

In the following, a combination of the feasible solution of the LMI (4.26) and the GA is employed to tune the controller gains by minimizing the H_∞ norms of the transfer functions. The approach proposed in Ref. [71] is applied in this section to design a static–output feedback controller with minimized H_∞ norms of the transfer functions.

The outline of the GA used in this work is detailed as follows. It is noted that if the controller gain, K, is known, the LMI (4.26) will be linear and can be solved easily by LMI solver in MATLAB. Thus, using the GA MATLAB Toolbox, a random set of the controller gains will be selected. However, each controller needs to satisfy the stability requirements. If the controller gain satisfies the stability conditions, then, the minimization problem (4.26) will be solved by the LMI solver and the resulting γ will be assigned as the value of the cost function of the GA. Otherwise, if the closed-loop system

is unstable or the feasible solution of the LMI can not be found, a large number will be considered for the cost function in order to reduce its chance to exist in the next generation.

In addition, the closed-loop vertex subsystems and the closed-loop nominal system must be strictly Hurwitz [71]. Therefore, the sketch of the minimization loop is as the following:

$$
\begin{cases}
\text{Call the gains } K = \left[k_1, \ k_2\right] \text{from MATLAB GA Toolbox} \\[2ex]
\quad \text{if } \mathrm{Re}_{\max}(\lambda(\overline{A}_N)) < 0 \\[2ex]
\quad\quad \text{if } \max_{i=1,2}\left\{\mathrm{Re}_{\max}(\lambda(\overline{A}_i))\right\} < 0 \\[2ex]
\quad\quad\quad \text{if } \ 0 < k_1 < 4000 \quad 100 < k_2 < 600 \\[2ex]
\quad\quad\quad\quad \text{Solve the LMI optimization problem} \\[2ex]
\text{else} \\[2ex]
\quad\quad\quad\quad \text{Assign a large number to the cost function} \\[2ex]
\text{end}
\end{cases}
$$

Here, λ is an eigenvalue of the matrix. $\overline{A}_i$ denotes the closed-loop vertex subsystem while $\overline{A}_N = A_{\underline{\Sigma}} - B_{1\underline{\Sigma}}KC$ is the closed-loop nominal system, in which $A_{\underline{\Sigma}} = (1/r)\sum_{i=1}^{r=2} A_i$ and $B_{1\underline{\Sigma}} = (1/r)\sum_{i=1}^{r=2} B_{1i}$ stand for the nominal system matrix and the nominal input vector, respectively. The above algorithm continues until the minimum of the cost function γ is found and, consequently, an acceptable controller gain is achieved.

The elements of the control gain in the above algorithm are limited between certain values to avoid passing the actuator saturation.

4.6.2 Controlled Damping Force

After obtaining the optimized controller gain, the desired damping force is expressed in the form

$$f_d = k_1 \dot{z}_s + k_2 \dot{\theta} \tag{4.27}$$

Based on the Equation (3.13), the angular velocity of the control arm, $\dot{\theta}$, is related to the relative velocity of the suspension, $\Delta L = \dot{z}_D - \dot{z}_C$, as:

$$\dot{\theta} \approx -\frac{\Delta \dot{L}}{L_A \cos(\theta_1)} \tag{4.28}$$

Thus, by substituting Equation (4.28) in Equation (4.27), the damping force is expressed as:

$$f_d = k_1 \dot{z}_s - \frac{k_2}{L_A \cos(\theta_1)} \Delta \dot{L} \tag{4.29}$$

On the right hand side of the above equation, the first term shows the sky-hook damping force while the second is a passive damping force. In fact, the force derived by means of H_∞ output feedback control theory is a combination of the sky-hook and passive damper forces with optimized coefficients in accordance with suspension requirements.

The simplicity and cost reduction are the two main advantages of the proposed controller. It is noted that the absolute vertical velocity of the vehicle body can be measured by integrating the accelerometer signals. Hence, this controller takes feedback of two data

which are easily measurable. Moreover, its performance is more robust to the system uncertainties compared to the other controllers. The benefits of the controller compared to other popular types of semi-active control strategies were discussed in Section 3.3.

Remark: The purpose of the semi-active control suspension system is to regenerate the desired damping force obtained from the controller by a semi-active damper located between the wheel and the chassis. However, the issues regarding the semi-active damper dynamics and the force tracking are not discussed in this chapter and will be addressed in the next chapter.

In order to analyze the control performance, two cases are considered. In the first case the parameters λ_1 and λ_2 are set equal to 1000 and 100, respectively, with focus on the ride quality while in the second one they are set equal to 1500 and 500, respectively, with focus on both the ride quality and tire grip. The obtained minimized γ^* and optimal gains are presented in Table 4-1.

Table 4-1 Controller specifications

	γ^*	Optimal Gains	Focus
Case 1	32.28	(2400, 100)	Ride quality
Case 2	39.99	(1500, 500)	Stability

The main parameters used for the GA are the population size of 50, the crossover fraction of 0.8, the maximum generation of 100, and Gaussian mutation function.

4.7 Evaluation of Controller Performances

Using the optimized controller gains from full state feedback controller (K), and output feedback controller (K1 and K2) the vehicle performance and stability are evaluated in

this section for different road disturbances such as potholes and random inputs. As mentioned earlier, the function of these controllers are to improve the ride quality while keeping the stability limitations within acceptable domain. In addition to that, the suspension kinematic performance subjected to those controllers is evaluated.

4.7.1 Bump response

The properties of the bump road disturbance are the same as that mentioned in Section 3.3. Different aspects of the dynamic and kinematic suspension performances when subjected to this input are illustrated through Figure 4.2 to Figure 4.5. In terms of the dynamic performance, the simulation results indicate that the improvement in the full state feedback acceleration response is less than that of the output feedback controller (K1) whereas improvement in other performances is much better. Regarding ride quality, K1 shows the best effectiveness of the system by reducing PTP and settling time values of the acceleration response compared to the other systems. However, K reduces the PTP value of the vertical displacement, the control arm rotation and suspension deflection.
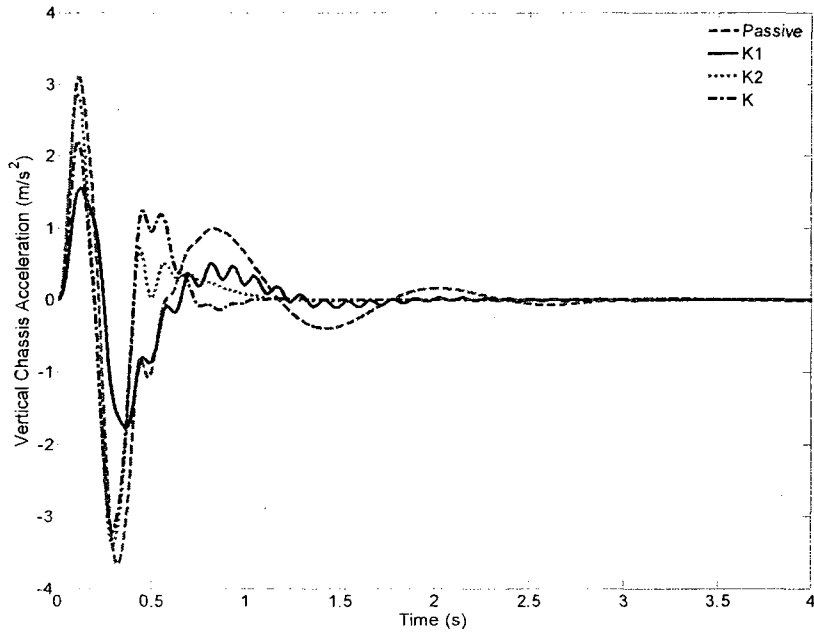
Figure 4.2 Vehicle vertical acceleration response subject to bump disturbance

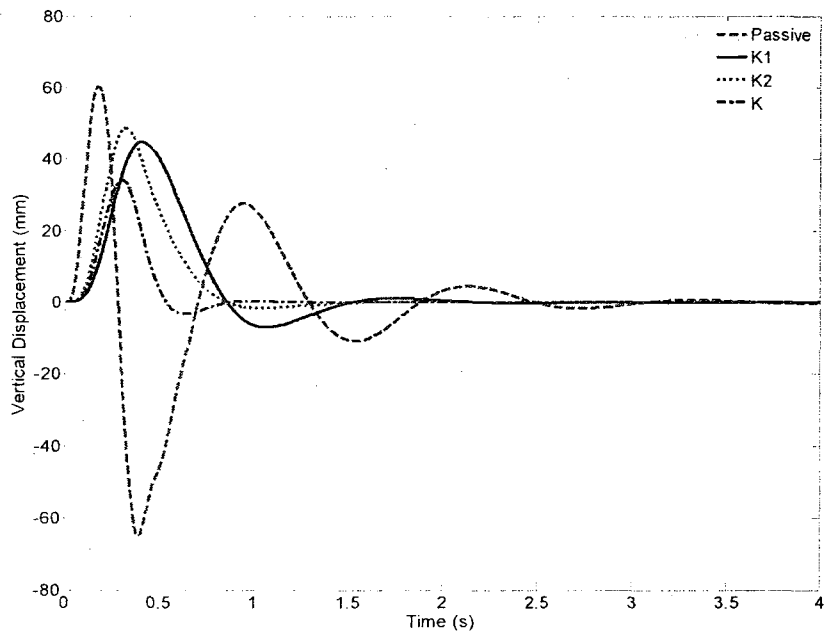**Figure 4.3 Vehicle vertical displacement subject to bump disturbance**
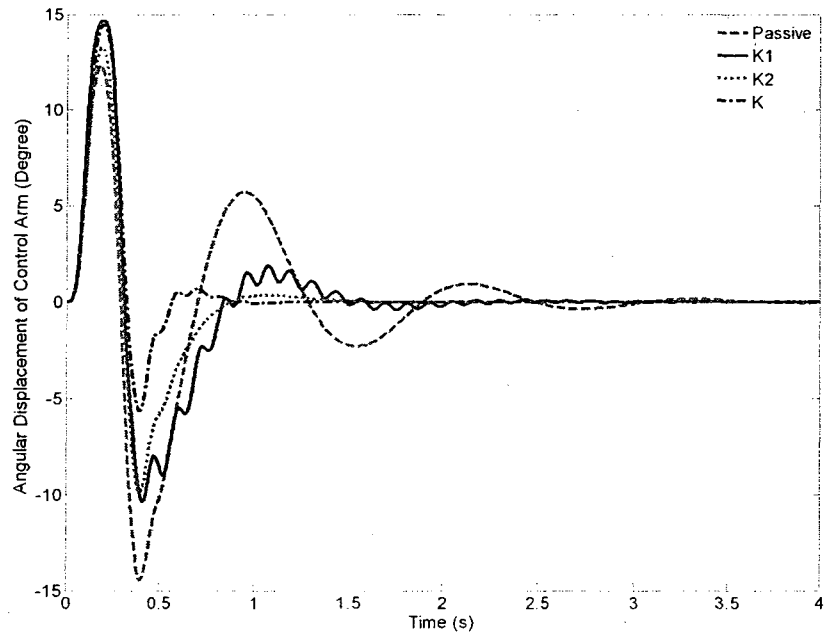
104

Figure 4.4 Control arm rotation subject to bump disturbance
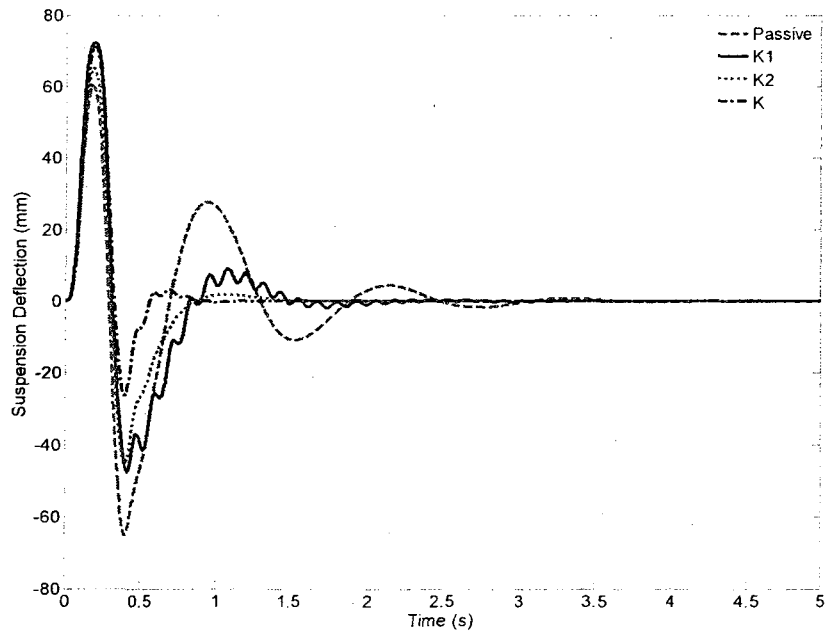

Figure 4.5 Vehicle suspension deflection subject to bump disturbance

In terms of the kinematic performance, all controllers modify the alteration of the kinematic parameters. Figure 4.6 shows the wheel camber angle alteration. As shown in

this figure, all controllers reduce the PTP and settling time of the camber angle significantly compared to the passive system resulting in longer tire life and superior stability. Figure 4.7 illustrates the wheel toe angle alteration. It should be noted that the variation of this parameter plays an important role in vehicle stability and even small reduction of this parameter could affect vehicle stability positively. The toe angle variation is modified by the all systems well; however, the parameter K shows a lower PTP and settling time. K1 reduces those values as well at the expense of introducing some chattering to the performance. Regarding the track width alteration, Figure 4.8 shows that K improves the performance of this parameter significantly compared to other control systems and passive one by reducing the PTP value and diminishing the oscillation. Although K1 reduces the PTP value of this parameter close to that of K, the chattering of the response may affect both the vehicle stability and tire performance. The caster and king-pin angles variation are plotted in Figure 4.9 and Figure 4.10. As mentioned already, these parameters are important in steering. From these figures, it can be seen that although K reduces the PTP values of these two parameters well, K2 makes the trend of these two parameters sluggish thereby making vehicle steering easier. In addition, K and K2 reduce the variation of the parameters well. It should be noted that the sluggish trend of these two angles gives more time to the driver to handle the vehicle. However, K1 introduces some chattering causing discomfort in steering. As a result, all controllers improve the vehicle performance well in which full state feedback controller has the superior improvement and output feedback controllers have a performance between that of passive and the full state feedback controller systems. As shown in the above figures, different controllers can affect the handling performance differently.
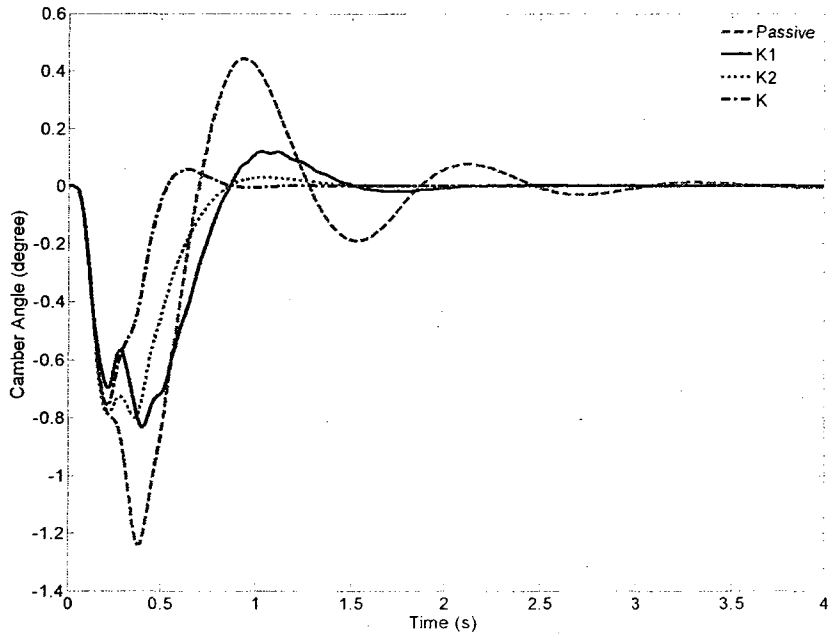
Figure 4.6 Camber angle alteration subject to bump disturbance
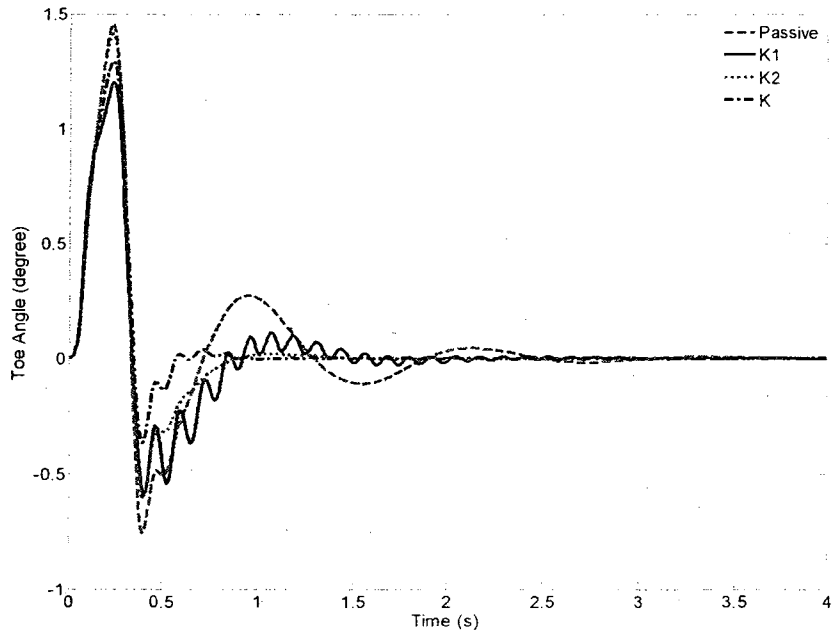
Figure 4.7 Toe angle alteration subject to bump disturbance
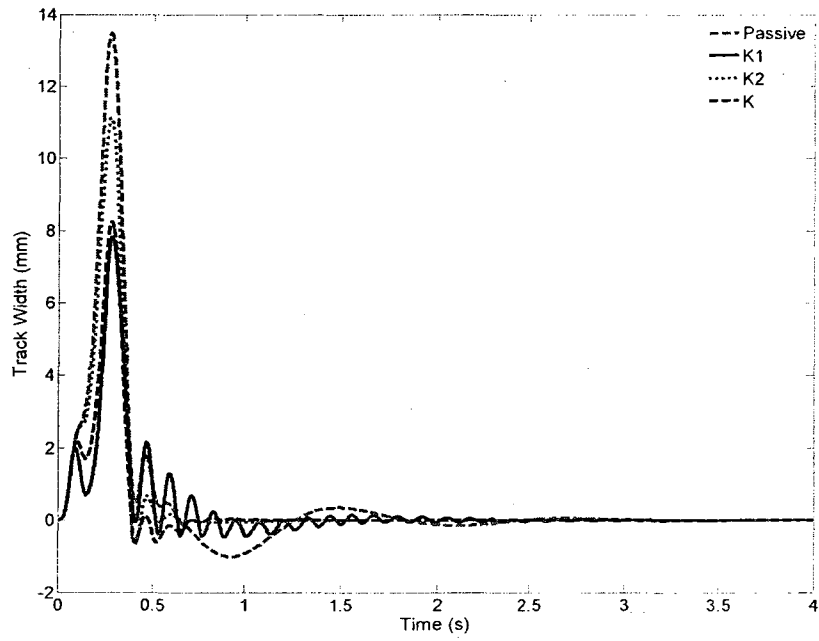
Figure 4.8 Track width alteration subject to bump disturbance
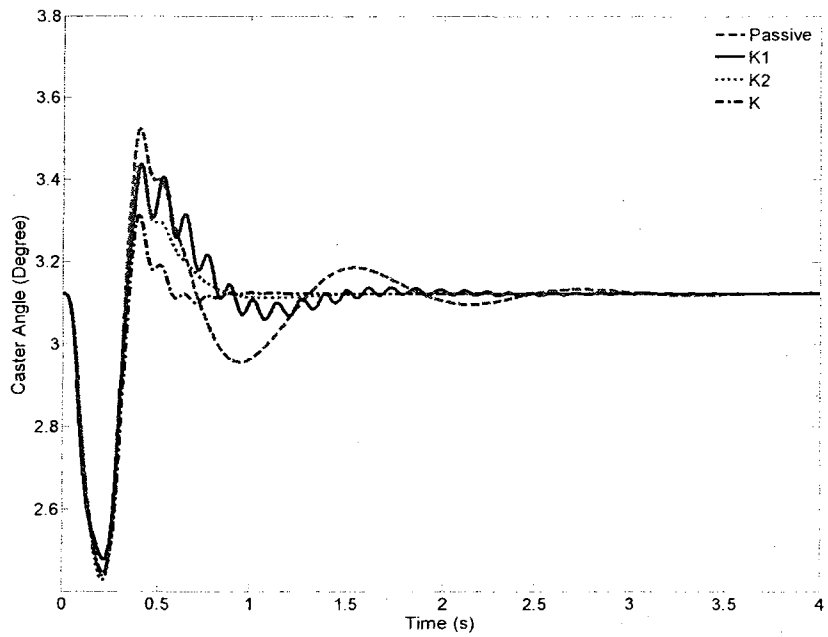
Figure 4.9 Caster angle alteration subject to bump disturbance

108
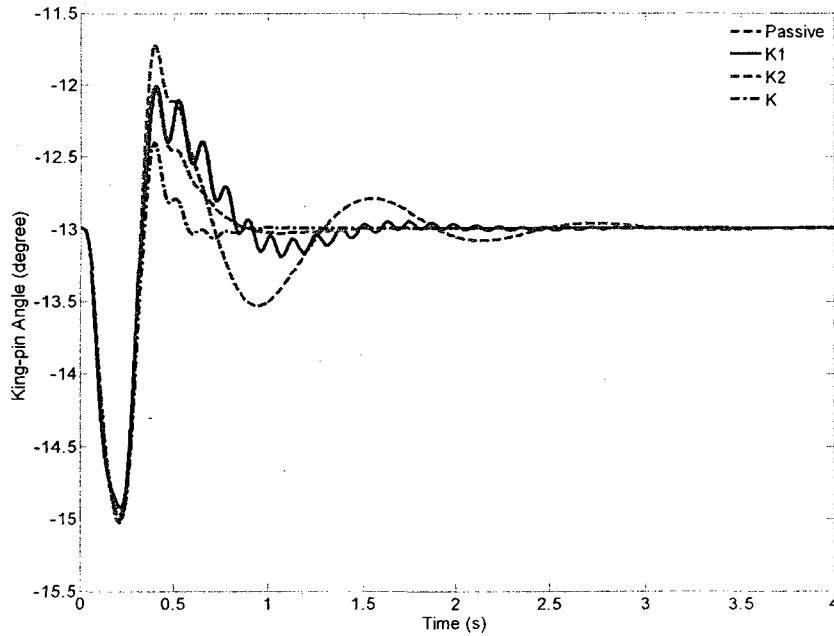
Figure 4.10 King-pin angle alteration subject to bump disturbance

4.7.2 Random road disturbance

The road disturbances to which the vehicle is subjected to are typically expressed as a random process with a ground Power Spectral Density (PSD) of

$$
S_g(\Omega) = \begin{cases} S_g(\Omega_0)\left(\dfrac{\Omega}{\Omega_0}\right)^{-n_1} & \text{if } \Omega \le \Omega_0 \\[4mm] S_g(\Omega_0)\left(\dfrac{\Omega}{\Omega_0}\right)^{-n_2} & \text{if } \Omega \ge \Omega_0 \end{cases}
\tag{4.30}
$$

Here $\Omega_0 = 1/(2\pi)$ is considered. Using the spectral representation method [72], the road irregularities can be simulated with the following series, assuming that forward velocity of the vehicle, V, is constant,

$$
z_r = \sum_{n=1}^{N_f} s_n \sin(n\omega_0 t + \varphi_n)
\tag{4.31}
$$

Here $s_n = \sqrt{2S_g(n\Delta\Omega)\Delta\Omega}$ and $\Delta\Omega = 2\pi/L$ where L is the length of the road segment. In addition, $\omega_0=(2\pi/L)V$ and φ_n are treated as random variables, with a uniform distribution in the interval $[0, 2\pi)$. Assume that $S_g(\Omega_0)=256\times10^{-6}$ m^3, $n_1=2$, $n_2=1.5$, V = 120 Km/h and L=100 m. Using the above formula, an example of the typical road profile, belonging to the poor quality, is generated and shown in Figure 4.11.
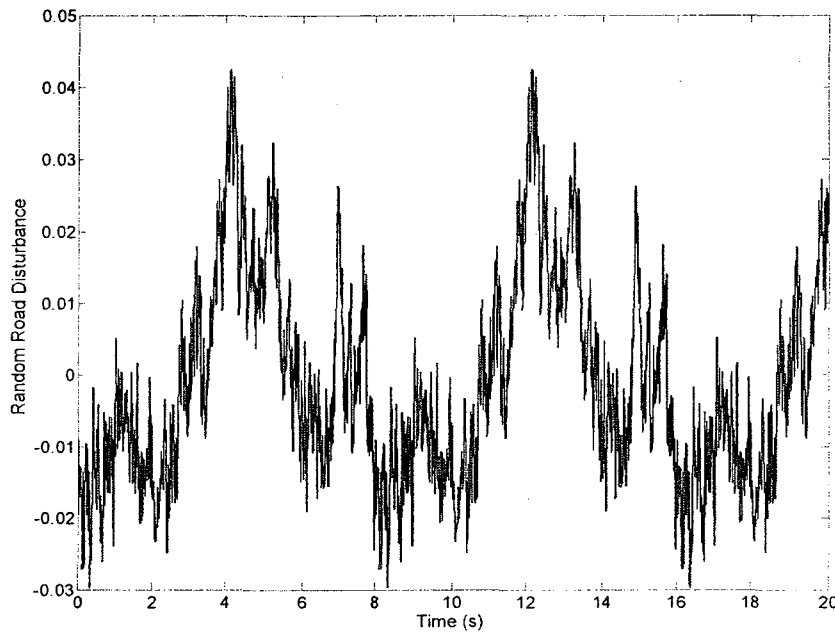
Figure 4.11 Example of poor road profile

The RMS values of the acceleration response, $\ddot{z}_s$, the control arm rotation, θ; the suspension deflection, and the kinematic parameters subject to random irregularities for vehicle forward velocities V=60 Km/h and V=120 km/h are calculated and summarized in Table 4-2 and Table 4-3, respectively. Referring to those tables, it can be seen that K1 improves the ride quality well compared to other systems at the expense of the deterioration of the suspension deflection and angular displacement of the control arm. Full state feedback controller, K, improves the ride quality reasonably well compared to that of the passive system while it keeps the control arm rotation and suspension

deflection close to those of passive system. However, K2 keeps the dynamic performance close to that of the passive system. It can be seen from these tables that all the controllers reduce the camber angle variation well, especially K, while deteriorating the toe angle. Track width alteration is modified by K and K2 only slightly whereas it is deteriorated by parameter K1. The contribution of controllers on the performances of the caster and king-pin angles is negligible.

Table 4-2   RMS values of the performance parameters subject to rough road disturbances and forward velocity V=60 km/h

	K1	K2	K	Passive
Acceleration(m/s^2)	0.73	1.13	0.94	1.10
Control arm rotation (degree)	3.97	2.05	2.54	2.46
Suspension Deflection (mm)	18.89	9.74	12.03	11.70
Camber angle (degree)	0.22	0.22	0.11	0.26
Toe angle (degree)	0.41	0.25	0.31	0.25
Caster angle (degree)	3.15	3.13	3.15	3.13
Kingpin angle (degree)	12.96	12.97	12.92	12.98
Track width (mm)	2.78	2.01	2.07	2.05

Table 4-3 RMS values of the performance parameters subject to rough road disturbances and forward velocity V=120 km/h

	K1	K2	K	Passive
Acceleration(m/s^2)	0.90	1.36	1.14	1.33
Control arm rotation (degree)	4.90	2.50	2.92	2.93
Suspension Deflection (mm)	23.34	11.89	13.96	13.97
Camber angle (degree)	0.24	0.21	0.13	0.29
Toe angle (degree)	0.49	0.28	0.33	0.28
Caster angle (degree)	3.14	3.12	3.13	3.12
Kingpin angle (degree)	12.99	13.01	12.99	13.02
Track width (mm)	2.98	2.10	2.08	2.37

4.8 Vehicle Body Roll Centre

As mentioned in Section 2.6.5, the vehicle roll centre should be designed close to the ground in order to have superior roll stability at the cost of kinematic performance deterioration especially that of toe angle and track width. According to the results explained in previous section, it is possible to improve the kinematic performance of the MacPherson suspension by semi-active control strategies. Based on these results, it would be possible for suspension designer to design the roll centre so that better vehicle

stability during the cornering is achieved while modifying the kinematic performance by an appropriate control strategy.

4.9 Summary

Many control strategies have been developed to improve overall vehicle performance, including both ride quality and stability conditions. However, most studies have used a simple quarter vehicle model for control design, where the effect of the controller on the wheel motions affecting handling and stability of a vehicle is ignored. In the present chapter, the new dynamic model of the MacPherson suspension system has been employed to design a full state H_∞ robust control for ride quality and stability condition enhancement using new states of the system. In addition, the theory of H_∞ output feedback control has been employed to optimize the control gains of the modified sky-hook controller according to suspension objectives.

Using three-dimensional kinematic model of the MacPherson suspension, the effects of the controller on the wheel motions such as the camber and toe angles as well as the track width alterations have been investigated. The simulation results showed that both proposed robust designs provide superior kinematic and dynamic performances compared to the passive system. However, the H_∞ output feedback control has significant benefits compared to the full state feedback controller due to its simplicity and practical implementation.

CHAPTER 5

HARDWARE-IN-THE-LOOP SIMULATION AND ANALYSIS

The last phase of the research involves the current generation for tuning the actuator and producing desired force developed by the controller. A mathematical inverse model of the MR damper is developed to tune the current (voltage) signal so as to track the desired damping force generated by the controller unit. In order to do this, experiments are conducted to characterize the Magneto-Rheological damper. Using the measured data and the least squares method a mathematical model of MR damper is developed to estimate the required current supply. The effectiveness of the damper model is demonstrated for different road input irregularities by integrating Hardware-In-the-Loop Simulation (HILS) procedure.

5.1 Introduction

Magneto-Rheological (MR) dampers have gained increased attention in vibration attenuation in different applications such as bridges, helicopter rotors, and suspension seats. Analytical and experimental studies have demonstrated the superior performance of MR dampers in vehicle suspension application compared to conventional hydraulic dampers [8, 41, 45, 50, 53, 73, 74, 79].

In a MR damper, Magnetorheological fluid, comprising of micron sized particles of iron which are suspended in the oil, are used instead of oil. In this type of dampers, the damping coefficient (viscous characteristics) of the damper will be changed whenever a polarization induced in suspended particles occurs. The MR damper is categorized as a

continuously controlled semi-active damper. Unlike fully active hydraulic actuators, the MR damper provides a variable damping force with low power requirements. Fast reaction time, usually less than 2 milliseconds, and very low power requirement (on the average, 3W per shock) are the main advantages of MR dampers. At the same time, having a high minimum damping coefficient is its disadvantage [7]. However, rapid variation in damping properties and desired performance which is in between that of passive and fully active device with a reliable fail-safe manner by providing adequate damping in the case of the control hardware malfunction makes this actuator applicable in the vehicle suspension systems.

In reality, due to high nonlinearities the generated force depends on the motion of the actuator in addition to the command force, and the actuator dynamics plays a significant role in the control design algorithm. Moreover, the input signal of the actuator is current or voltage and, hence, it is important to tune current (voltage) signal so that the command force from control unit can be achieved accurately.

In order to tune the current (voltage), three main control feedback systems are proposed in the literature. The first approach (A_1) considers the combination of the dynamics of the actuator and chassis together and tries to generate a proper current so that the objectives are obtained [75, 76]. However, as mentioned before, the dynamic behaviour of a semi-active actuator such as MR damper is highly nonlinear and developing its accurate dynamic model for control purposes is not a trivial task. This shortcoming increases the control complexity and deteriorates practical performance of the system. Figure 5.1 represents the block diagram of this control system.
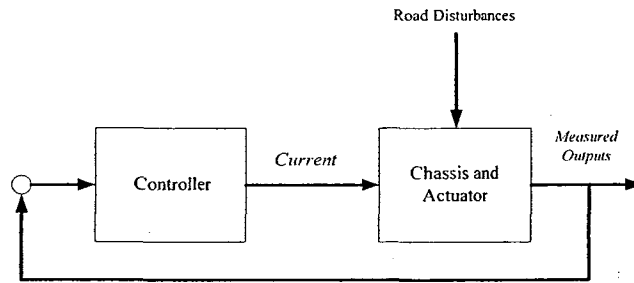
Figure 5.1 The block diagram of the first approach to control ride quality

The second approach (A_2) isolates the dynamics of the actuator from the plant and generates the required current signal using an internal controller. Proposed in references [77, 78], A_2 includes two loops in which one produces desired force for suspension control and the other one is created to track the command (desired) force and to take care of actuator nonlinearities. Figure 5.2 shows the block diagram scheme of this control suspension system. In this figure, while the outer controller generates the desired force based on the suspension control objectives, the duty of the inner controller is to track the command force by actuator. For this approach an extra sensor is required for each wheel to measure the force produced by the actuator resulting in increasing design cost. In addition, this sensor is sensitive to noise and may deteriorate the effectiveness of the whole control system.
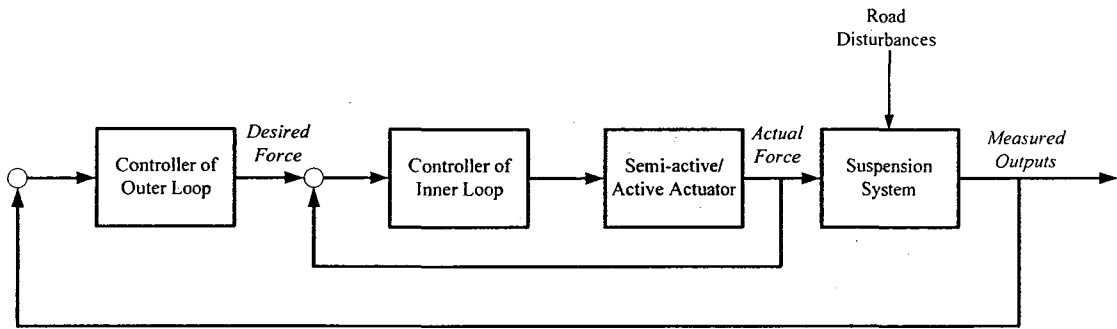
Figure 5.2 The block diagram of the second approach to control ride quality
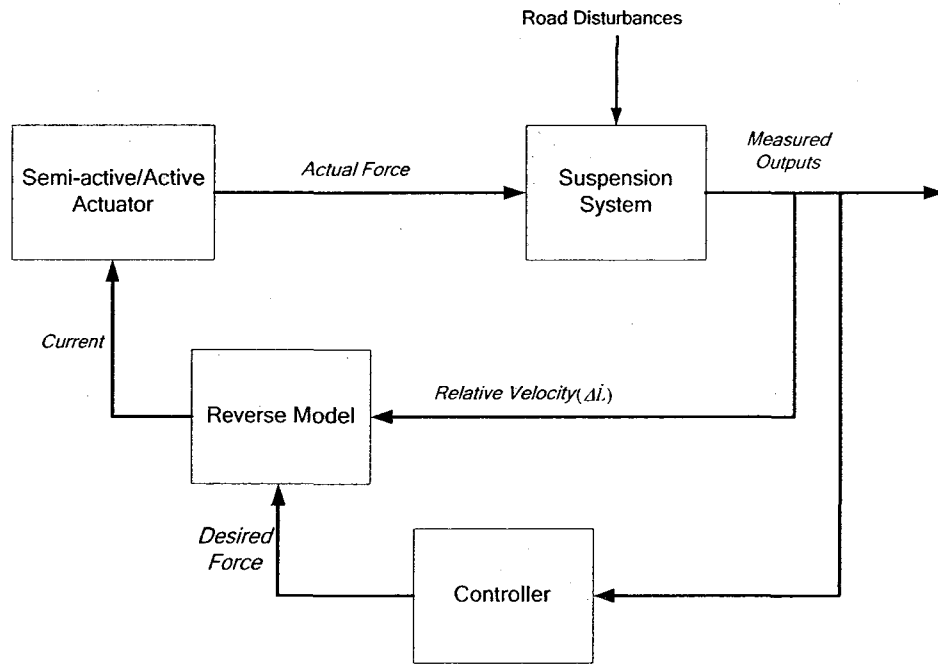
Figure 5.3 The block diagram of the third approach of ride quality control

In order to isolate the nonlinearities of the actuator from ride control design and simultaneously generate current input without measuring output force, a third control approach (A_3) was proposed in References [50, 65, 80].

Figure 5.3 illustrates the block diagram of this control architecture. In this approach, in order to improve the ride quality and stability of the vehicle, a desired control force is

117

developed by a proper control strategy. The generated desired force then will be input to an inverse model of the actuator such as MR damper. In this approach, the nonlinearities of the actuator are isolated from ride control design and also the cost of design is reduced. These two main advantages make this approach applicable in the car suspension systems compared to the two previous approaches.

5.2 Experiment Approach

Two main obstacles in the practical usage of the MR damper for control applications are its inherent hysteresis and highly nonlinear dynamics. Thus, the modelling of MR dampers is really important for accurate analysis. Different models such as Bouc-wen hysteresis model [81], fuzzy model [82], visco-elastic model [83], polynomial model [84], and neural network model [85-87] are developed to predict the dynamic performance of a MR damper. Although the models represent the MR damper behaviour reasonably well, they include a highly nonlinear formulation with many parameters required to be identified.

In order to cope with the MR damper modelling, and to save the cost and time of development, Hardware-In-the-Loop (HIL) simulation method is used in the laboratory to evaluate the performance of the MacPherson MR suspension system. Easy adjustment of the parameter and low-cost test facilities are main advantages of this method compared to a full car setup in the laboratory. The HILS comprises three parts including interface, hardware, and software. In the software part, a simulation of the controlled MacPherson suspension system under road disturbances is performed using MATLAB/SIMULINK environment. The relative velocity of MR damper and desired force, obtained from controller, are achieved as the input signal of the hardware part. In the hardware part, the

required current for damping changes is amplified and force generated by MR damper is measured from hydraulic tester and fed back into computer simulation. The hardware and software parts communicate to each other in a real-time manner through the dSPACE interface. A schematic of the experiment is shown in Figure 5.4.

As shown in the Figure, the software portion includes the MacPherson suspension model, control algorithm, and the inverse model of the MR damper. The hardware part involves the MR damper, a servo-hydraulic vibration test system, a power supply for the damper, and a force sensor for acquiring the damper force signal. The interface component connects the hardware and software portions through DSP processor and I/O boards. More details regarding the experiment components and methodology may be found in Reference [88].
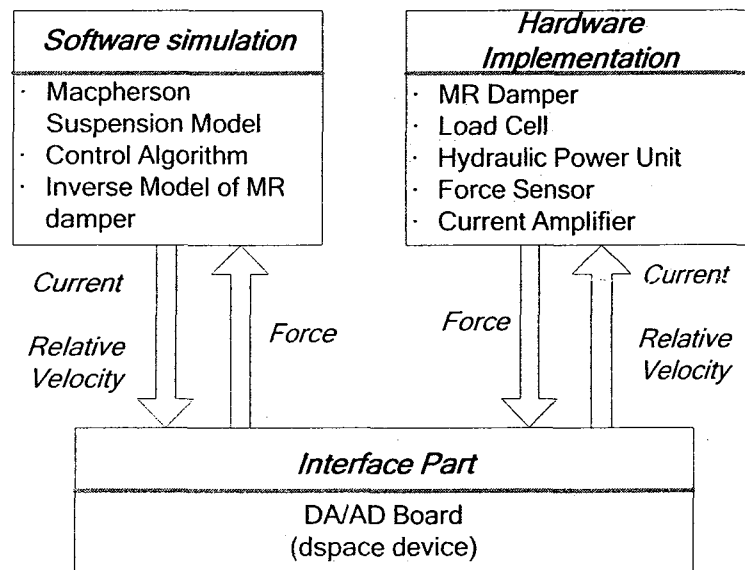

Figure 5.4 Schematic diagram of the HILS for the MacPherson MR suspension system

5.3 MR Damper Characterization

A *CARRERA*^{TM} *MagnetoShock*^{TM} MR damper is considered for the control performance evaluation of the current work. The physical characteristics of the damper may be found on the company website [89]. The principal objective is to develop an inverse mathematical model of the MR damper. Different experiments are conducted in the following to characterize the MR damper performance precisely. It is known that the damping characteristics of a MR damper is highly related to the excitation and input current. Using the HILS, different simulations are carried out under different excitations and current signals so as to assess and develop a mathematical formulation of dynamic performance of the MR damper. Because of the limited stroke of the candidate MR damper and its current signal capacity, the travel of the suspension system and the control current signal are limited to 762 mm and 1.5 Amp, respectively, to ensure safety of the test system and the damper. In addition, the harmonic inputs with different amplitudes and frequencies are considered as excitations to the MR damper. Laboratory tests are conducted to characterize the force-velocity properties and time response performance of candidate MR damper over a wide range of excitation condition.

In this experiment, the MR damper is placed on an electro-hydraulic vibration exciter in which the top frame is fixed and considered as initial frame. The base of the exciter can move and simulate the road disturbances (see Figure 5.5). The exciter integrates three sensors including a force transducer installed on the inertial frame, a position sensor (LVDT), and a velocity sensor. The last two sensors are placed on the exciter to measure the instantaneous position and velocity of MR damper. The damper is excited under different harmonic displacement excitations in 0 to 15 Hz frequency range which

includes the predominant frequencies in the vehicular ride motions and the wheel hub vibrations.
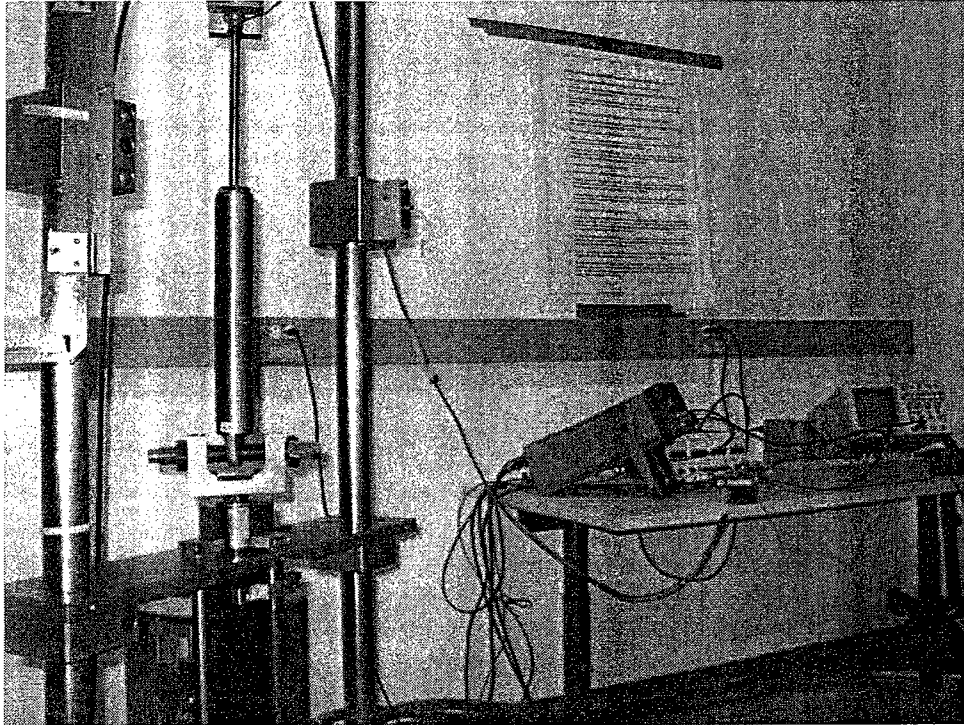
Figure 5.5 Experiment facilities

In the laboratory various tests are carried out at different frequencies with constant amplitudes subject to current signal variation to assess the effect of the current signal and frequency parameters on the dynamic performance of the MR damper. In addition, the performance of the MR damper is examined subject to different amplitudes with constant frequency and current signal. The tests are conducted for frequencies 0.1, 0.5, 1.5, 2.5, 5, 10, 12.5, and 15 Hz with amplitudes 2.5, 5, 12.5, 25, 50, and 75 mm. The current has been changed between 0 to 1.5 Amp. The lower amplitudes of the harmonic excitations are considered in order to avoid crossing the damper velocity limits. The examples of the MR damper response subject to harmonic excitations with frequencies 0.5 Hz and 12.5 mm amplitude, 1.5 Hz and 12.5 mm amplitude, 5 Hz and 2.5 mm amplitude, and 15 Hz

and 2.5 mm amplitude under different current signal inputs are illustrated in Figure 5.6

through Figure 5.9, respectively.

Figure 5.6 MR damper response subject to harmonic input with 0.5 HZ frequency and 12.5 mm amplitude

Figure 5.7 MR damper response subject to harmonic input with 1.5 HZ frequency and 12.5 mm amplitude
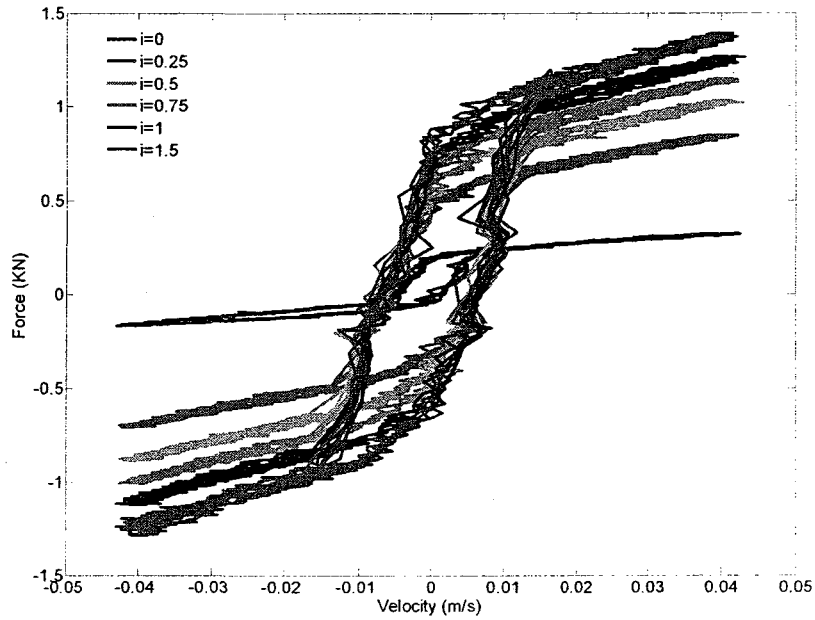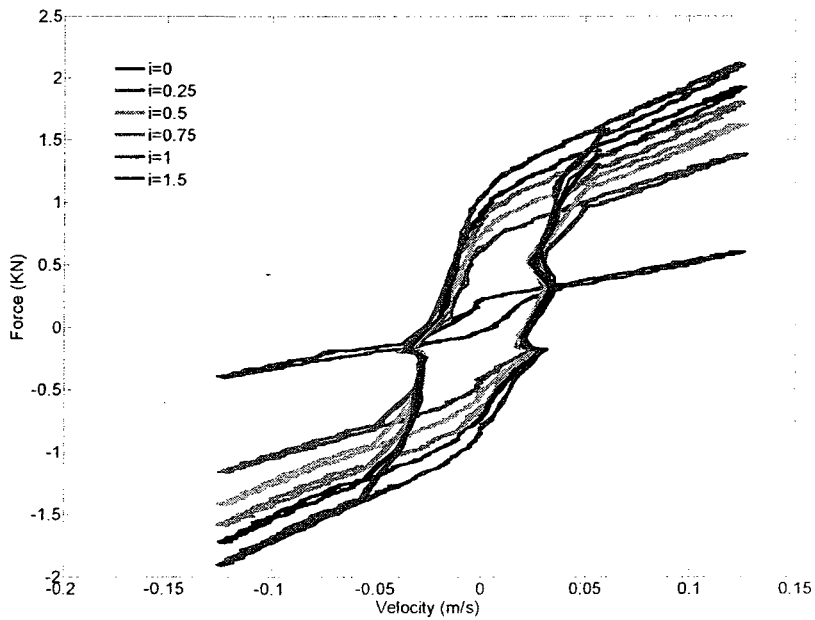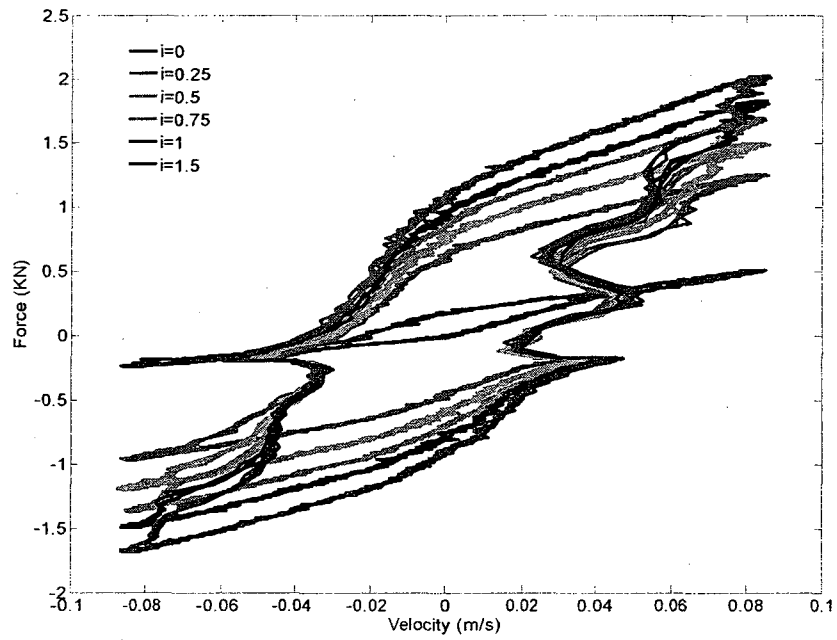
Figure 5.8 MR damper response subject to harmonic input with 5 HZ frequency and 2.5 mm amplitude
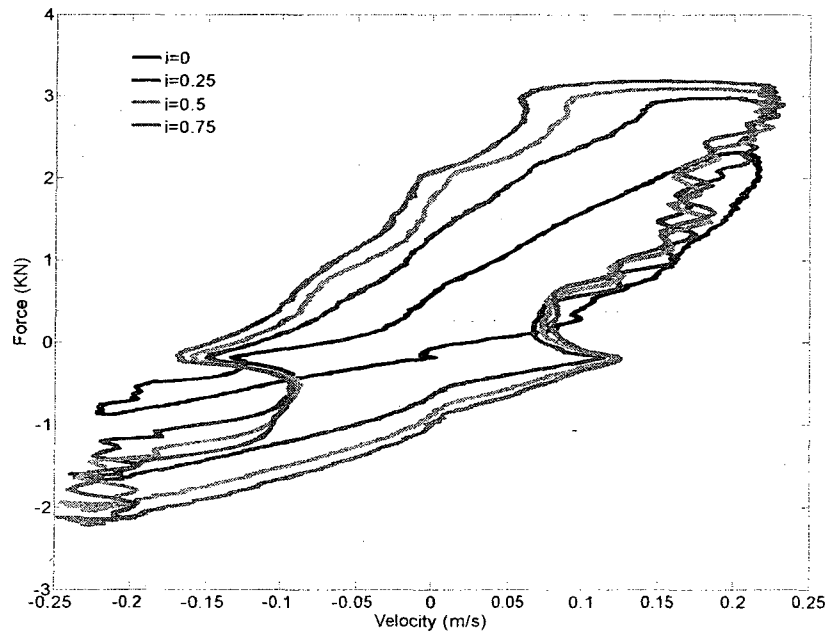
Figure 5.9   MR damper response subject to harmonic input with 15 HZ frequency and 2.5 mm amplitude

It is observed from these figures that such nonlinear damper properties are highly dependent on the excitation frequency and current signal. The results shown in figures clearly indicate that by increasing the excitation frequency the hysteresis effects will be magnified in pre-yield (low velocity) conditions and by increasing the current signal the damping force will be increased. The f-v characteristics further show that for a certain velocity the damping force will increase almost linearly by increasing the current signal, especially for those higher than 0.25 Amp.

Figure 5.10 and Figure 5.11 depict the MR damper response subjected to harmonic excitations with current signals 0 and 0.75 Amp, respectively. The frequency is set equal to 0.5 Hz in these cases to assess the effect of the harmonic amplitude excitation on the dynamic response of the MR damper. It is seen from these figures that the amplitude amplification does not affect the dynamic performance of the MR damper in post-yield conditions whereas affecting the pre-yield conditions by changing of the hysteresis slope. Generally speaking, the MR damper behaviour is almost independent from excitation amplitudes.

Figure 5.10 MR damper response subject to harmonic input with 0.5 HZ frequency and 0 Amp current signal

Figure 5.11 MR damper response subject to harmonic input with 0.5 HZ frequency and 0.75 Amp current signal
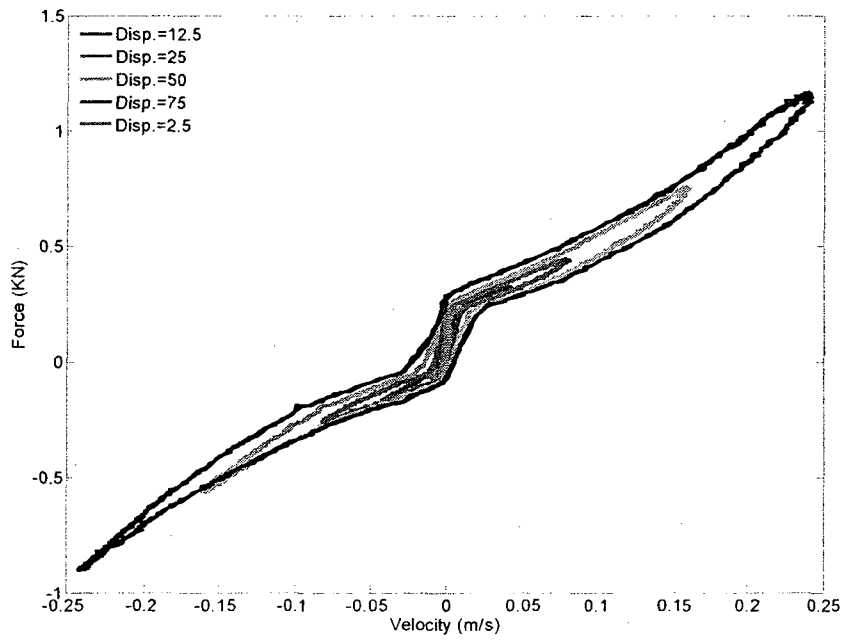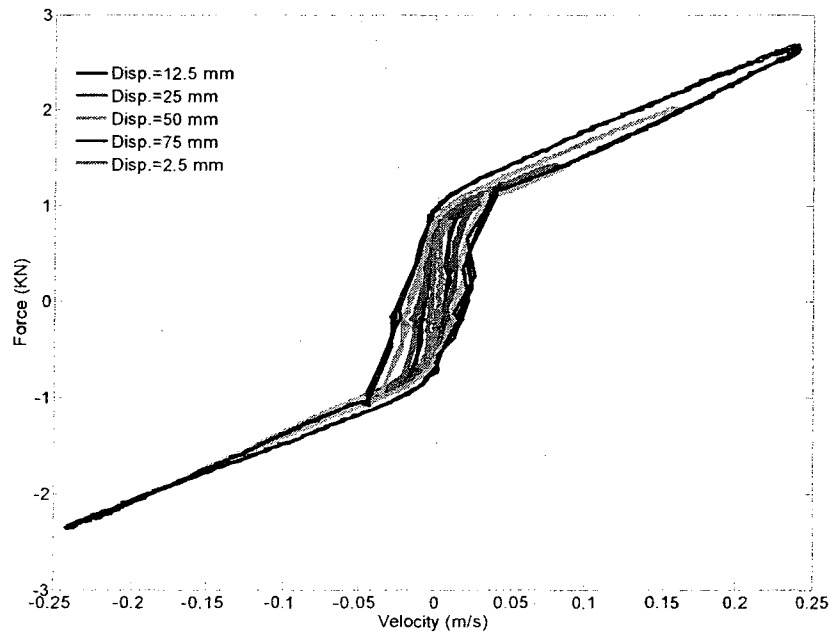
125

In summary, the *f-v* plots show that the MR damper characteristics can be represented as symmetric bi-nonlinear curves with hysteresis phenomena in pre-yield conditions and by linearly increasing force at post-yield conditions. In addition, the force will be saturated at a certain force value. Therefore, the damping force of MR damper can be formulated as a function of piston velocity and current signal, with appropriate consideration for the force saturation.

5.4 Inverse Mathematical Modeling of MR Damper

Considerable research has been conducted to capture the MR damper characteristics by developing its appropriate mathematical model in order to facilitate the formulation of an effective controller for estimating desirable controlled variations in the damping force. For example, Shames and Cozzarelli [90] proposed Bingham plastic model in which material behaviour was assumed as rigid in the pre-yield conditions, whereas shear flow was modelled by a viscous damping coefficient in post-yield conditions. Considering plastic material performance in pre and post yield conditions, Stanway et al. [91] proposed a nonlinear model of MR damper. Dyke et al. [92] developed a damper model on the basis of the Bouc-Wen hysteresis model. Although these models are sufficiently accurate to predict the damping force, they are highly nonlinear functions of both controlled current signal and piston velocity causing complexity in current estimation and increasing computational effort. In addition to these shortcomings, they represent the damping force as a function of the current signal and piston velocity, whereas in suspension control system a straightforward formula (inverse dynamics model) representing the current signal as a function of the controlled damping force and piston velocity is desired. Researchers in references [93] and [94] proposed inverse models of a

MR damper in which current signal can be tuned based on the desired force and piston velocity; however, it involves highly nonlinear formulations causing computational complexity thereby limiting the practical implementation. As a simple model, Choi and Lee [84] proposed a polynomial formulation for the MR damper force in which the polynomial variables are power of piston velocity while their coefficients are a linear function of current signal. Although it is possible to estimate this current signal from this formulation easily, a number of parameters are required to be identified using measured data. In addition, due to age and working conditions, these parameters are subject to the change in time. The purpose of the current research is to come up with a simple current signal estimation which makes the control algorithm more practical. The examples of abovementioned models are shown in Table 5-1.

5.4.1 Piecewise polynomial model of the MR damper

The overriding focus of the current research is on the practicality, implementation, and robustness of the control algorithm rather than the perfection of the model matching. Thus, a piecewise polynomial model of MR damper is developed according to the f-v plots obtained from the experiment data. According to the performance of MR damper plotted in Figure 5.6 to Figure 5.11, the damping force relatively changes linearly by increasing the current signal for a certain piston velocity.

Therefore, the current signal at a specific piston velocity can be estimated from the following relation

$$\frac{i}{i_{max}} = \frac{f - f_{min}}{f_{max} - f_{min}} \qquad (5.1)$$

Table 5-1   Mathematical Models of MR damper

	Model Formulation	**Definition of Parameters**
Bouc-wen Model [94]	$F = \alpha z + c_0(\dot{x} - \dot{y}) + k_0(x - y) + k_1(x - x_0)$ $\dot{z} = -\gamma\|\dot{x} - \dot{y}\|z\|z\|^{n-1} - \beta(\dot{x} - \dot{y})\|z\|^n + A(\dot{x} - \dot{y})$ $\dot{y} = \dfrac{1}{c_0 + c_1}\left\{\alpha z + c_0\dot{x} + k_0(x - y)\right\}$	F=Damping force x = damper displacement y = the internal pseudo-displacement of the damper z = evolutionary variable that describes the hysteresis behavior of the damper k_1= the accumulator stiffness c_0=viscous damping at large velocities x_0 = initial displacement of the spring k_1 α = the evolutionary coefficient n, A = shape parameters of the hysteresis loops
Polynomial Model [84]	$F = \displaystyle\sum_{j=1}^{n}(b_j + c_j i)v^j$	F=Damping force v = piston velocity b_j, c_j = constatnt coefficients i=current signal
Inverse Dynamic Model [94]	$i(t) = -\dfrac{1}{k_6}\ln\left[\dfrac{k_4 - \|F_d\| + \|\widetilde{F}_\eta(t)\|}{k_5}\right]$ $\widetilde{F}_\eta(t) = \left(1 + \dfrac{wh}{2A_p}\right)\dfrac{12\eta LA_p}{wh^3}A_p$	i = Current signal k_4, k_5, and k_6= constant values F_d= desired damping force L= the effective axial pole length A_p = the cross sectional area of the piston w = the width of rectangular plate h = the width of the gap between two parallel plates η = the Newtonian viscosity τ_0= the fluid yield stress

where, the i stands for the current signal, f_{max} and f_{min} correspond to the minimum and maximum damping forces subjected to the minimum and maximum current signals, respectively. In this case, the minimum and maximum current signals (i_{min}, i_{max}) are set to 0 and 1.5 Amp. By substituting the desired damping force derived from Equation (5.1), it is possible to estimate the required current signal so that the real damping force delivered by the MR damper is close to desired force as much as possible. The next step in the modelling is deriving a proper formulation for the f_{max} and f_{min}. According f-v curves shown in Figure 5.6 to Figure 5.11, the f-v plot of the candidate MR damper has been divided into six regions in terms of the piston velocity and the maximum and minimum forces of each region are represented by first or second order polynomials. It is worth mentioning that the hysteresis issue is ignored in the current formulation which is reasonable from design point of view. The selected areas are as shown in Table 5-1.

Table 5-2 Piecewise polynomial region of MR damper f-v performance

Piston Velocity (m/s)	Maximum Damping Force (N)	Minimum Damping Force (N)
$v > 0.1$	$c_0 + c_1 v + c_2 v^2$	$b_0 + b_1 v + b_2 v^2$
$0.02 < v < 0.1$	$c_3 + c_4 v$	$b_3 + b_4 v$
$-0.02 < v < 0.02$	$c_5 + c_6 v + c_7 v^2 + c_8 v^3$	$b_5 + b_6 v + b_7 v^2 + b_8 v^3$
$-0.1 < v < -0.02$	$c_9 + c_{10} v$	$b_9 + b_{10} v$
$v < -0.1$	$c_{11} + c_{12} v$	$b_{11} + b_{12} v$

The next step in the formulation is to identify the parameters of the abovementioned polynomials using the measured data acquired under a wide range of excitation

conditions. The model parameters are estimated through least square regression method described as:

$$J = \sum_{n=1}^{k1} \sum_{m=1}^{k2} \left(f_{sa}(v) - f_{dm} \right)^2$$ (5.2)

where f_{sa} is the damping force estimated from the polynomial piecewise polynomial model, and f_{dm} is the measured damping force. Through the least square regression, the summation of squared errors between f_{sa} and f_{dm} is minimized over a wide range of data described by indices n, and m. The indices n and m describe the number of excitation frequencies and the number of amplitude excitation considered in formulation. Since the polynomial formula is not a function of a frequency excitation, just the data obtained for frequency excitations 0.5, and 1.5 Hz are considered for parameter identifications. The amplitudes employed are 25 and 12.5 mm. The MATLAB constrained optimization toolbox with its function "lsqcurvefit" is integrated to minimize the error function (5.2).

Table 5-3 Identified piecewise polynomial model

Piston Velocity (m/s)	Maximum Damping Force (N)	Minimum Damping Force (N)
$v > 0.1$	$1280.36+4224.22v+11280.52v^2$	$332.12+607.14v+12098.96v^2$
$0.02 < v < 0.1$	$728.89+10624.23v$	$200.23+3015.87v$
$-0.02 < v < 0.02$	$115.02+42388.91v-$ $520.44.06v^2+1252616.37v^3$	$91.74+13842.16v+23063.56v^2-$ 13371050.39_8v^3
$-0.1 < v < -0.02$	$-652.14+8927.2v$	$-29.64+2736.24v$
$v < -0.1$	$-861.48+6943.07v$	$202.94+4507.91v$

The solutions are obtained for the fixed 0 and 1 Amp current signals. The identified parameters for the piecewise polynomials are summarized in Table 5-3. The model performance is investigated and analyzed in the following section.

5.4.2   Validation of inverse model of MR damper

In this section, the piecewise polynomial model developed for the MR damper is validated for the variety of excitations through different amplitudes, frequencies, and current signals in comparison with the real damping force measured from test facilities. Since the main purpose of the modelling is to tune the current signal so as to track the controlled desired force, the time response of the model is evaluated in the following, as well. For example, the time response of MR damper subject to harmonic excitations along with frequencies 0.5, 1.5, 2.5 and 7.5 Hz and 2.5, 12.5, and 25 mm subjected to the current signals 0 and 1 Amp are considered and illustrated in Figure 5.12-Figure 5.27. For the minimum and maximum current signals (0 and 1 Amp), as can be seen in those figures, the model predicts the damping force well at low frequencies and predict it at high frequencies reasonably well. At the high frequencies, there is an error around 500 N in the peak of extension while the error in the peak of contraction is less than 100 N. The error in the peak of contraction is ignorable for those with maximum current signal. As obviously shown in these figures, the hysteresis loop does not affect the time response of the model and it is logical to ignore its effects on the system response from design point of view.

131

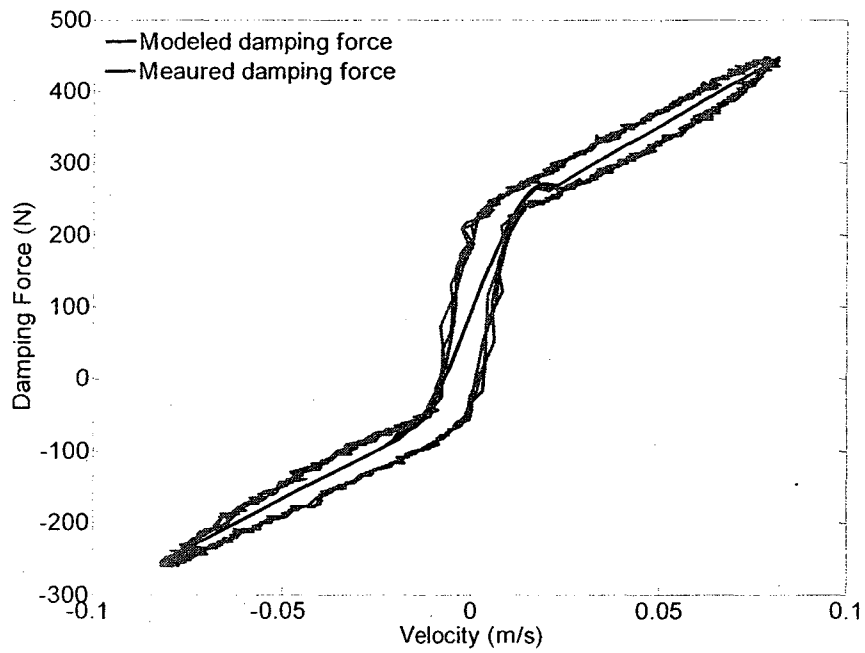Figure 5.12 *f-v* plot of MR damper for excitation with 0.5 Hz frequency and 25mm Amplitude subject to 0 Amp current signal

Figure 5.13 Time response of MR damper for excitation with 0.5 Hz frequency and 25mm Amplitude subject to 0 Amp current signal

Figure 5.14 *f-v* plot of MR damper for excitation with 1.5 Hz frequency and 25mm Amplitude subject to 0 Amp current signal
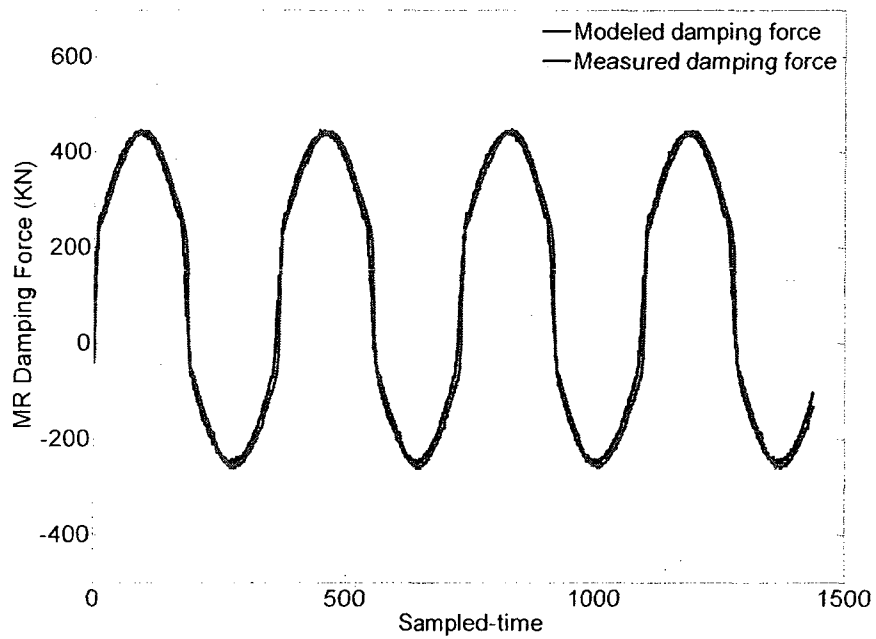

Figure 5.15 Time response of MR damper for excitation with 1.5 Hz frequency and 25mm Amplitude subject to 0 Amp current signal

Figure 5.16 *f-v* plot of MR damper for excitation with 2.5 Hz frequency and 12.5mm Amplitude subject to 0 Amp current signal

Figure 5.17 Time response of MR damper for excitation with 2.5 Hz frequency and 12.5mm Amplitude subject to 0 Amp current signal
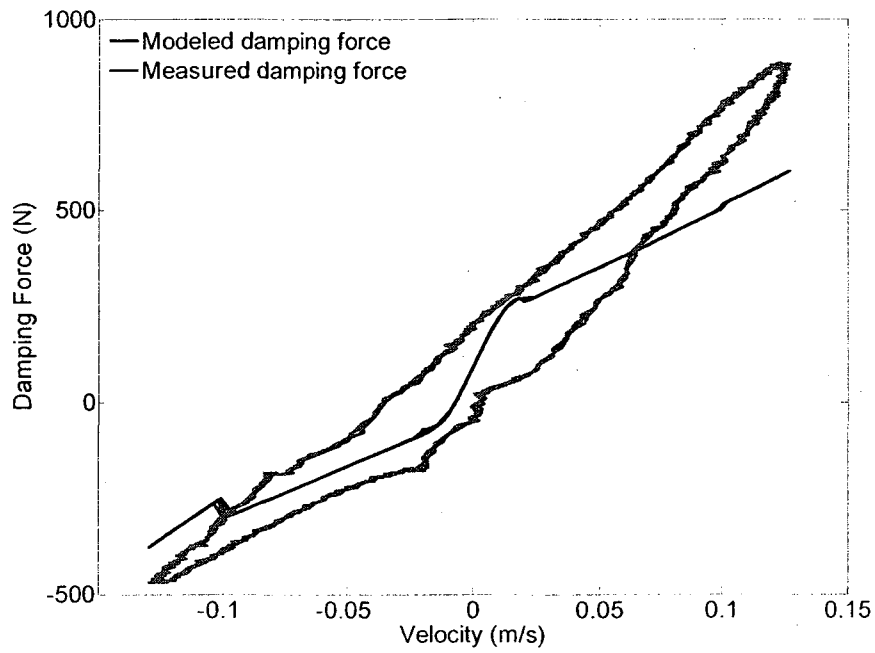
Figure 5.18 *f-v* **plot of MR damper for excitation with 7.5 Hz frequency and 2.5mm Amplitude subject to 0 Amp current signal**
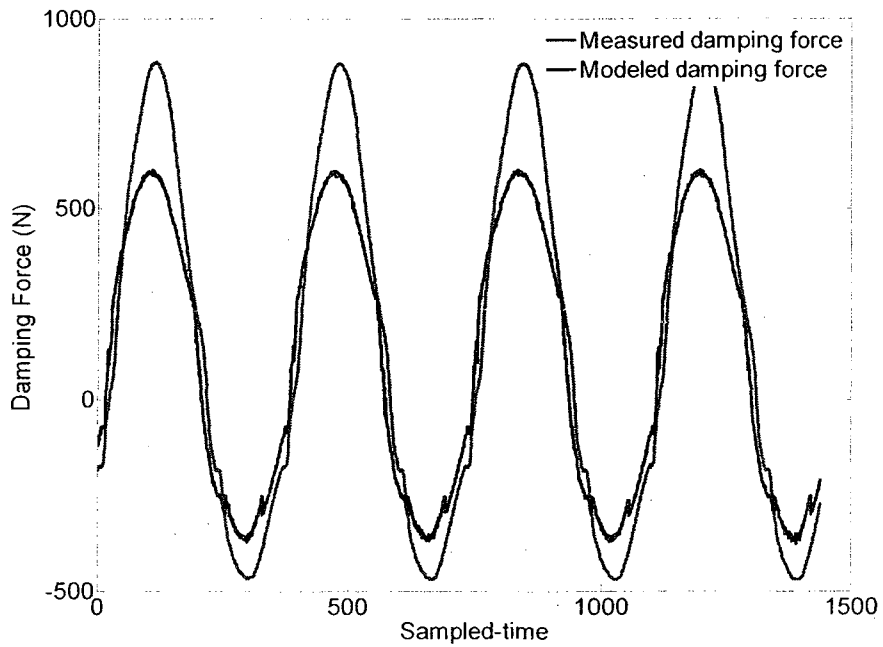
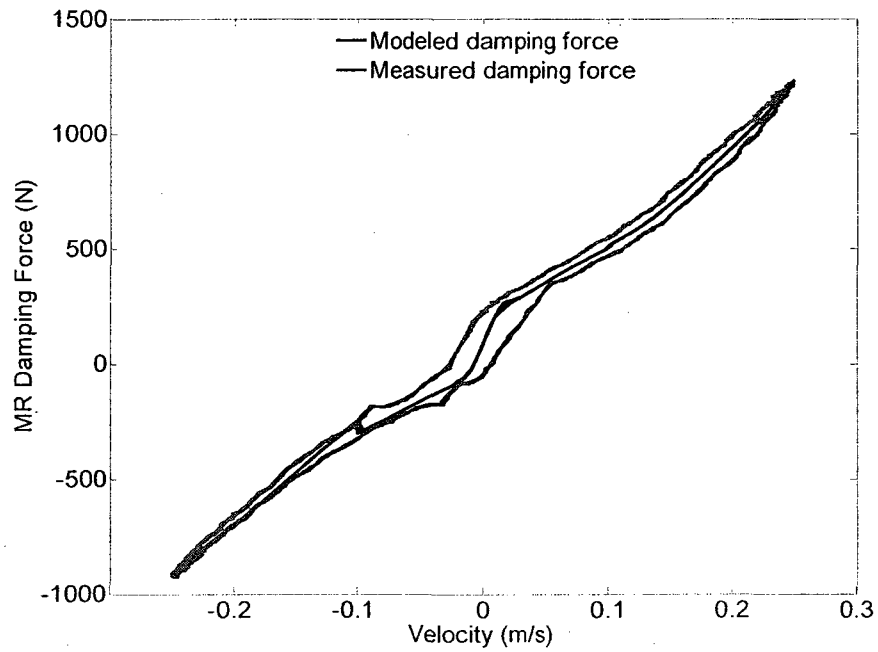**Figure 5.19 Time response of MR damper for excitation with 7.5 Hz frequency and 2.5mm Amplitude subject to 0 Amp current signal**

135
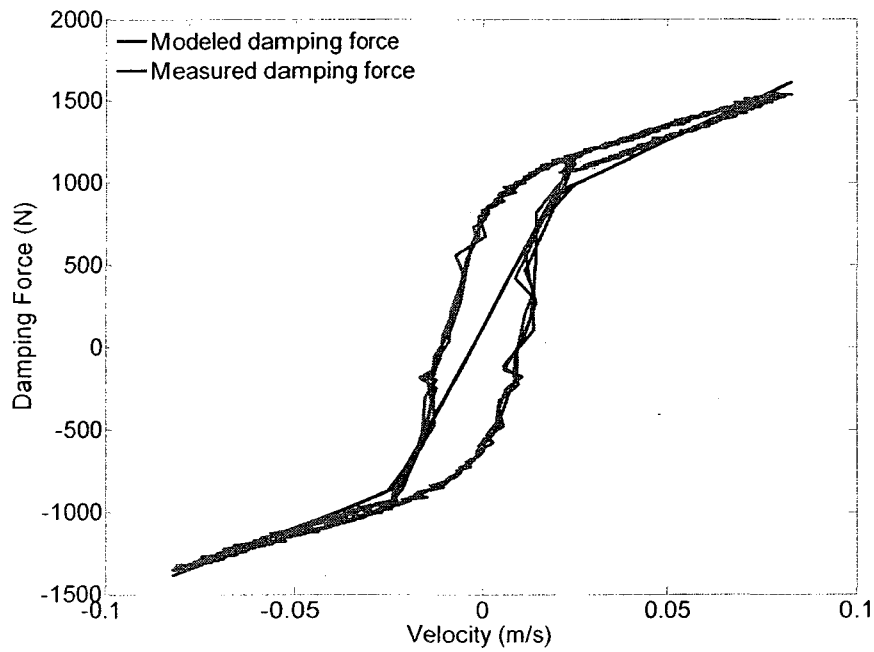
Figure 5.20 *f-v* plot of MR damper for excitation with 0.5 Hz frequency and 25mm Amplitude subject to 1 Amp current signal
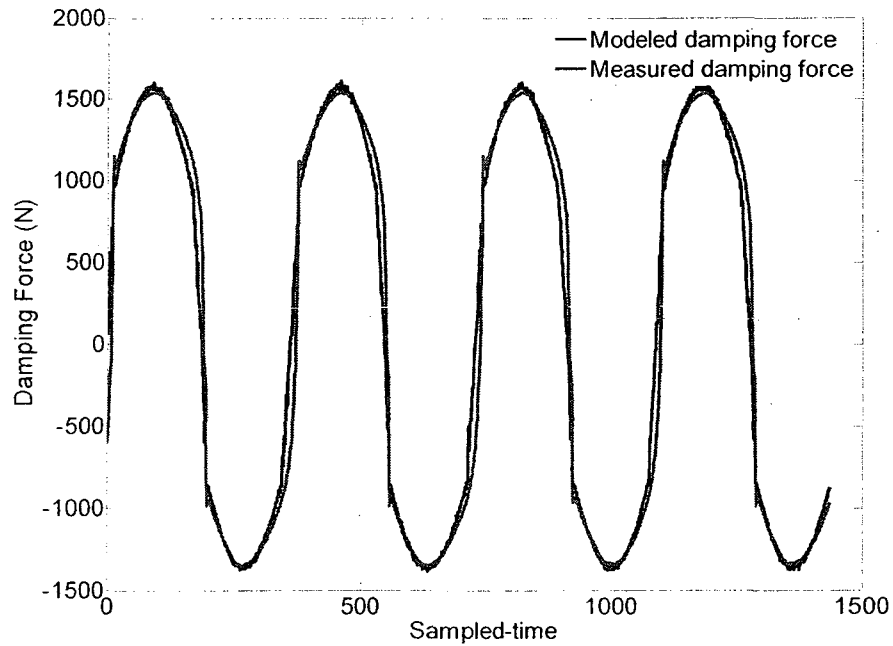
Figure 5.21 Time response of MR damper for excitation with 0.5 Hz frequency and 25mm Amplitude subject to 1 Amp current signal
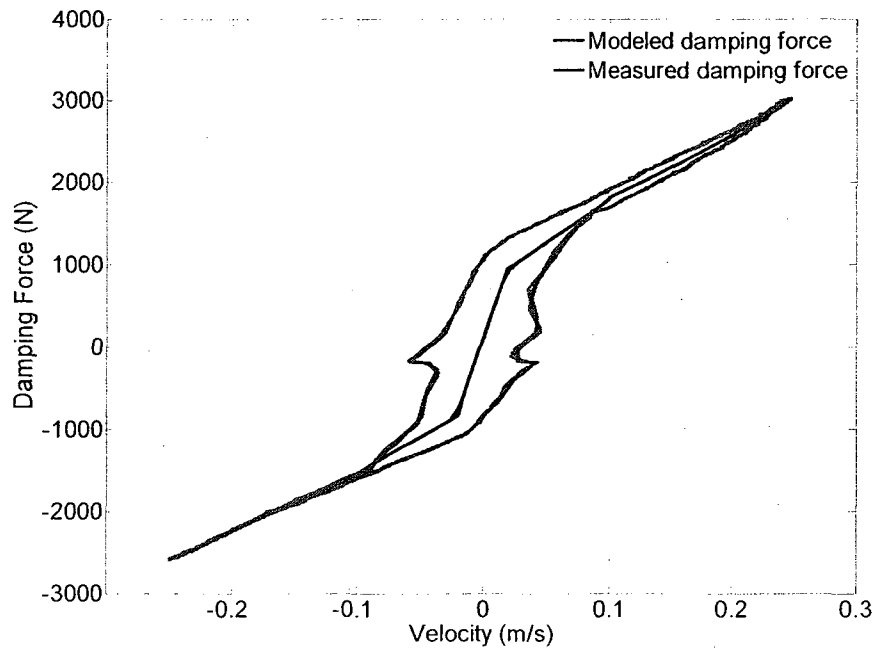
Figure 5.22 *f-v* plot of MR damper for excitation with 1.5 Hz frequency and 25mm Amplitude subject to 1 Amp current signal
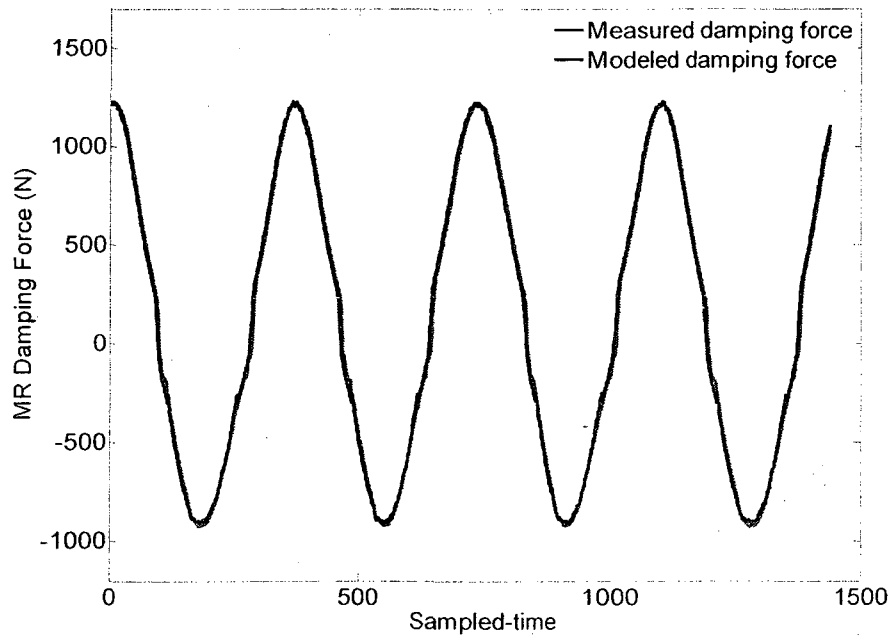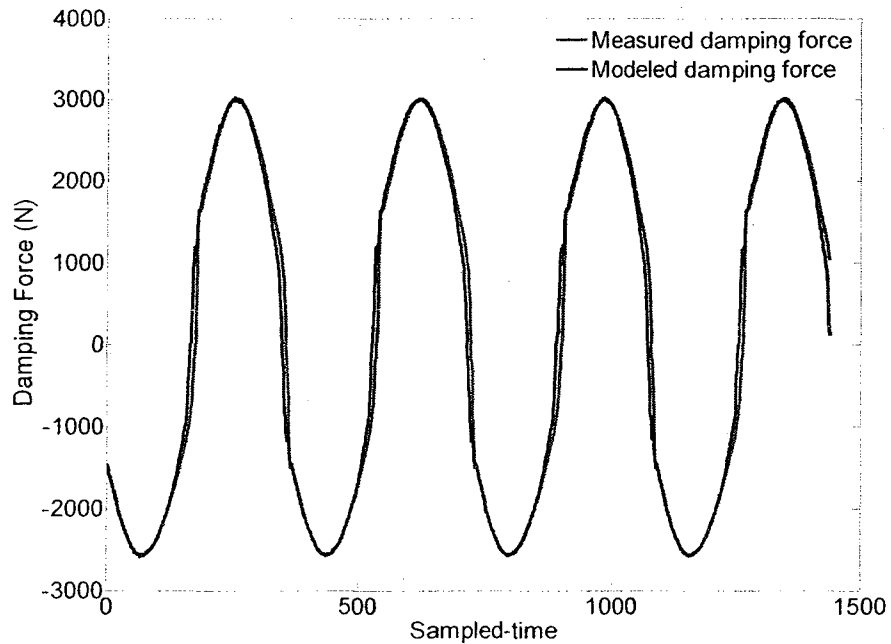

Figure 5.23 Time response of MR damper for excitation with 1.5 Hz frequency and 25mm Amplitude subject to 1 Amp current signal
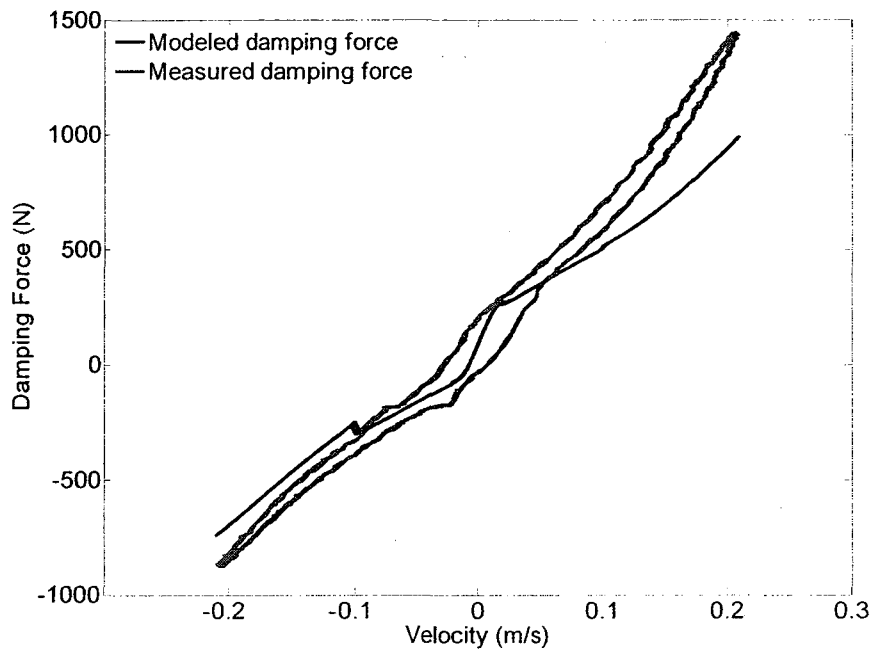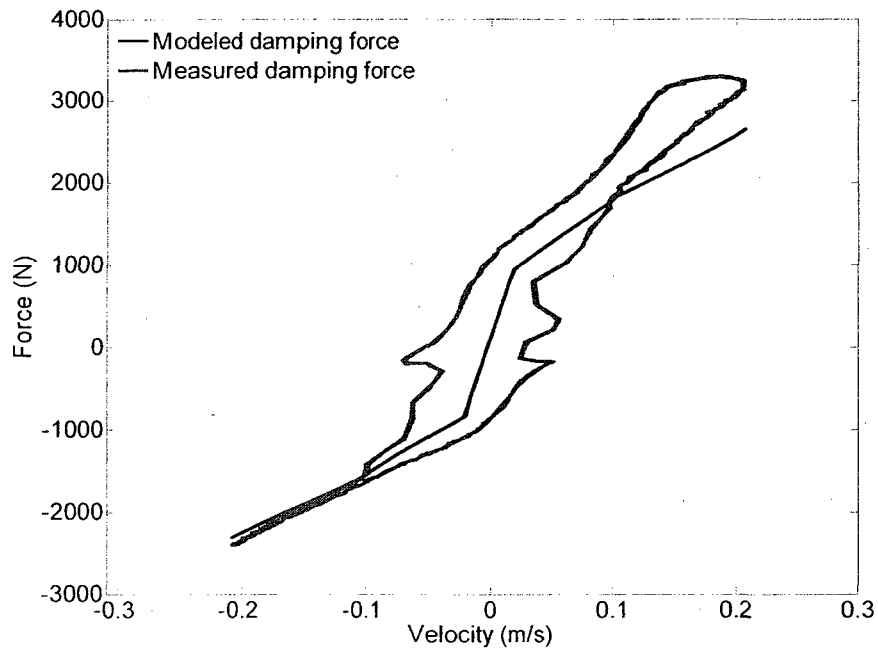
Figure 5.24 *f-v* plot of MR damper for excitation with 2.5 Hz frequency and 12.5mm Amplitude subject to 1 Amp current signal
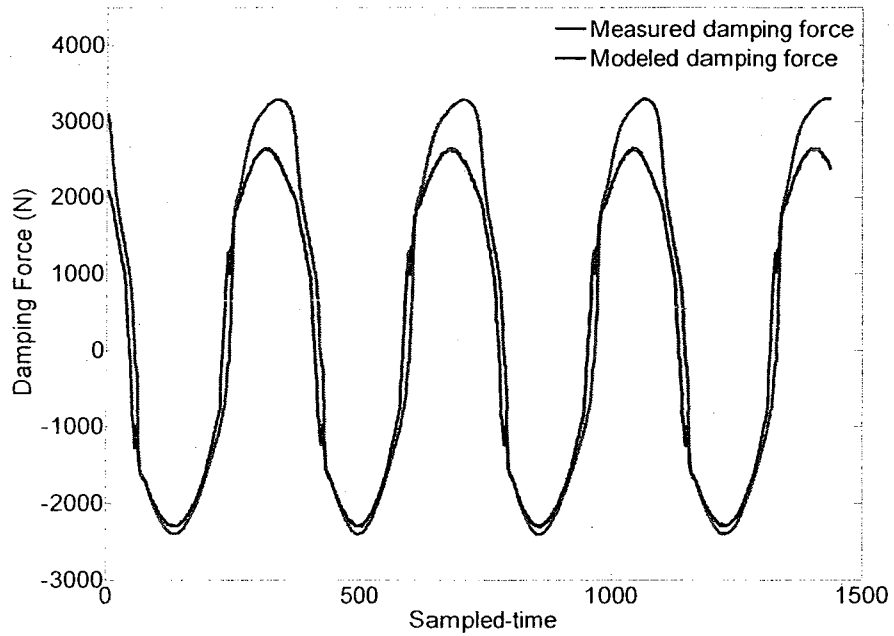
Figure 5.25 Time response of MR damper for excitation with 2.5 Hz frequency and 12.5mm Amplitude subject to 1 Amp current signal
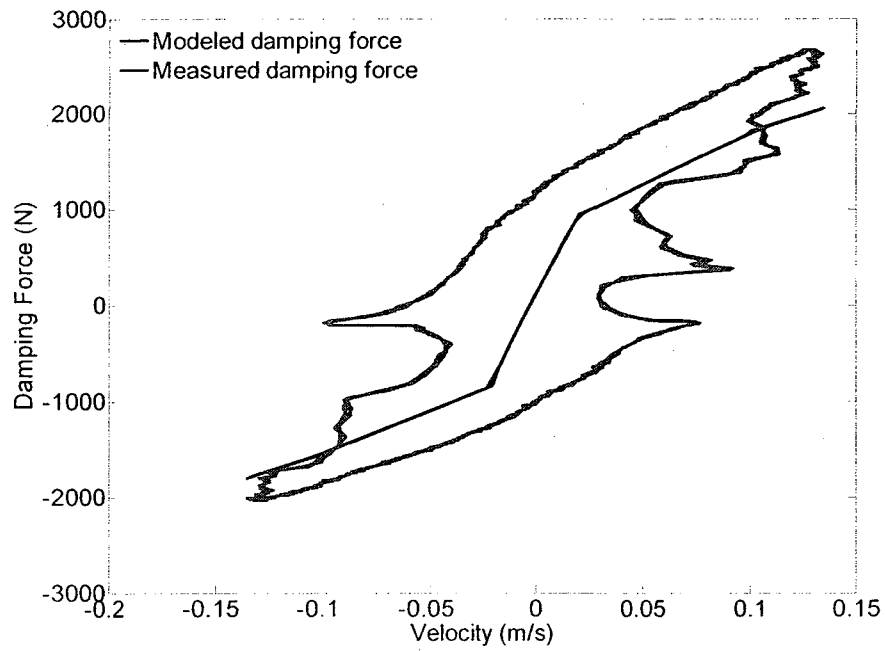
Figure 5.26 *f-v* plot of MR damper for excitation with 7.5 Hz frequency and 2.5mm Amplitude subject to 1 Amp current signal
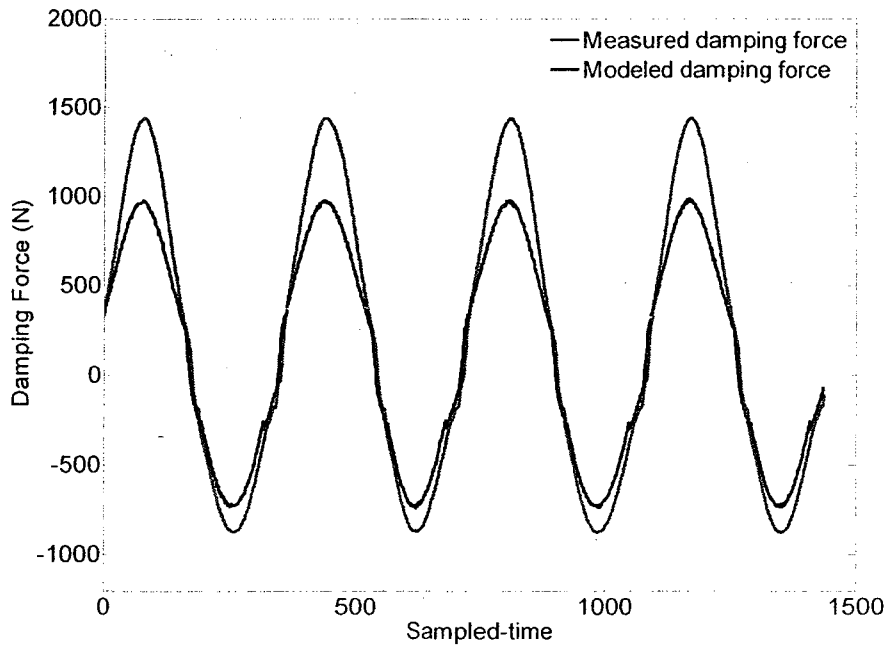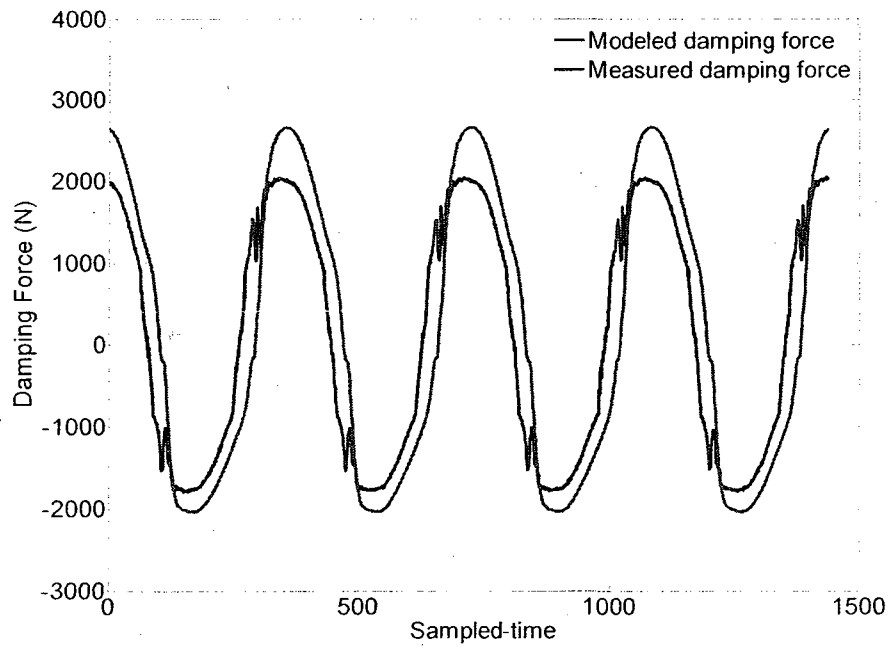

Figure 5.27 Time response of MR damper for excitation with 7.5 Hz frequency and 2.5mm Amplitude subject to 1 Amp current signal

5.5 Current Generation

By developing the mathematical model of the MR damper, it is possible to tune the current signal so that the real force generated by the MR damper follows the desired force obtained by the control system part. However, two main points should be taken into account during current tuning. The first one is the passivity constraint and the second one is the force saturation. As mentioned in Section 1.3.2, the passivity constraint comes from the energy dissipating function of MR damper, which is obvious from f-v plot of the MR damper. In f-v plot there is no force in the second and forth quadrants of the plot meaning if the damping force and the piston velocity have the same sign the damper dissipates the system energy and otherwise there is no force. The mathematical description of the constraint is shown in Equation (1.3). In addition to this constraint, the MR damper force is limited and will be saturated at a certain damping force. The saturation of damper can be shown mathematically by the following relation:

$$
f = \begin{cases} f_{max} & if\ f_{max} \leq f_d \\ f_d & if\ f_{min} \leq f_d \leq f_{max} \\ f_{min} & if\ f_d \leq f_{min} \end{cases}
\qquad (5.3)
$$

For large desired damping forces, the actuator saturation would be unavoidable, thus, the control performance of the MR damper would be less perfect in rough road disturbances. Considering two aforementioned constraints the algorithm for current generation is shaped as following:

$$
\begin{cases}
if & f_d > f_{max} \\
\quad f_d = f_{max} \\
elseif & f_d < f_{min} \\
\quad f_d = f_{min} \\
elseif & f_d v < 0 \\
\quad f_d = f_{min} \\
else \\
\quad f_d = f_d \\
end \\
i = \dfrac{(f_d - f_{min})}{(f_{max} - f_{min})} i_{max}
\end{cases}
$$

5.6 Controller Performance with Integrated MR Damper

In this section, the performance of the controller is validated through HIL simulation. The procedure was explained in Section 5.2 and shown in Figure 5.4. According to that procedure, the performance of the controller is plotted in Figure 5.28, Figure 5.29, and Figure 5.30 subjected to harmonic road excitations with 10 mm amplitude and 1 Hz, 2 Hz, 5 Hz, and 10 Hz frequencies, respectively. The controller gain selected for simulation is K1=[2400, 100]. As shown in those figures there is a time delay between the measured and desired forces because of the hardware signal communications. The time delay for the current system is 2 milliseconds. The figures show that the damper follows the desired force with good accuracy. However, there is a small difference between those forces during the contraction period. This discrepancy has been arisen from malfunction of the MR damper. Unfortunately, the rod of the MR damper has buckled during the MR damper characterization procedure, causing to add up an extra friction force to the damper during contraction period. The friction is between the rod and the piston.
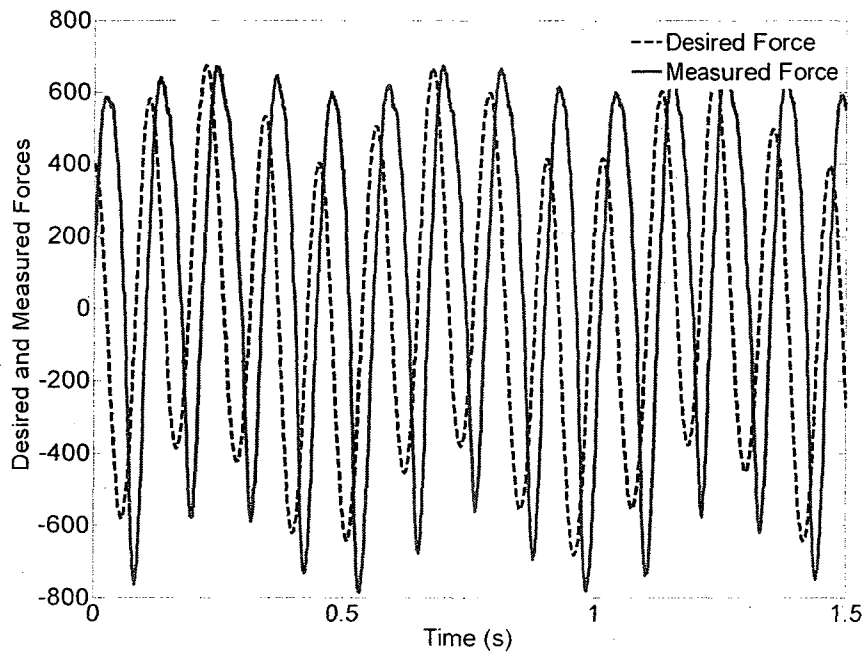
Figure 5.28 Measured and desired forces obtained through HIL simulation subject to a harmonic road excitation with 0.01 m amplitude and 3 Hz frequency
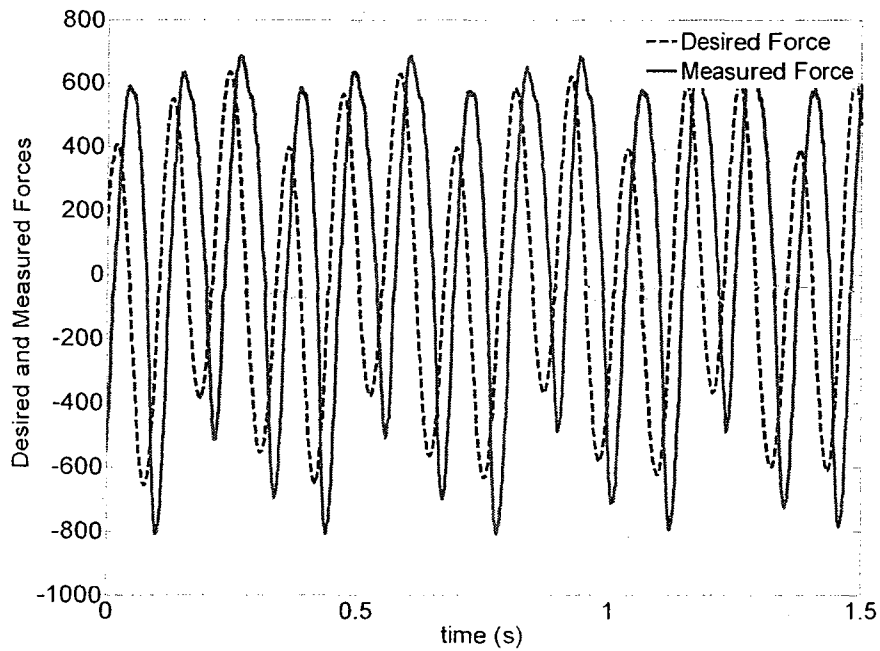
Figure 5.29 Measured and desired forces obtained through HIL simulation subject to a harmonic road excitation with 0.01 m amplitude and 3 Hz frequency

142
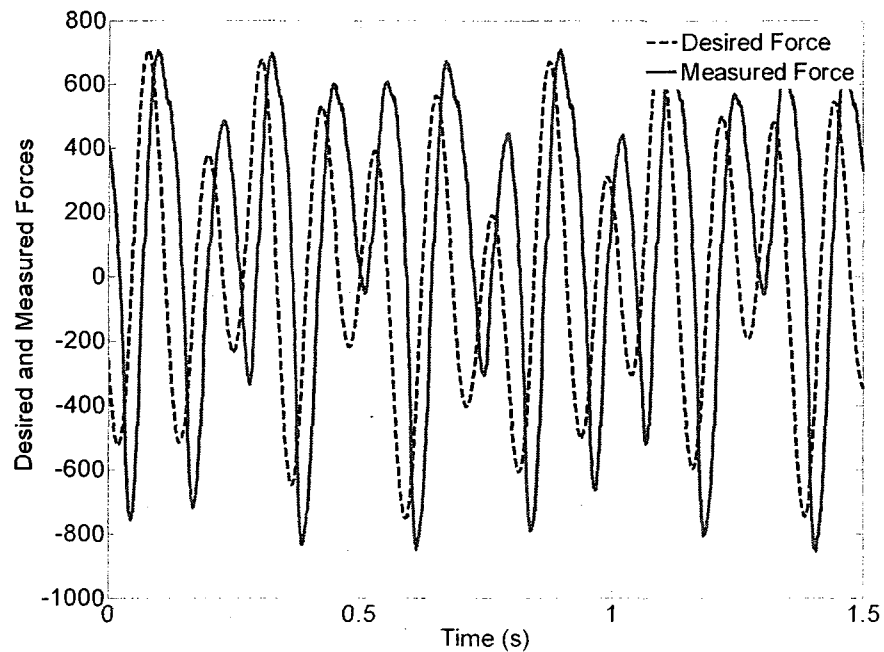
Figure 5.30 Measured and desired forces obtained through HIL simulation subject to a harmonic
road excitation with 0.01 m amplitude and 5 Hz frequency

5.7 Summary

There exists a large body of research on the modelling and characterization of MR

dampers. However, there is a lack of simple and practical models applicable to vehicle

suspension systems. Using a candidate MR damper, its dynamic performance is

characterized and a simple model of that applicable to suspension system is proposed.

The effectiveness of the proposed model is shown by comparing the measured damping

force with that predicted for a variety of excitations with different amplitudes,

frequencies, and current signals. The accuracy of the control force tracking by the

candidate MR damper is shown by HIL simulation.

143

CHAPTER 6

CONCLUSIONS AND RECOMMENDATIONS FOR FUTURE WORK

The ride vibration of a vehicle is important from both passenger comfort and car safety points of view. Poor ride quality combined with longer hours of operation causes driver fatigue and may affect the driver's concentration and sensory reactions thereby reducing vehicle safety. The unevenness and road disturbances causing ride quality deterioration are transmitted to the vehicle cabin through the vehicle suspension system. The suspension system is a multilink dynamic system with complex structure and its function is to distribute the energy, and phase it over the period and to dissipate it through a damper. Usually, a soft suspension provides a good passenger ride quality at the expense of good handling and stability characteristics. Thus, it is important that the suspension be designed so that a compromise between the requirements is achieved. In order to accomplish that, the active and semi-active vehicle suspension systems have received a great deal of attention from researchers for more than three decades. Although the active suspension provides a great improvement over a wide range of frequencies and road disturbances, its complex circuit and structure make its implementation difficult in practice. In contrast, the semi-active systems have a simple structure with minimal power requirements. In this type of systems, the damping of the suspension can be continuously changed according to an appropriate control policy.

The present work was undertaken in order to understand the behaviour of semi-active suspension systems equipped with MR dampers and to develop a new kinematic and

dynamic model of MacPherson suspension system and to provide a practical control design.

6.1 Dissertation Summary

In order to include the kinematic structure in considering the dynamic response of a specific suspension system, namely MacPherson suspension system, a new control oriented dynamic model of the suspension has been developed. The rotational motion of the wheel subject to the control arm transverse motion is considered in the modelling. In addition to that, geometrical aspects of the system such as strut inclination and wheel camber rotation are included in the modelling. It has been shown that the model exhibits a superior dynamic performance of MacPherson suspension system compared to that of the conventional model, widely used by researchers. In order to avoid complexity, the highly nonlinear model has been linearized about the system equilibrium point. Moreover, it is shown that the structure of the system affects on the pole locations of the dynamic model.

The point that has not received enough attention from the previous researchers in the field of vehicle suspension control is the wheel motions under the control force variation. The wheel motions are important in tire grasp, handling, steering, and stability of the vehicle. In order to evaluate the wheel motions subjected to the damping force variation, a three-dimensional kinematic model of MacPherson suspension has been developed. The accuracy of model is validated by a three-dimensional kinematic model of the system simulated in ADAMS software environment. It is shown that the model represents the kinematic performance of the system with high accuracy. In addition, some geometry

parameters affecting handling performance of the vehicle are defined and their contributions on the overall vehicle performance are described and discussed.

Next, the three popular semi-active control strategies, namely hybrid skyhook-groundhook controller, modified skyhook controller, and passive-skyhook controller, are described. Their contributions on the ride quality, stability, and kinematic performance of the MacPherson suspension system are compared. As a result, it is concluded that the different control strategies can improve ride quality and tire grip in a similar way whereas their influences on the suspension kinematic performance are completely different.

Different sophisticated control strategies have been used by researchers for control of the vehicle suspension; however, the robust control theory has received more attention because of its ability in dealing with model uncertainties and in dealing with frequency specifications. A full state feed back control strategy is designed using H_{∞} control theory and Linear Matrix Inequality (LMI) technique optimization. In order to reduce the design cost and to make the controller more practical, following the H_{∞} output feedback control theory; two different controllers are developed to improve vehicle suspension specifications. In order to solve the minimization problem of output feedback controller, a combination of LMI and Genetic Algorithm (GA) methods is chosen owing to the bilinear nature of the problem. The resulting controller has a structure similar to that of the skyhook-passive controller in which the controller gains are optimized based on the vertical displacement and acceleration responses as well as control arm rotation response. It is shown that despite the simple structure of the output feedback controller, it can achieve a performance close to that of a full state feedback controller.

A MR damper is selected as the candidate dissipative component of the semi-active suspension to generate the force calculated from the control unit. In order to tune the current signal of the MR damper according to the command force generated by the control unit, an inverse dynamic model of the damper is required. Various experiments are carried out in the laboratory in order to characterize the dynamic performance of the MR damper. The results showed that the MR damper force behaves approximately linearly as a function of the current signal at a certain damper velocity. Accordingly, a simple and practical model of MR damper was developed using the data acquired through the laboratory tests and the MR damper performance. The model is validated by the experimental data and the results show that it represents the MR damper performance reasonably well for vehicle suspension control applications.

The last part of the thesis deals with the effect of the MR damper dynamics on the control performance. In order to take care of highly nonlinear characteristics of the MR damper and make the control design more reliable, a real MR damper is integrated in the feedback loop. Simulations are carried out using the Hardware-In-the Loop Simulation (HILS) technique. The effectiveness of the inverse model of MR damper is shown and discussed.

The main contributions of the research are highlighted as follows:

1- The kinematic performance of the suspension system is integrated in control design procedure, the point that was not given enough attention by previous researchers.

2- Using a new dynamic model of Macpherson suspension system, it is shown that the combination of the passive and skyhook damping forces has the best contribution on

improvement of Macpherson suspension performance compared to other controllers. In addition, it is shown that neither the ideal skyhook nor pure ground-hook controllers are effective for Macpherson suspension system

3- Using robust control theory, an output feedback robust control is designed and its gains are optimized by means of the combination of LMI and GA solvers. It should be noted that, the designed controller has simple structure and is robust against model uncertainties compared to previous controllers proposed in the literature.

4- A piecewise polynomial model of MR damper is developed to predict MR damper performance and an algorithm is developed to estimate the current signal of MR damper. The algorithm has a simple structre and it is applicable on controlled suspension systems.

6.2 Recommended Future Works

Many research studies have been carried out in the field of vehicle suspension control design, however, this field of research is still open and several aspects of that have not received enough attention. The following subsections describe some areas that need to be studied in this area.

6.2.1 Control-oriented modeling of specific suspension systems

A simplified model composing two lumped masses which are connected through linear stiffness has been widely used to represent the dynamics of the suspension system. The model is very simple in which the structural effects of the mechanism on the dynamic response has been ignored. Since different suspension systems with complex structure are available, it is recommended that the modelling of a specific suspension system such as

double-wishbone and multi link systems may be developed. Having a superior model of suspension system is necessary for a reliable control design.

6.2.2 Roll centre control

One of the important parameters in studying both the ride quality and stability of the vehicle is its roll centre. It is known that while cornering the vehicle tends to roll around this point. The location of this point can be determined from the suspension structure and would be changed by vehicle's motion. The roll centre is inversely related to other kinematic parameters such as track width and camber angle. The lower roll centre provides better stability at the cost of track width and camber angle deteriorations. It is recommended that in using semi-active control strategies the variation of the roll centre be controlled while the other kinematic parameters are adjusted passively or vice-versa.

6.2.3 Inverse MR damper modeling

Having an accurate and practical inverse model of a MR damper is essential in the suspension control design. Thus, the development of an accurate inverse model of MR damper would be immensely useful.

Bibliography

1. Gillespie T. D., 1992, Fundamentals of vehicle dynamics, *Society of Automotive Engineering, Inc.*

2. Wong J. Y., 1993, Theory of ground vehicles, Second edition, *John Wiley & Sons.*

3. Reimpell J., Stoll H., and Betzler J. W., 2001, The automotive chassis: engineering principles, Second Edition, *Butterworth Heinmann.*

4. Hrovat, D., 1997, Survey of advanced suspension developments and related optimal control applications, *Automatica*, **33**(10), 1781-1817.

5. Tseng H. E., and Hedrick J. K., 1994, Semi-active control laws – optimal and sub optimal, *Journal of Vehicle System Dynamics*, **23**(1), 545-569.

6. Giua A., Seatzu C., and Usai G., 1999, Semi active suspension design with an optimal gain switching target, *Journal of Vehicle System Dynamics*, **31**(4), 213-232.

7. Giua A., Mlas M., Seatzu C., and Usai G., 2004, Design of a predictive semi active suspension system, *Journal of Vehicle System Dynamics*, **41**(4), 277-300.

8. Canale M., Milanese M., and Novara C., 2006, Semi active suspension control using fast model predictive techniques, *IEEE Transactions on Control Systems Technology*, **14**(6), 1034-1046.

9. Sohn H. C., and Hong K. T., 2004, An adaptive LQG control for semi-active suspension systems, *International Journal of Vehicle Design*, **34**(4), 309-325.

10. Sinha A., 2007, Linear Systems Optimal and Robust Control, *CRC Press, Taylor & Francis Group.*

11. Song X., Ahmadian M., Southward S., and Miller L., 2005, An adaptive semi active control algorithm for magnetorheological suspension systems, *Journal of Vibration and Acoustics*, **127**(5), 493 - 502.

12. Chen P., and Huang A., 2005, Adaptive sliding control of non-autonomous active suspension systems with time-varying loadings, *Journal of Sound and Vibration*, **282**, 1119-1135.

13. Fialho I., and Balas G., J., 2002, Road adaptive active suspension design using linear parameter-varying gain-scheduling, *IEEE Transactions on Control Systems Technology*, **10**(1), 43-54.

14. Liete V. J., and Peres P. L., 2005, Pole location control design of an active suspension system with uncertain parameters, *Journal of Vehicle System Dynamics*, **43**(8), 561-579.

15. Sie W., Lian R., and Lin B., 2006, Enhancing grey prediction fuzzy controller for active suspension systems, *Journal of Vehicle System Dynamics*, **44**(5), 407-430.

16. Thompson A. G., and Pearce C. E., 2001, Performance index for a preview active suspension applied to a quarter-car model, *Journal of Vehicle System Dynamics*, **35**(1), 55-66.

17. Donahue M. D., 2001, Implementation of an active suspension, preview controller for Improved rides comfort, M. Sc. Thesis, *The University of California at Berkeley, California*.

18. Stensson A., Splund C., and Karlsson, 1994, The nonlinear behavior of a MacPherson suspension mechanism, *Journal of Vehicle System Dynamics*, **39**(3), 85-106.

19. Jonsson M., 1991, Simulation of dynamical behavior of a front wheel suspension, *Journal of Vehicle System Dynamics*, **20**(5), 269-281.

20. Fallah M. S., Mahzoon M., and Eghtesad M., 2004, Kinematical and dynamical analysis of MacPherson suspension using displacement matrix method, *Iranian Journal of Science and Technology*, **32**(B4), 325-339.

21. Suh C. H., 1989, Synthesis and analysis of suspension mechanism with use of displacement matrices, *SAE Technical Paper Series*, Paper No. 890098.

22. Mantaras D. A., Luque P., and Vera C., (2004), Development and validation of a three-dimensional kinematic model for the MacPherson steering and suspension mechanism, *Journal of Mechanism and Machine Theory*, **39**, 603-619.

23. Chen K., and Beale, D. G., 2003, Base dynamic parameter estimation of a MacPherson suspension mechanism, *Journal of Vehicle System Dynamics*, **39**(3), 227-244.

24. Habibi H., Shirazri K. H., and Shishesaz M., 2008, roll steer minimization of MacPherson strut suspension using genetic algorithm method, *Journal of Mechanism and Machine Theory*, **43**(1), 57-67.

25. Kim C., and Ro P. I., 2000, "Reduced Order Modeling and Parameter Estimation for Quarter Car Suspension System," *Journal of Automobile Engineering, IMechE*, Vol. 214, Part D, 851-864.

26. Hong K. S., Jeon, D. S., and Sohn, H. C., 1999, A new modeling of the MacPherson suspension System and its optimal pole-placement control, Proceedings of the 7th Mediterranean Conference on Control and Automation (MED99) Haifa, Israel, June 28-30.

27. Sohn H. C., Hong K. S., and Hedrick, J. K., 2000, Semi-active control of the MacPherson suspension system: hardware-in-the-loop simulations, *Proceedings of the 2000 IEEE, International Conference on Control Applications*, Anchorage, Alaska, USA, September 25-27.

28. Spong M. W., and Vidyasagar M., 1989, Robot dynamics and control, *John Wiley & Sons, Inc. New York, NY*.

29. Choi, S., B., Song, H., J., Lee, H., H., Lim, S., C., and Kim, J. H., 2003, Vibration control of a passenger vehicle featuring magnetorheological engine mounts, *International Journal of Vehicle Design*, **33**(1-3), 2-16.

30. Dominguez, A., Sedaghati, R., and Stiharu, I., 2004, modeling the hysteresis phenomenon of magnetorheological dampers, *Journal of Smart Materials and Structures*, **13**, 1351-1361.

31. Liao, W., H., and Lai, C., Y., 2002, Harmonic analysis of a magnetorheological damper for vibration control, *Journal of Smart Materials and Structures*, **11**, 288-296.

32. Heisler H., 1999, Vehicle and Engine Technology, Second Edition, *Society of Automotive Engineers*.

33. Fallah, M. S., Bhat, R., and Xie, W. F., 2009, "New model and simulation of MacPherson suspension system for ride control applications", *Vehicle System Dynamics*, Vol. **47**(2), pp. 195-220.

34. Chapra S. C., and Canale R. P., 2002, *Numerical methods for engineering*, Fourth Edition, McGraw-Hill.

35. Karnopp D., Crosby M. J., and Harwood R. A., 1974, Vibration control using semi-active force generators, *Trans. ASME, Journal of Engineering for Industry*, **96**(2), 619-626.

36. Valasek M., Novak M., Sika Z., and Vakulin O., 1997, Extended ground-hook new concept of semi-active control of truck's suspension, *Journal of Vehicle System Dynamics*, **27**(5), 289-303.

37. Ahmadian M., and Vahdati N., 2006, Transient response of semi-active suspensions with hybrid control, *Journal of Intelligent Materials Systems and Structures*, **17**, 145-153.

38. Ahmadian M., and Pare C., 2000, A quarter-car experimental analysis of alternative semi-active control methods, *Journal of Intelligent Materials Systems and Structures*, **11**, 604-612.

39. Goncalves F. D., and Ahmadian M., 2003, A hybrid control policy for semi-active vehicle suspensions, Journal of Shock and Vibration, **10**, 59-69.

40. Ahmadian M., Song X., and Southward S., 2004, No-jerk skyhook control method for semi-active suspensions, *Journal of Vibration and Acoustics*, **126**, 580-584.

41. Batterbee D., C., and Sims, N., D., 2007, Hardware-in-the-loop simulation of magnetorheological dampers for vehicle suspension systems, Proceedings of the I MECHE Part I, *Journal of Systems & Control Engineering*, **221**(2), 265-278.

42. Yi K., and Song B. S., 1999, A new adaptive sky-hook control of vehicle semi-active suspensions, Proceedings of the I MECHE Part D, *Journal of Automotive Engineering*, **213**(3), 293-303.

43. Sohn, H. C., Hong, K., S., and Hedrick, J., K., 2002, Modified skyhook control of semi-active suspensions: a new model, gain scheduling, and hardware-in-the-Loop tuning, *Journal of Dynamic Systems, Measurement, and Control*, **124**(1), 158-167.

44. Liu Y., Waters T. P., and Brennan M. J., 2005, A comparison of semi-active damping control strategies for vibration isolation of harmonic disturbances, *Journal of Sound and Vibration*, 280, 21-39.

45. Shen Y., Golnaraghi M., R., and Heppler G. R., 2006, Semi-active vibration control schemes for suspension systems using magnetorheological dampers, *Journal of Vibration and Control*, **12**(1), 3-24.

46. Savaresi M. S., and Spelta C., 2007, Mixed sky-hook and ADD: Approaching the filtering limits of a semi-active suspension, *Journal of Dynamic Systems, Measurement, and Control*, **129**(4), 382-392.

47. Jalili N., 2002, A comparative study and analysis of semi-active vibration-control systems, *Journal of vibration and Acoustics*, 124, 593-605.

48. Dixit R. K., and Buckner, 2005, Sliding mode observation and control for semi-active vehicle suspensions, *Journal of Vehicle System Dynamics*, **43**(2), 83-105.

49. Sammier D., Sename O., and Dugard L., 2003, Sky-hook and H_∞ control of semi-active suspensions: some pratical aspects, *Journal of Vehicle System Dynamics*, **39**(4), 279-308.

153

50. Du H., Sze K. Y., and Lam J., 2005, Semi-active H∞ control of vehicle suspension with magnetorheological dampers, *Journal of Sound and Vibration,* **283**(3-5), 981-996.

51. Hayakawa K.,, Matsumoto K., Yamashita M., Suszuki Y., Fujimori K. and Kimura H., 1999, Robust H∞ output feedback control of decoupled automobile active suspension systems, *IEEE Transactions on Automatic Control,* **44**(2), 392-396.

52. Yamashita M., Fujimori K., Hayakawa K., and Kimura H., 1994, Application of H∞ control to active suspension systems, *Automatica,* **30**(11),1717-1729.

53. Zribi M., and Karkoub M., 2004, Robust control of a car suspension system using magnetorheological dampers, *Journal of Vibration and Control,* **10**, 507—524.

54. Gaspar P., Szaszi I., and Bokor J., 2003, Design of robust controllers for active vehicle suspension using the mixed μ synthesis, *Journal of Vehicle System Dynamics,* **40**(4), 193-228.

55. Dai H., Zhang H., and Zhang W., 1998, Robust performance analysis of active suspension with model uncertainty using structured singular value, μ approach, *Journal of Vehicle System Dynamics,* **29**(1), 635-647.

56. Kashani R., and Kiriczi S., 1992, Robust stability analysis of LQG-controlled active suspension with model uncertainty using structured singular value, μ, method, *Journal of Vehicle System Dynamics,* **21**, 361-384.

57. Chen H., and Guo K. H., 2005, Constrained H∞ control of active suspensions: an LMI approach, *IEEE Transactions on Control System Technologies,* **13**(3), 412 - 412.

58. Chen H., Liu Z. Y., and Sun Y. P., 2005, Application of constrained H∞ control to active suspension systems on half-car models, *Journal of Dynamic Systems, Measurements, and Control,* **127**(3), 345-354.

59. Chen H., Liu Z. Y., Sun P. Y., and Yu Y. S., 2004, H∞ active suspension control based on moving horizon strategy, *Proceedings of the 5th World Congress on Intelligent Control and Automation,* June 15- 19., Hangzhou, China.

60. Fialho I. J., and Balas G., J., 2000, Design of nonlinear controllers for active vehicle suspensions using parameter-varying control synthesis, *Journal of Vehicle System Dynamics,* **33**(5), 351-370.

61. Du H., Lam J., and Sze K. Y., 2005, Design of non-fragile H∞ controller for active vehicle suspensions, *Journal of Vibration and Control,* 11, 225—243.

62. Son H. Y., Jeong S. G., Choi J. Y., Kim J. K., Cheon Y. S., Paek Y. I., Kwon S. H., and Lee M. H., 2001, A robust controller design for performance improvement of a semi-active suspension system, *IEEE ISIE*, Pusan, Korea.

63. Lucente G., and Rossi C., 2005, Multi-objective control of semi-active suspension systems, *IEEE ISIE*, June 20-23, Dubrovnik, Croatia.

64. Du H., and Zhang N., 2008, Designing H_∞/GH_2 static-output feedback controller for vehicle suspensions using linear matrix inequalities and genetic algorithms, *Journal of Vehicle System Dynamics*, **46**(5), 385-412.

65. Choi S., Lee H., and Park Y., 2002, H_∞ control performance of a full-vehicle suspension featuring magnetorheological dampers, *Journal of Vehicle System Dynamics*, **38**(5), 341-360.

66. Zhou K., and Doyle J. C., 1998, *Essentials of Robust Control*, Prentice-Hall, Inc.

67. Zhang H., 2003, *Robust LPV Control of a Magnetic Bearing Suspension System with a Convex Optimization Approach*, PhD dissertation, University of Virginia.

68. Fallah M. S., Long H., Xie, W. F., and Bhat R., 2008, Computationally Efficient Robust Model Predictive Control of Shimmy Vibration in Aircraft Landing Gears, , *Journal of Aircraft*, **45**(6), 1872-1880.

69. Boyd S., Ghaui L., Feron E., and Balakrishnan V., 1994, *Linear Matrix Inequalities in System and Control Theory*, The Society for Industrial and Applied Mathematics (SIAM).

70. Jamshidi M., 2003, *Robust Control Systems with Genetic Algorithms*, CRC Press LLC.

71. Sun C. C., Chung Y. H., and Chang W. J., 2005, "H2/H_∞ robust static output feedback control design via mixed genetic algorithm and linear matrix inequality", *Journal of Dynamic Systems, Measurement, and Control*, **127**(4), pp. 715-722.

72. Verros G., Natsiavas S., and Papadimitriou C., 2005, "Design optimization of quarter-car models with passive and semi-active suspensions under random road excitation". *Journal of Vibration and Control*, **11**(5), 581—606.

73. Zapateiro M., Luo N., and Vehi J., 2009, "Vibration control of a class of semiactive suspension system using neural network and backstepping techniques", *Journal of Mechanical Systems and Signal Processing*, In press.

74. Eslaminasab N., and Golnaraghi F., 2009, "A semi-active control strategy for vibration isolation to improve the ride comfort of vehicles", *International Journal of modelling, Identification, and Control*, **7**(3), 282-293.

75. Chang P., and Huang A., 2006, Adaptive sliding control of active suspension systems with uncertain hydraulic actuator dynamics, Journal of Vehicle System Dynamics, **44**(5), 357-368.

76. Lin J. S., and Kanellakopoulos I., 1997, Road-adaptive nonlinear design of active suspensions, *Proceedings of American control conference*, Albuquerque, NM, 714-718.

77. Chantranuwathana S., and Peng H., 1999, Force tracking control for active suspensions-theory and experiments, International Conference on Control applications, Kohala coast-Island of Hawai, USA, August 22-27.

78. Alleyne A., Liu R., and Wright H., 1998, On the limitation of force tracking control for hydraulic active suspensions, Proceedings of the American Control Conference, Philadelphia, Pennsylvania, June.

79. Zhang Y. and Alleyne A., 2005, A practical and effective approach to active suspension control, *Journal of Vehicle System Dynamics*, **43**(5), 305-330.

80. Wang E. R., Ma Q. X., Rakheja S., and Su C. Y., 2005, Force tracking control of vehicle vibration with MR dampers, Proceedings of the 2005 IEEE International Symposium on Intelligent Control, Limassol, Cyprus, June 27-29.

81. Spencer B. F., Dyke S. J., Sain M. K., and Carlson J. D., 1997, ""Phenomenological for magnetorheological dampers, Journal of Engineering Mechanics, **123**(3), 230-238.

82. Schurter K. C., and Roschke P., N., 2000, "Fuzzy modeling of a magnetorheological damper using ANFIS", *Proceedings of the IEEE International Conference on Fuzzy Systems*, 122-127.

83. Wereley N. M., Pang L., and Kamath G., 1998, "Idealized hysteresis modeling of electrorheological and magnetorheologic dampers", *Journal of Intelligent Material Systems and Structures*, **9**(8), 642-649.

84. Choi S., Lee H., and Park Y., 2001, "A hysteresis model for the field-dependent damping force of a magnetorheologicaldamper", *Journal of Sound and Vibration*, **245**(2), 375-383.

85. Chang C. C., and Roschke P., 1998, "Neural network modeling of a magnetorheological damper", *Journal of Intelligent Material Systems and Structures*, **9**(9), 755-764

86. Sun W., Hu H., and Weng J., 2006, "Design, testing, and modeling of a magnetorheological damper with stepped restoring torque", *Journal of Intelligent Material Systems and Structures*, **17**(4), 335-340.

87. Boada M. J. L., Calvo J. A., Boada B. L., and Dia V., 2009, "Modeling of a magnetorheological damper by recursive learning lazy learning", *International Journal of Non-Linear Mechanics*, In press.

88. Ma X. Q., 2006, *Dynamic characterization of a magneto-rheological fluid damper and synthesis of a semi-active suspension seat*, PhD dissertation, Concordia University.

89. Carrera website, http://www.carrerashocks.com/

90. Shames I. H., and Cozzarelli F. A., 1992, *Elastic and inelastic stress analysis*, Princton Hall, Englewoos Cliffs, New Jersy.

91. Stanway R., Sproston J. L., and El-Wahed A. K., 1996, "Application of electrorheological fluids in vibration control: a survey", *Journal of smart Materials and Structures*, 5(4), 464-482.

92. Dyke S. J., Spencer B. F., Sain M K., and Carlson J. D., 1996, "Seismic response reduction using magetorheological dampers", IFAC 13th triennial world congress, USA, 145-150.

93. Xia P. Q., 2003, "An inverse model of MR damper using optimal neural network and system identification", *Journal of Sound and Vibration*, 5(2), 1009-1023.

94. Tsang H. H., Su R.K.L., and Chandler A.M., 2006, "Simplified inverse dynamics models for MR fluid dampers", *Journal of Engineering Structures*, 28(3), 327-341.

95. Ma X. Q., Rakheja S., and Su C. Y., 2007, Development and relative assessments of models for characterizing the current dependent hysteresis properties of magnetorheological fluid dampers, *Journal of Intelligent Material Systems and Structures*, 18, 487-502.